FROM DISCOVERY TO MECHANISM: CHARACTERIZING PRC1584 AS A NOVEL IRRESISTIBLE ANTIMALARIAL AGENT

by

REAGAN SIERRA HANEY

(Under the Direction of Maria Belen Cassera)

ABSTRACT

Malaria remains a major global health burden, driven largely by *Plasmodium falciparum* and worsened by resistance to artemisinin-based combinations. This dissertation investigates PRC1584, a β-carboline antimalarial lead with rapid, potent activity against asexual blood stages, most pronounced from late ring to early trophozoite. Brief exposures trigger morphological quiescent/pyknotic forms reminiscent of dihydroartemisinin-associated dormancy, however, ring-stage dormancy can arise independently of any specific agent. Cross-resistance sensitivity profiling showed that parasites with the Kelch13-C580Y mutation are more sensitive in certain conditions than wild type strains, suggesting that endocytic pathways linked to K13 may play a role in how this mechanism works. Electron microscopy demonstrated disrupted cytostomes with abnormal invaginations and fewer endocytic or digestive vesicles that contained hemoglobin. Biochemical fractionation and heme quantification revealed a reduction in parasite heme levels as well as less hemozoin formation. These results indicate that PRC1584 disrupts cytostome-mediated hemoglobin uptake and subsequent delivery to the digestive vacuole. Together, these findings position PRC1584 as a fast-acting

disruptor of cytostome-mediated hemoglobin uptake, an essential pathway for parasite growth. To enable target discovery using chemoproteomics, two analogs were developed: an intermediate scaffold (PRC1859) and a diazirine–azide photoaffinity probe (PRC1860). Under continuous exposure, both preserved parent-like potency and reproduced PRC1584-like morphology, supporting on-pathway action suitable for chemoproteomic capture. At the same time, repeated attempts to select stable PRC1584-resistant lines were unsuccessful, indicating that resistance is unlikely to develop easily—PRC1584 appears to have an "irresistible" profile under the conditions tested. Although definitive molecular targets were not identified, this work delivers validated probes and workflows that establish a practical foundation for future target identification. Altogether, the dissertation characterizes PRC1584 as an antimalarial with nanomolar potency against asexual blood stages and an unusual efficacy signature that includes collateral sensitivity in artemisinin-tolerant parasites, durable effects after brief exposure, and failure to select resistance *in vitro*. These properties argue for the development of PRC1584 analogs primarily as a combination partner—a targeted starvation agent orthogonal to heme detoxification and peroxide activation—that can be scheduled to complement rapid-clearing schizonticides, suppress recrudescence, and maintain activity in K13-variant settings while minimizing cross-resistance.

INDEX WORDS: Malaria, *Plasmodium falciparum*, Drug Discovery, Kelch13, Artemisinin Resistance

FROM DISCOVERY TO MECHANISM: CHARACTERIZING PRC1584 AS A NOVEL IRRESISTIBLE ANTIMALARIAL AGENT

by

REAGAN SIERRA HANEY

BS, University of Idaho, 2019

A Dissertation Submitted to the Graduate Faculty of The University of Georgia in Partial Fulfillment of the Requirements for the Degree

DOCTOR OF PHILOSOPHY

ATHENS, GEORGIA

2025

FROM DISCOVERY TO MECHANISM: CHARACTERIZING PRC1584 AS A NOVEL ANTIMALARIAL COMPOUND

by

REAGAN SIERRA HANEY

Major Professor:	Maria Belen Cassera
Committee:	Dennis Kyle
	Lance Wells
	Tania Rozario

Electronic Version Approved:

Ron Walcott
Vice Provost for Graduate Education and Dean of the Graduate School
The University of Georgia
December 2025

DEDICATION

I would like to dedicate my dissertation to my family, friends, academic mentors (past and present), professional mentors, and the community at UGA for their patience, love, and steady belief in me. Without you, I would not be the person or scientist I am today. I also dedicate this work to future patients and caregivers affected by malaria, the reason careful science matters. And to every first-generation student and anyone who has struggled but kept going, many of us are not handed a golden platter; the work is hard, the effort is real, and the progress is worth it. To my past self, who kept choosing the next step, I am proud of you.

Most importantly, I dedicate this dissertation to my grandpa, Jerry Haney (1938-2016), whose quiet courage, and stubborn optimism shaped my own. One of the last things he said to me was, "*Wow—you will be the first doctor in the family.*" At the time I planned to become a veterinarian; life changed after he passed, but the promise did not—I still became a doctor, just a different kind. Your lessons about dignity, persistence, and doing the right thing traveled with me from the first pipette to the final page. I carry you with me, always.

ACKNOWLEDGEMENTS

First and foremost, I am deeply grateful to my advisor and mentor, Dr. Maria Belen Cassera. I first met Belen during my UGA interview weekend and was immediately drawn to her work and her way of thinking. From my very first rotation, she believed in me (even when imposter syndrome was loud) and gave me the space to grow while challenging me to think more critically and work more independently. The scientist I am today is possible because she trusted me to learn at my own pace and held the bar high.

To the entire Cassera Lab, thank you for years of support, good humor, and everyday problem-solving. A special thank you to Dr. Emilio Fernando Merino for keeping the lab running smoothly and in top shape. To my fellow graduate students, Emily Bremers and Leticia Do Amaral—thank you for the coffee runs, tea breaks, reality checks, and the safe space to vent; you made the hard days lighter. And to all the undergraduate students I had the privilege to mentor during my PhD: working with you was one of the best parts of this journey.

I am grateful to my committee—Dr. Dennis Kyle, Dr. Lance Wells, and Dr. Tania Rosario—for your guidance, thoughtful feedback, and steady confidence in my potential, especially at times when I struggled to see it myself.

My path to graduate school was shaped by mentors at the College of Southern Idaho: Kathy Clark, Amy Rice Doestch, Sarah Harris, and Megan Jacobson. Your encouragement and

practical help made graduate school imaginable and attainable. Thank you for opening doors and insisting I walk through them.

To my small circle of women who held me up—Jana Carpenter, Yasmin Anderson, and Kendall Clay—thank you for showing up with advice, laughter, and love exactly when I needed it. To the friends I met my first semester, the LT committee, our traditions and ridiculous themed parties were lifelines; I didn't expect to find a lifelong group of friends in graduate school, and I'm so glad I did. I'm also thankful for the many friends and colleagues in the Biochemistry Department and the Center for Tropical and Emerging Global Diseases who made UGA feel like home.

I want to thank my mom, Lisa Haney, for being my cheerleader through most of my undergraduate and graduate years. Even though our relationship changed, I recognize and appreciate the role you played in who I am today. To Maria Alvarez, thank you for pushing me forward when I was tired and reminding me of what I'm capable of. To my forever besties—Beth Roach, Carlos Romero Anaya, and Daniel Rega—thank you for your unwavering support across time zones and seasons. And to my rave besties—Arely Ayala, Ashley Ayala, Reanne Lokelani—thank you for pulling me out of the lab and into the joy of the moment, and for reminding me to breathe, dance, and savor the good.

Finally, to everyone along the way who offered a kind word, a troubleshooting session, or a shared snack at exactly the right time—thank you. This dissertation carries all your fingerprints.

TABLE OF CONTENTS

Page

Defining PRC1584's biological profile, stage specificity, and time–kill/recovery behavior....121

LIST OF TABLES

Page

LIST OF FIGURES

Page

ABREVIATIONS

ACT artemisinin combination therapy

ADME absorption–distribution–metabolism–excretion

ART artemisinin

ART-R artemisinin resistance

BTB/POZ broad-complex, tramtrack, and bric-à-brac

CQ chloroquine

CuAAC Copper(I)-catalyzed Azide–Alkyne Cycloaddition

DHA dihydroartemisinin

DMPK drug metabolism and pharmacokinetics

EM electron microscopy

ER endoplasmic reticulum

HTS high throughput screening

IDC intraerythrocytic cycle

IPP isopentenyl diphosphate

K13 *Pfk13*, kelch13

LiP-MS limited proteolysis–mass spectrometry

MMV Medicines for Malaria Venture

MOA mechanism of action

PK/PD pharmacokinetics/pharmacodynamics

QSA quiescence survival assay

RBC red blood cell

RSA ring survival assay

SAR structure activity relationship

SP sulfadoxine-pyremethamine

TCP target candidate profile

TPN total protein number

TPP target product profile

UPR unfolded protein response

WB western blot

CHAPTER 1

INTRODUCTION

Background: Malaria as a Global Health Challenge

Malaria remains one of the most pressing global health concerns. In 2023, an estimated 263 million cases of malaria were reported worldwide, resulting in approximately 597,000 deaths—a troubling increase of 11 million cases compared to the previous year[1]. This reversal of earlier progress underscores the fragility of current control efforts and the urgent need for sustained intervention. The disease disproportionately affects low- and middle-income countries, with Sub-Saharan Africa accounting for 94% of all cases and 95% of all deaths[1]. Among the six human malaria parasites: *Plasmodium falciparum*, *P. vivax*, *P. malariae*, *P. ovalecurtisi, P. ovalewallikeri*, and *P. knowlesi*. *P. falciparum* is the most virulent, causing most severe disease and nearly all malaria-related deaths. Children under the age of five remain the most vulnerable, accounting for roughly three-quarters of global malaria deaths due to their limited immunity and restricted access to prompt treatment[1]. The burden of malaria extends beyond direct mortality. Recurrent infections contribute to chronic anemia, maternal and fetal complications, and neurocognitive impairments in children, all of which perpetuate cycles of poverty and poor health. In economic terms, malaria imposes a formidable burden on individuals, health systems, and national economies.

Endemic countries may lose up to 1.3% of annual gross domestic product (GDP) to malaria through productivity losses, healthcare costs, and absenteeism[2]. At the household level,

recurrent infections contribute to income instability and educational setbacks, with infected children experiencing long-term cognitive and academic impairments. Although the costs of control programs range from $0.11 to $39.06 per capita for control initiatives and $0.18 to $27 per capita for elimination efforts, these investments are considered highly cost-effective. In numerous contexts, benefit-cost ratios often surpass 100, attributable to increased labor productivity, lower healthcare expenditures, and improved educational outcomes[3]. These data highlight the need for ongoing financial and political support to eradicate malaria, especially in areas moving from control to elimination. Over the past two decades, global investments in malaria control through insecticide-treated bed nets, indoor residual spraying, and the widespread adoption of artemisinin-based combination therapies (ACTs) led to dramatic reductions in malaria incidence and deaths[4]. However, progress has stalled in recent years, hindered by a combination of insecticide resistance, drug-resistant parasite strains, climate-related disruptions, and chronic funding shortfalls[5, 6].

Despite decades of global investment, funding for malaria control has consistently fallen short of what is needed to sustain elimination efforts, hindering the scale-up of existing tools and the implementation of new interventions. The COVID-19 pandemic further strained malaria programs by disrupting access to diagnostics, delaying treatment delivery, and impeding the distribution of interventions[6]. These setbacks contributed to resurgent case numbers in several high burden countries, particularly those with fragile healthcare systems. This pattern reflects the decline of mid-20th century eradication initiatives, which initially demonstrated short-term effectiveness but ultimately fell short as financial support and political commitment diminished. Currently, artemisinin resistance has become prevalent in regions of East and Central Africa due to systemic challenges such as insufficient pharmaceutical regulation, the administration of

substandard or monotherapy drugs, and limited surveillance capacity[7]. Together, these challenges emphasize the urgent need for resilient health systems, sustained investment, and new therapeutics with distinct modes of action to avoid repeating past failures[6]. A central priority is the development of antimalarial agents that effectively target both drug-resistant parasites and less recognized forms, such as dormant ring-stage parasites. These forms are associated with treatment failures and sustained transmission, highlighting a key vulnerability in current therapeutic approaches. Overcoming this challenge is essential to advancing future antimalarial drug discovery initiatives.

The *Plasmodium falciparum* Lifecycle and Points of Vulnerability

P. falciparum alternates between the human host and the female *Anopheles* mosquito, progressing through liver**,** asexual blood, and sexual/transmission stages. The overview below maps this lifecycle before detailing stage-specific vulnerabilities.

Infection begins when an infected mosquito injects sporozoites into the human host while feeding. Point of action: Sporozoites need to quickly move through and enter liver cells; strategies that prevent mosquito-to-human transmission or stop sporozoite invasion can halt infection before symptoms appear[8]. Sporozoites then rapidly travel to the liver, where they invade hepatocytes and undergo a clinically silent round of asexual replication. A single sporozoite can produce 10,000 to more than 30,000 merozoites within a hepatocyte[9]. Treatment relevance: Parasites rely on de novo pyrimidine synthesis (via DHODH) and mitochondrial electron transport processes throughout both blood and liver stages. During the liver stage, their intracellular existence and asymptomatic proliferation highlight these metabolic pathways as

promising targets for causal prophylaxis. Therapeutic interventions directed at these mechanisms can eradicate the infection before clinical manifestations arise in the blood stage[10-13].

After several days, these merozoites are released into the bloodstream, initiating the symptomatic blood-stage cycle[5, 14]. Once inside red blood cells (RBCs), *P. falciparum* progresses through the intraerythrocytic developmental cycle (IDC), comprising morphologically distinct ring, trophozoite, and schizont stages over approximately 48 hours. Intervention focus: Stage identity determines drug sensitivity: ring stages are characterized by limited heme availability and are particularly susceptible to impairments in endocytic flux, translation, and ion homeostasis. In contrast, trophozoites possess abundant heme and are primarily affected by agents that disrupt food vacuole function or interfere with hematin detoxification. Schizonts experience increased DNA replication, proteostasis, and egress mechanisms[15-17]. Within 6–8 days of liver emergence, parasite densities reach approximately 50/μL of blood (equivalent to about 100 million parasites in an adult), at which point infection becomes detectable by microscopy or rapid diagnostic tests, and the symptomatic stage of infection begins. The incubation period is typically 12–14 days from the infecting bite[9]. Treatment relevance: Because early asexual expansion is often below the limit of detection at presentation, early rings predominate; regimens need rapid ring-stage activity and sustained exposure that outlasts the dormancy window to reduce biomass before peak symptoms.[18-20].

By the end of the erythrocytic cycle (Figure 1.1), parasites have consumed most of the host RBC contents and undergone several nuclear divisions. The schizont then ruptures, releasing 6–30 merozoites, each capable of invading new RBCs and repeating the cycle. Clinical manifestation of malaria results from both direct RBC destruction releasing their content to the blood stream and host inflammatory responses. Treatment intervention: Inhibitors administered at later stages

that disrupt DNA synthesis, proteasome activity, or egress can diminish burst size and decelerating parasite replication[21]. During the IDC, a small subset of parasites commits to sexual development through gametocytogenesis, a process that is initiated by activation of the transcription factor *ap2-g*, which triggers expression of genes required for sexual differentiation.

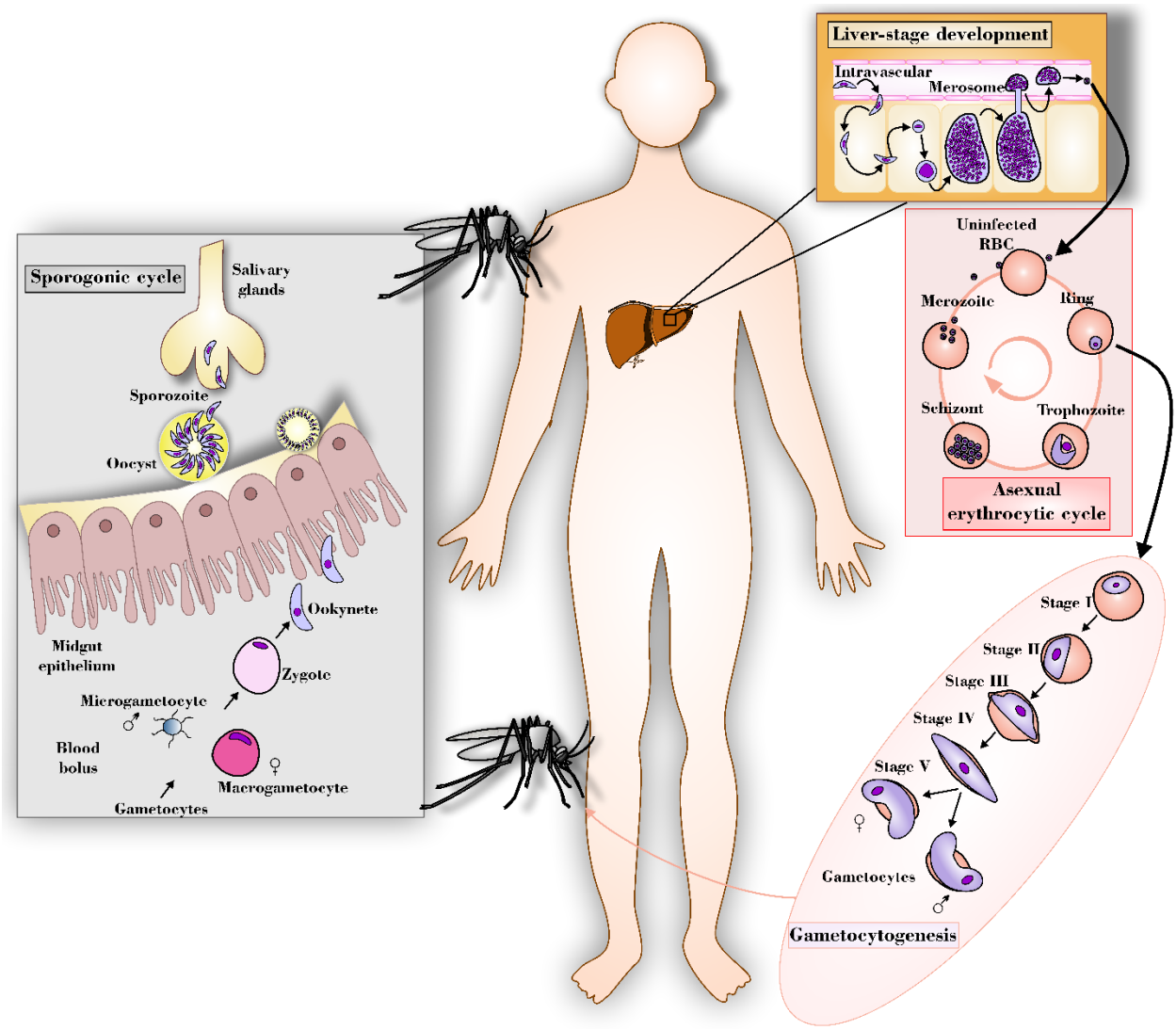

Figure 1.1 *Life cycle of Plasmodium falciparum.* The parasite alternates between mosquito and human hosts, progressing through sporozogonic, liver, and blood stages. Reproduced with permission from Kingston & Cassera, *Antimalarial Natural Products*, Springer Nature (2022).

Committed parasites progress through five morphologically distinct gametocyte stages (I–V) over approximately 10–12 days. Stages I–IV are sequestered in extravascular niches such as the bone marrow and spleen, where they mature largely hidden from immune surveillance and drug exposure[22]. Mature stage V gametocytes re-enter peripheral circulation, where they can be taken up during a mosquito blood meal. Treatment intervention: Early gametocyte differentiation and mitochondrial/ATP homeostasis are drug targets, but mature stage V forms are insensitive to most frontline drugs active in the asexual stages—thus transmission-blocking agents or combinations that target early stages are needed[23]. In the mosquito midgut, gametocytes rapidly differentiate into gametes, undergo fertilization, and eventually form oocysts that release sporozoites, completing the transmission cycle[6, 14]. Point of action: The processes of midgut traversal and oocyst/sporogony rely on specific signaling and bioenergetic pathways. Interventions targeting vectors, as well as the use of endectocides, can effectively decrease subsequent transmission, even after clearance of human blood-stage infection[24].

Gametocytes, as non-replicative sexual forms, are relatively insensitive to most frontline drugs and can persist in the bloodstream after clinical cure, enabling ongoing transmission even from asymptomatic carriers[25]. Notably, early ring-stage parasites can enter a reversible dormant state that transiently suppresses multiple cellular processes, enabling survival after short drug exposures, particularly with artemisinin-based therapies[26, 27]. This dormancy-like phenotype is a defining feature of reduced sensitivity to artemisinin (ART) and differs from classical target-site mutation resistance mechanisms. *Pfkelch13* mutations represent a key mechanism linked to delayed clearance and ring-stage survival. Artemisinin tolerance/resistance is multifactorial: beyond *Pfkelch13*, additional loci and non-genetic adaptations— including altered proteostasis, stress-response signaling, and changes in hemoglobin endocytosis/digestion—also shape the

phenotype.[28-30]. Point of action: effective regimens should retain activity in early rings, minimize reliance on heme availability for activation as it is the case of ART, and sustain exposure and efficacy beyond dormancy windows while pairing blood-stage killing with transmission-blocking coverage[19, 31, 32].

In summary, the biology of *P. falciparum* presents both opportunities and barriers for therapy; effective regimens must eliminate asexual blood and liver stages, overcome ring-stage dormancy, target transmission stages, and sidestep diverse resistance mechanisms.

Historical Perspective on Antimalarial Drug Development and Resistance

The history of antimalarial drug development reflects both scientific progress and the parasite's extraordinary capacity for adaptation. The first effective treatment, quinine, was derived from the bark of the cinchona tree and used widely by the 17th century[33]. Although effective, quinine's side effects and limited availability motivated the development of synthetic alternatives[34, 35]. Chloroquine (CQ), a 4-aminoquinoline compound introduced during World War II, became the backbone of global malaria control programs due to its efficacy, affordability, and long half-life. However, widespread use led to the rapid emergence of resistance.

CQ resistance was first reported in Thailand in 1957 and quickly spread to South America and Africa, driven largely by mutations in the *P. falciparum* chloroquine resistance transporter gene (*pfcrt*) and multidrug resistance gene (*pfmdr1*)[36, 37]. This trajectory repeated with sulfadoxine-pyrimethamine (SP), introduced in the late 1960s[38]. Resistance, fueled by the stepwise accumulation of mutations in the *P. falciparum* dihydrofolate reductase (*pfdhfr)* and *P. falciparum* dihydropteroate synthase (*pfdhps)* genes, spread from Asia to Africa and rendered SP

ineffective within decades[39, 40]. The collapse of CQ and SP efficacy prompted the global transition to ACTs in the early 2000s. ART and its derivatives act fast but disappear from blood within hours, leaving residual parasites that can rebound if given alone. ACTs pair ART with a long-residence partner (e.g., lumefantrine, piperaquine, amodiaquine) to provide sustained exposure over several asexual cycles, achieving radical clearance and narrowing the resistance-selection window[41]. Yet by the late 2000s, partial ART resistance emerged in the Greater Mekong Subregion[29]. It is now known to be primarily associated with mutations in the *Pfkelch13* gene, which delays parasite clearance and reduces treatment efficacy. These resistant strains have since appeared in East and Central Africa, raising alarms about the long-term sustainability of ACTs[7].

Compounding the problem, resistance to partner drugs such as piperaquine and lumefantrine is also spreading. Polymorphisms in *P. falciparum* chloroquine resistance transporter (*pfcrt*) and *P. falciparum* multidrug resistance 1(*pfmdr1*) genes modulate drug transport within the digestive vacuole and are implicated in reduced partner drug sensitivity. Recent molecular surveillance in Uganda has demonstrated decreased lumefantrine susceptibility linked to *pfmdr1* mutations, even in the absence of *pfkelch13* mutations, highlighting that partner drug resistance can arise independently and may foreshadow complete ACT failure[37, 42]. This convergence of resistance mechanisms has led to treatment failures in Southeast Asia and now threatens control efforts in parts of Africa[42].

Overall, these results indicate that drug resistance is an ongoing battle. *P. falciparum* can utilize gene mutations or amplifications that once conferred resistance to older antimalarial drugs to undermine the efficacy of new therapies as well. The lessons from history are clear: monotherapies inevitably select for resistance, while sustained, globally coordinated combination

strategies and robust molecular surveillance are essential. With ACT efficacy under threat, the development of next generation antimalarials featuring novel mechanisms of action, improved pharmacokinetics, and activity against resistant and dormant parasite stages is critical to sustaining treatment success and advancing toward malaria elimination.

Ring-Stage Plasticity and Artemisinin Resistance

ART and its derivatives are activated by heme (ferrous protoporphyrin IX) to generate short-lived carbon-centered radicals that covalently alkylate parasite proteins (and other macromolecules), leading to proteome damage and death[43]. This mechanism is potent in trophozoites when hemoglobin digestion supplies abundant heme, yet stage-specific profiling shows early rings can be highly susceptible under continuous drug exposure, whereas short ART pulses reveal the well-described ring-stage survival phenotype which is amplified by Kelch13 (K13) mutations[20, 44, 45]. Ring-stage survival after short ART exposure was first described in Cambodian clinical isolates with delayed parasite clearance *in vivo*[29]. *In vitro*, this phenotype is measured by the ring-stage survival assay (RSA), in which early rings receive a 6-hour dihydroartemisinin (DHA) pulse and are then returned to drug-free medium for outgrowth [46]. Cultures with >1% survival are classified as having reduced ART susceptibility, whereas DHA-sensitive cultures typically show <1% survival. Importantly, the underlying ability to enter a reversible growth-arrest ("ring-stage dormancy" or quiescence) is not contingent on ART resistance—both sensitive and resistant parasites can transiently arrest after short pulses. K13 mutations and related factors increase the likelihood and durability of that dormancy, which is why RSA survival is higher in those lines.[26].

Dormant rings display reduced transcriptional activity, slowed protein translation, and altered cellular morphology, allowing survival through drug pressure before resuming normal development once drug pressure subsides[26, 27]. This adaptive program has been linked to translational repression via eIF2α phosphorylation and altered PI3P-mediated trafficking[30, 47]. Central to this phenotype is K13, a Broad-Complex, Tramtrack, and Bric-à-brac (BTB; also called POZ)–Kelch protein with an N-terminal BTB/POZ dimerization domain and a C-terminal Kelch β-propeller, localized to vesicular structures and cytostomes at the parasite plasma membrane. K13 is thought to function as an adaptor in a ubiquitin ligase complex, potentially regulating endocytic trafficking and vesicle-mediated hemoglobin uptake[44, 47]. Mutations in K13, such as C580Y or R539T, reduce hemoglobin endocytosis, limiting the heme availability and thereby ART activation[48]. By delaying hemoglobin ingestion and metabolic activity, ring-stage parasites can effectively "wait out" short-lived ART exposure.

K13-independent pathways also contribute to plasticity. Transcriptomic analyses show that resistant parasites upregulate stress-response genes, including those involved in the unfolded protein response (UPR), redox balance, and protein folding[27, 49]. Gene set enrichment analysis of DHA-treated ring stages has further revealed enrichment of endoplasmic reticulum (ER) and proteostasis-related pathways, consistent with an integrated stress-adaptation program that increases drug tolerance, rather than resistance in the strict genomic sense. Because ART derivatives clear quickly from blood, a minority of early rings that survive brief exposure can resume growth once levels decline. ACTs therefore pair ART with a long-acting partner to cover this window and prevent recrudescence. When resistance to partners such as piperaquine or lumefantrine arises, this protective tail is lost, increasing the risk of rebound parasitemia and treatment failure.[50].

Experimental systems such as selection-linked integration targeted gene disruption (SLI-TGD) knockdowns and rapamycin-inducible 'knock sideways' (FKBP-FRB) mislocalization have confirmed that a functional K13 is essential for parasite survival and contributes to artemisinin-tolerance phenotypes[15, 51]. Conditional depletion of K13 or introduction of mutant alleles recapitulates resistance phenotypes and highlights its role in vesicular dynamics, hemoglobin import, and possibly stress signaling[15]. Overall, ring-stage plasticity represents a multifaceted survival strategy combining metabolic downregulation, vesicular trafficking control, and stress response regulation to endure ART exposure. These adaptations, driven primarily by K13 mutations but reinforced by accessory pathways, allow *P. falciparum* to tolerate fast-acting drugs, necessitating revised strategies for drug discovery and therapeutic design that can overcome this stage-specific resilience mechanism.

The Drug Discovery Pipeline and the Role of Hit-to-Lead Optimization in Antimalarial Development

The development of a new drug is a lengthy and resource-intensive process, often exceeding a decade and costing more than a billion dollars[52]. Attrition rates are high: of the thousands of compounds entering discovery pipelines, fewer than 10% ultimately progress to clinical approval[53]. This pipeline consists of sequential phases—hit discovery, hit-to-lead optimization, lead optimization, preclinical development, and clinical trials—each serving as a critical filter to eliminate compounds with poor efficacy, safety, or pharmacokinetic properties[54].

Modern discovery typically begins with identifying chemical matter capable of producing a measurable biological effect. In traditional pipelines, this process starts with high-throughput screening (HTS) of hundreds of thousands of compounds or with fragment-based approaches,

yielding “hits” that show acceptable potency and possess desirable physicochemical features[55]. These hits are triaged through medicinal chemistry, computational modeling, and structure–activity relationship (SAR) studies to produce “leads” with improved potency, selectivity, and desirable pharmacokinetic/pharmacodynamic (PK/PD) properties[56]. Key preclinical assays at this stage include *in vitro* potency testing, cytotoxicity evaluation, absorption–distribution–metabolism–excretion (ADME) profiling, and resistance selection studies, especially in the case of infectious diseases[57].

Hit-to-lead optimization represents the first rigorous checkpoint in this process. Hits are rarely drug-like; they often suffer from poor solubility, metabolic instability, cytotoxicity, or limited bioavailability[58]. The hit-to-lead stage aims to address these liabilities through iterative medicinal chemistry, refining potency, selectivity, solubility, metabolic stability, and permeability, while simultaneously identifying off-target effects, early toxicity, and resistance liabilities[59]. This step is particularly critical in malaria because parasites must be targeted within red blood cells, adding permeability and intracellular trafficking to the list of chemical hurdles[19]. Early go/no-go decisions at this stage can prevent costly failures later in preclinical or clinical phases[60].

Rather than starting from human molecular targets, malaria programs are organized around public-health priorities: rapid clearance, single-visit regimens, pediatric suitability, and low cost. The Medicines for Malaria Venture (MMV) and partner organizations have formalized these needs in Target Product Profiles (TPPs) and Target Candidate Profiles (TCPs)[19]. TPPs outline the minimal and ideal characteristics of deployable medicines: oral dosing, affordability, heat stability for storage in tropical climates, safety in children and pregnant women, and low

propensity for resistance[61]. TCPs, in turn, map compounds to therapeutic roles across the parasite lifecycle[62]:

- TCP1 – Fast-acting compounds that rapidly clear blood asexual parasites including compounds with schizonticide activity and long-duration blood.
- TCP3 – Radical cure agents with activity against hypnozoites (*P. vivax*) or dormant liver forms.
- TCP4 – Chemopreventive agents to protect high-risk populations.
- TCP5 – Transmission-blocking agents with activity against mature gametocytes.
- TCP-6: Transmission-blocking agents by targeting the insect vector (endectocides)

While *P. falciparum* does not form hypnozoites, TCP1 and TCP5 are especially relevant in endemic regions: the former ensures durable cures in the face of antimalarial resistance, while the latter interrupts transmission[1]. Increasingly, compounds are also evaluated for "irresistibility"—the inability to select resistant mutants *in vitro* and *in vivo*—a property now highly valued as potency[63].

These priorities have driven a shift away from purely target-based discovery. While rational inhibitors of validated parasite enzymes (e.g., dihydrofolate reductase, dihydroorotate dehydrogenase, or PI4K) have shown promise, many failed due to poor cell penetration, rapid resistance, or lack of whole-parasite efficacy[64]. In contrast, phenotypic screening, which is the direct testing of compounds against live parasites, has yielded several first-in-class leads with novel modes of action[65]. Notable examples include cipargamin (KAE609), a PfATP4 inhibitor, and ganaplacide (KAF156), an imidazolopiperazine with multistage activity, both of which emerged from HTS campaigns and advanced to clinical development[66]. M5717, an elongation factor 2 inhibitor with a long half-life in blood, illustrates the power of phenotypic hits with

unique PK properties, enabling single-dose potential[67]. Other compounds, such as KDU691 (phosphatidylinositol 4-kinase [PI4K] inhibitor), DSM265 (dihydroorotate dehydrogenase [DHODH] inhibitor), and fosmidomycin (methylerythritol phosphate [MEP] pathway inhibitor), highlight the challenges of target-based approaches: despite clear targets, many stalled due to safety, resistance, or insufficient efficacy[64, 68].

Antimalarial compounds discovered by phenotypic screenings depend on rigorous mechanistic deconvolution, historically a bottleneck[69], to understand their mechanism of action (MOA). Recent innovations have transformed this step, such as:

- *In vitro* evolution with whole-genome analysis (IVIEWGA): entails subjecting parasites to compound pressure, sequencing the emerging populations, and identifying recurrent resistance mutations or gene amplifications. These variants are of particular interest when they (i) localize to a single gene or pathway, (ii) alter compound potency, and (iii) correspond to plausible binding or functional sites. In many cases, mutations can be mapped to the molecular target or to the molecular mechanism mediating the resistance phenotype[70].
- Thermal proteome profiling and limited proteolysis–mass spectrometry (LiP-MS): involves quantifying ligand-induced shifts in protein stability or protease accessibility across the proteome. A direct binder typically shows dose-dependent thermal stabilization (or destabilization) in intact cells/lysate or site-specific protection/exposure of peptides. Convergence criteria—such as consistent shifts observed across replicates, competition with an inactive or competitor analog, and alignment of time- and dose-response curves—help identify the molecular target or pathway by mapping the stabilized proteins to known cellular functions[71, 72].

- Photoaffinity probes: involve adding a photoreactive group (e.g., diazirine) and a clickable chemical handle (e.g., alkyne/azide) to allow protein pulldown and identification by mass spectrometry. In whole parasites, a short exposure to UV light covalently links the probe to nearby binding proteins. Click chemistry is then used to attach either biotin or a fluorophore, enabling protein enrichment, identification by mass spectrometry, or visualization. In this method, a genuine target is identified by several criteria: (i) it displays strong, saturable labelling within cells; (ii) the parent compound can compete for binding, causing a dose-dependent decrease in labelling; (iii) labelling occurs at concentrations and durations that match the kinetics of cell death; and (iv) the signal aligns with structure-activity relationships, distinguishing between active and inactive analogues[73, 74].
- pH fingerprint assays (live-cell cytosolic pH tracing)[75]: this approach encompasses loading parasites with a pH-sensitive fluorophore (e.g., BCECF-AM) and tracking real-time cytosolic pH (pH_i) changes after compound addition in the presence or absence of ion and transport challenges. Inhibitors of specific transporters produce characteristic pH_i signatures such as:
    - PfATP4 (Na^+ efflux P-type ATPase): blocking this enzyme disrupts Na^+ balance, causes acidification, and leads to irregular pH_i recovery, often with Na^+ influx or volume shifts. The effect is quick and can be tested using ionophores like monensin.
    - The inhibition of the PfFNT (lactate/H^+ transporter): leads to cytosolic alkalinization during glycolytic lactate export. This effect can be reversed

depending on the stimulus, such as upon glucose pulsing or alteration of external pH conditions.

- MOA link: When a compound's pH profile (i) matches the reference pattern of PfATP4 or PfFNT, (ii) displays a clear dose–response and rapid effect, (iii) is shifted in a competitive manner by changes in substrate or ion concentration, and (iv) correlates with resistance mutations in the relevant gene (PfATP4 or PfFNT), this nominates the transporter as its primary target. Additional confirmation comes from methods like electrophysiology or Na^+ imaging, allelic replacement experiments, and analysis of chemical genetics such as cross-resistance profiles.

In all the approaches outlined, comprehensive drug target validation through cellular and biochemical methods remains essential. Collectively, these strategies integrate chemical biology with parasite genetics to facilitate target identification, SAR optimization, and resistance risk evaluation.

Contributions to collaborative initiatives aimed at advancing drug discovery efforts

Throughout these years, alongside my work characterizing the mechanism of action of PRC1584, I have had the privilege to contribute to Dr. Cassera's group's collaborative efforts focused on the discovery and development of safer antimalarial drugs. Provided below is a summary of my contributions to each collaborative publication, which also forms the foundation of my thesis.

Malaria Box-Inspired Discovery of N-Aminoalkyl-β-carboline-3-carboxamides, a Novel Orally Active Class of Antimalarials (Co-author)[76]

Our project started by using a pharmacophore based on the apicoplast-targeting antimalarial MMV008138 to virtually screen around 13,000 compounds from the GSK collection, leading to the selection of candidates from the "Malaria Box." Through these efforts, we identified tetrahydro-β-carboline TCMDC-140230 as a promising compound for resynthesis and further antiplasmodial evaluation.

All four stereoisomers of TCMDC-140230 were obtained, but none of those inhibited *P. falciparum* growth potently. Instead, a minor oxidative byproduct obtained during amidation—an aromatized β-carboline amide designated as 7e and referred to as PRC1584 throughout this dissertation—demonstrated low nanomolar potency. This serendipitous switch from a tetrahydro- to β-carboline core to a β-carboline marked a pivotal inflection point of our research and set the bases of my thesis work as this novel class is not targeting the MEP pathway in the apicoplast. My role was to perform dose-dependent growth inhibition assays to determine the EC_{50} values of 7e analogs and to perform isopentenyl diphosphate (IPP) metabolic-rescue experiments to determine if these analogs were still acting through a different and potentially novel MOA independent of the apicoplast.

In addition, the team performed an extensive SAR around the C-3 carbonyl and pendant amines. My dose-dependent growth inhibition assays showed a clear on/off switch: esters and acids were inactive (>10 μM), neutral amides were weak, and activity clustered in amides bearing a basic side chain, of which the N-(2-methylamino)ethyl substituent in 7e was best. These data guided the medicinal chemistry to keep a protonated side-chain amine in the series.

In parallel, we explored A- and D-ring substitutions. My profiling across these variants demonstrated that 3′,4′-dichloro substitution on the D-ring consistently delivered the highest potency (again exemplified by 7e), while unsubstituted or mono-chloro analogs lost ground. That structure-level clarity helped us focus on a narrow chemical neighborhood rather than broad, inefficient searches.

Because clinical translation depends on robustness against existing resistance mechanisms, we extended testing beyond Dd2 to 3D7, W2, 4G, and a KAE609-resistant strains, and confirmed potency using orthogonal assays (DNA replication, purine biosynthesis, and LDH activity). Compound 7e maintained low nanomolar potency across resistant strains, supporting no cross-resistance with current know mechanisms. These assays were crucial for selecting compounds for *in vitro* drug metabolism and pharmacokinetics (DMPK) and *in vivo* work.

In summary, 7e was "discovered" not by direct design but by disciplined follow-through on an unexpected byproduct and my contribution was to (i) validate its potency and non-MEP mechanism via IPP-rescue assays, (ii) aiding in mapping early SAR that highlighted the essential basic amide side chain and 3′,4′-dichloro D-ring, (iii) demonstrate cross-strain robustness, and (iv) help triage candidates for DMPK and efficacy studies, collectively moving 7e from a serendipitous event to an orally active early lead antimalarial.

Optimization of the β-Carboline-3-Carboxamide Scaffold and My Role in Advancing PRC1584 (7e) (Co-author)[77]

Following the initial discovery of PRC1584 (compound 7e), our next goal was to further refine the specific structural features that governed its potency, selectivity, and pharmacological behavior. In the follow-up study, *β-Carboline-3-Carboxamide Antimalarials: Structure–Activity*

Relationship, ADME-Tox Studies, and Resistance Profiling (Mathew et al., ACS Infectious Diseases, 2024), we systematically explored 91 analogs. In this work, I used dose-dependent growth inhibition assays to determine the EC_{50} values of analogs varying in A-ring methylation, C_1-phenyl substitution, and C_3-amide side-chain composition. My results confirmed the essentiality of a protonated amine on the amide substituent and revealed that electron-withdrawing D-ring halogens, particularly 3′,4′-dichloro and 3′,4′,5′-trichloro patterns, produced the steepest potency gains. These findings guided our medicinal chemists toward the most productive chemical space, culminating in the identification of compound 42a (referred to as PRC1697 in this dissertation), which doubled the potency of PRC1584 while preserving its favorable resistance profile.

Together, these two research projects established the β-carboline-3-carboxamide series—initiated by the discovery of PRC1584—as a new, orally active antimalarial chemotype with a distinct mechanism of action. My contributions bridged the discovery and optimization phases: validating the original hit biologically, aiding in mapping early SAR trends, confirming mechanistic novelty, and helping define the next steps for pre-clinical development.

Key Outstanding Questions Driving the Development of PRC1584 as an Antimalarial Agent

PRC1584's potency, safety and oral availability justified deeper investigation to understand its MOA and molecular target(s). The work that followed aimed to develop orthogonal assays and chemical tools to aid in establishing a mechanistic framework that enables rational optimization and anticipates resistance liabilities.

How does PRC1584 act as an antimalarial?

PRC1584 is a potent β-carboline with rapid activity concentrated at the ring to trophozoite stage transition. My early morphology assessments by electron microscopy (EM) suggested cytostome abnormalities and perturbed hemoglobin trafficking, but the direct molecular target(s) and primary pathway were unknown. This uncertainty limited our ability to anticipate toxicity (especially in children and during pregnancy) and to steer medicinal chemistry rationally. Despite knowing MOA is not strictly required for progression of novel antimalarials, it strengthens development. For example, identifying PfATP4 as the target of cipargamin enabled prospective resistance surveillance and de-risked clinical advancement[66], whereas chemotypes with unclear or promiscuous action have often failed later due to unexpected toxicity (e.g., halofantrine; DM1157) or have selected resistance rapidly when not paired appropriately (e.g., atovaquone monotherapy)[78-80]. PRC1584 merits mechanistic definition because its phenotype partly overlaps with ART including rapid kill in ring stages, pyknotic/dormancy-like morphological phenotype after brief drug exposure, while behaving differently in terms of resistance.

ART tolerance is associated with mutations in *Pfkelch13* (e.g., C580Y) that reduce hemoglobin endocytosis, lowering heme availability for ART activation and increasing ring-stage survival under short pulses[81-83]. Surprisingly, across isogenic backgrounds, PRC1584 shows collateral sensitivity in PfK13-C580Y mutant parasites by inhibiting mutant parasite growth more strongly than in the wild type. This inverted relationship to K13 (ART tolerance vs PRC1584 hypersensitivity) supports a distinct mechanism of action for PRC1584 and steered our mechanistic investigations toward the process of hemoglobin uptake and degradation.

What is the impact of PRC1584 on hemoglobin uptake and heme detoxification?

At the outset, morphology and EM hinted that PRC1584 perturbs cytostome architecture and the ring to trophozoite transition, raising the possibility that hemoglobin uptake and downstream hemozoin formation are affected. However, the primary step (digestive vesicle formation vs vesicle trafficking vs food-vacuole processing) and its timing remained undefined. Therefore, we assessed whether PRC1584 alters the heme/hemozoin content and causes changes along the endocytosis → food vacuole → crystallization pathway using fractionation-based heme and hemozoin measurements and ultrastructural analysis after short drug exposure. The abnormal morphology and structural analysis of cytostomes and digestive vesicles observed by EM and the detection of reduced heme and hemozoin levels in PRC1584-treated parasites further aligned with perturbations of the cytostome-mediated hemoglobin uptake/trafficking supporting our hypothesis that PRC1584 disrupts hemoglobin uptake and degradation, thus, starving the parasites from amino acid precursors. These experiments were designed to narrow the MOA that in turn will guide the identification of potential molecular targets.

What is the resistance potential of PRC1584?

Drug resistance has undermined every frontline antimalarial: CQ, SP, and, more recently, ART–based combinations[84]. Early observations with PRC1584 suggested a higher barrier to resistance: standard *in vitro* selections did not yield stable mutants, no cross-resistance to DHA was detected, and parasites bearing PfK13-C580Y (linked to ART tolerance) showed collateral sensitivity to PRC1584.

Key questions remain, including whether resistance develops, the fitness costs of such changes, the frequency of *de novo* resistance under realistic exposures, and how PRC1584

interacts with partner drugs (synergy, additivity, or suppression). To tackle these questions, I begin by re-evaluating whether PRC1584 has a greater resistance threshold. I use both continuous and stepwise or alternating drug exposures to test if resistance can be induced, and how frequently it occurs. All these approaches failed to select parasites resistant to PRC1584, thus, confirming its "irresistibility". These results were independently confirmed by the group of Dr. David Fidock (Columbia University) as part of our collaboration with Medicine for Malaria Venture (MMV).

In addition, we previously assessed the potential cross-resistance and sensitivity within this scaffold, PRC1548 was evaluated using the Antimalarial Resistome Barcode Sequencing (AReBar) pooled-screening assay[77]. This methodology employs genetically barcoded *P. falciparum* parasite lines, which were previously developed using the CRISPR/Cas9 genome editing to introduce a barcode cassette into a nonessential locus of each line[85]. Barcode sequencing subsequently quantifies the relative abundance of each line. Using this strategy, 51 distinct cell lines are pooled for direct competition assays in the presence of selected compounds, thereby encompassing diverse resistance mechanisms within both the 3D7 and Dd2 genetic backgrounds. These mutations cover a range of different biological functions including protein synthesis, nucleic acid synthesis and processing, mitochondrial function, and hemoglobin uptake and processing, thus addressing potential mechanisms of antimalarial action. Through this analysis, no mutant cell lines were recovered in PRC1584 treated samples, thus, no cross-resistance was detected.

Assessing PRC1584's resistance potential and cross-resistance profile is essential for developing it as a new antimalarial. These analyses also help identify suitable drug combinations

and evaluate whether PfK13-linked collateral sensitivity can be used effectively in regions with prevalent ART tolerance.

In summary, three unanswered questions drove this work.

1. **Mechanism of action.** PRC1584 is potent, but its molecular target and primary target pathway remain undefined. Until target engagement is established, chemistry is only guided based on phenotypic potency and overall safety, but more precise risks are hard to anticipate. My work concentrated on developing orthogonal assays and chemical tools to transition PRC1584 from demonstrating only phenotypic potency to establishing a solid mechanistic basis.
2. **Hemoglobin uptake and heme detoxification.** Morphology and structural analysis by EM implicated the ***cytostome and formation of digestive vesicle*** as part of the potential mechanism of action of PRC1584, and hint at downstream effects on hemozoin formation, a well-known drug target in *P. falciparum*. By identifying where PRC1584 first acts in the endocytosis → food vacuole → crystallization pathway, we aimed to clarify whether it defines a new mechanistic class rather than another vacuolar poison or heme-reactive agent.
3. **Resistance potential.** Our initial findings—namely, that PRC1584 does not select for mutants under standard conditions, shows no DHA cross-resistance, and exhibits collateral sensitivity to PfK13-C580Y—indicate it may have resistance-refractory properties worth further investigation.

Addressing these three unanswered questions is essential for determining the translational trajectory of PRC1584 and enhancing our understanding of malaria biology. Establishing a clear MOA and identifying a potential molecular target will help guide optimization of PRC1584, and leveraging insights into the formation and role of digestive vesicles could expand the antimalarial target landscape. Furthermore, developing a comprehensive resistance profile will support the design of novel drug combinations, which is particularly important in areas where K13-mediated ART tolerance is prevalent.

Specific Aims

This dissertation examines three critical aspects related to PRC1584 as a potential novel antimalarial: its biological footprint, mechanism of action, and resistance profile, including the observed collateral sensitivity in *Pfkelch13* C580Y mutant parasites.

Aim 1: Define PRC1584's biological activity and phenotypic effects.

Rationale: Early studies revealed that PRC1584 exhibits nanomolar potency against asexual blood stages. However, a systematic characterization of its biology is needed to establish its therapeutic profile and relevance to MMV Target Candidate Profiles (TCPs).

Approach: This aim evaluates PRC1584's potency, stage-specific activity, and phenotypic consequences. Microscopy, viability assays, and gametocyte/gamete studies provide a comprehensive description of its effects on parasite development and transmission potential.

Connection to Unanswered Questions: Establishes a clear "what it does" map that the mechanistic and resistance studies build on.

Aim 2: Investigate the mechanism of action of PRC1584.

Rationale: Morphological data and biochemical assays suggest that PRC1584 interferes with hemoglobin trafficking, heme release, and cytostome function. These processes are essential for parasite survival but remain underexploited as drug targets. Understanding PRC1584's effects on these pathways will clarify its novelty and therapeutic potential.

Approach: Fractionation assays, biochemical measurements of heme/hemozoin, and electron microscopy were used to define how PRC1584 impacts hemoglobin metabolism and cytostome architecture.

Connection to Unanswered Questions: This aim addresses uncertainty surrounding PRC1584's MOA and its unique relationship to hemoglobin utilization.

Aim 3: Develop chemoproteomic tools and workflows to enable future identification of PRC1584 targets.

Rationale: The direct molecular target is still unidentified. Standard methods have not yielded resistant mutants, and K13 C580Y displays collateral sensitivity, consequently objective target discovery in *P. falciparum* is important but challenging.

Approach: Design and validate a β-carboline photoaffinity probe; optimize UV crosslinking, Copper(I)-catalyzed Azide–Alkyne Cycloaddition (CuAAC) biotin-tagging, and streptavidin-based detection; establish sample preparation workflows that are compatible with downstream mass spectrometry analysis.

Connection to Unanswered Questions: Provides a validated toolkit designed to enable future research to demonstrate target engagement and identify prospective molecular targets.

Together, these aims connect phenotypic definition (Aim 1) with pathway localization (Aim 2) and technical capacity for target discovery (Aim 3). The result is a mechanistic framework for PRC1584 and a set of methods that can accelerate next-generation antimalarial discovery.

REFERENCES

(1) Organization, W. H. *World malaria report 2024: addressing inequity in the global malaria response.* ; 2024.
(2) Mezieobi, K. C.; Alum, E. U.; Ugwu, O. P.; Uti, D. E.; Alum, B. N.; Egba, S. I.; Ewah, C. M. Economic burden of malaria on developing countries: A mini review. *Parasite Epidemiol Control* **2025**, *30*, e00435. DOI: 10.1016/j.parepi.2025.e00435 From NLM PubMed-not-MEDLINE.
(3) Shretta, R.; Avancena, A. L.; Hatefi, A. The economics of malaria control and elimination: a systematic review. *Malar J* **2016**, *15* (1), 593. DOI: 10.1186/s12936-016-1635-5 From NLM Medline.
(4) Bhatt, S.; Weiss, D. J.; Cameron, E.; Bisanzio, D.; Mappin, B.; Dalrymple, U.; Battle, K.; Moyes, C. L.; Henry, A.; Eckhoff, P. A.; et al. The effect of malaria control on Plasmodium falciparum in Africa between 2000 and 2015. *Nature* **2015**, *526* (7572), 207–211. DOI: 10.1038/nature15535 From NLM.
(5) Phillips, M. A.; Burrows, J. N.; Manyando, C.; van Huijsduijnen, R. H.; Van Voorhis, W. C.; Wells, T. N. C. Malaria. *Nat Rev Dis Primers* **2017**, *3*, 17050. DOI: 10.1038/nrdp.2017.50 From NLM Medline.
(6) Li, Q.; Liu, T.; Lv, K.; Liao, F.; Wang, J.; Tu, Y.; Chen, Q. Malaria: past, present, and future. *Signal Transduct Target Ther* **2025**, *10* (1), 188. DOI: 10.1038/s41392-025-02246-3 From NLM Medline.
(7) Rosenthal, P. J.; Asua, V.; Conrad, M. D. Emergence, transmission dynamics and mechanisms of artemisinin partial resistance in malaria parasites in Africa. *Nature Reviews Microbiology* **2024**, *22* (6), 373–384. DOI: 10.1038/s41579-024-01008-2.
(8) Loubens, M.; Vincensini, L.; Fernandes, P.; Briquet, S.; Marinach, C.; Silvie, O. Plasmodium sporozoites on the move: Switching from cell traversal to productive invasion of hepatocytes. *Mol Microbiol* **2021**, *115* (5), 870–881. DOI: 10.1111/mmi.14645 From NLM.
(9) White, N. J.; Pukrittayakamee, S.; Hien, T. T.; Faiz, M. A.; Mokuolu, O. A.; Dondorp, A. M. Malaria. *Lancet* **2014**, *383* (9918), 723–735. DOI: 10.1016/s0140-6736(13)60024-0 From NLM.
(10) Armstrong, J. F.; Campo, B.; Alexander, S. P. H.; Arendse, L. B.; Cheng, X.; Davenport, A. P.; Faccenda, E.; Fidock, D. A.; Godinez-Macias, K. P.; Harding, S. D.; et al. Advances in malaria pharmacology and the online guide to MALARIA PHARMACOLOGY: IUPHAR review 38. *Br J Pharmacol* **2023**, *180* (15), 1899–1929. DOI: 10.1111/bph.16144 From NLM.
(11) Wu, R. L.; Idris, A. H.; Berkowitz, N. M.; Happe, M.; Gaudinski, M. R.; Buettner, C.; Strom, L.; Awan, S. F.; Holman, L. A.; Mendoza, F.; et al. Low-Dose Subcutaneous or Intravenous Monoclonal Antibody to Prevent Malaria. *N Engl J Med* **2022**, *387* (5), 397–407. DOI: 10.1056/NEJMoa2203067 From NLM.
(12) Draper, S. J.; Sack, B. K.; King, C. R.; Nielsen, C. M.; Rayner, J. C.; Higgins, M. K.; Long, C. A.; Seder, R. A. Malaria Vaccines: Recent Advances and New Horizons. *Cell Host Microbe* **2018**, *24* (1), 43–56. DOI: 10.1016/j.chom.2018.06.008 From NLM.
(13) Combrinck, J. M.; Mabotha, T. E.; Ncokazi, K. K.; Ambele, M. A.; Taylor, D.; Smith, P. J.; Hoppe, H. C.; Egan, T. J. Insights into the role of heme in the mechanism of action of antimalarials. *ACS Chem Biol* **2013**, *8* (1), 133–137. DOI: 10.1021/cb300454t From NLM.
(14) Cowman, A. F.; Healer, J.; Marapana, D.; Marsh, K. Malaria: Biology and Disease. *Cell* **2016**, *167* (3), 610–624. DOI: 10.1016/j.cell.2016.07.055 From NLM Medline.
(15) Birnbaum, J.; Scharf, S.; Schmidt, S.; Jonscher, E.; Hoeijmakers, W. A. M.; Flemming, S.; Toenhake, C. G.; Schmitt, M.; Sabitzki, R.; Bergmann, B.; et al. A Kelch13-defined endocytosis

pathway mediates artemisinin resistance in malaria parasites. *Science* **2020**, *367* (6473), 51–59. DOI: 10.1126/science.aax4735 From NLM Medline.
(16) Olafson, K. N.; Ketchum, M. A.; Rimer, J. D.; Vekilov, P. G. Mechanisms of hematin crystallization and inhibition by the antimalarial drug chloroquine. *Proc Natl Acad Sci U S A* **2015**, *112* (16), 4946–4951. DOI: 10.1073/pnas.1501023112 From NLM.
(17) Collins, C. R.; Hackett, F.; Strath, M.; Penzo, M.; Withers-Martinez, C.; Baker, D. A.; Blackman, M. J. Malaria parasite cGMP-dependent protein kinase regulates blood stage merozoite secretory organelle discharge and egress. *PLoS Pathog* **2013**, *9* (5), e1003344. DOI: 10.1371/journal.ppat.1003344 From NLM.
(18) Owalla, T. J.; Okurut, E.; Apungia, G.; Ojakol, B.; Lema, J.; C. Murphy, S.; G. Egwang, T. Using the Ultrasensitive Alere Plasmodium falciparum Malaria Ag HRP-2™ Rapid Diagnostic Test in the Field and Clinic in Northeastern Uganda. *The American Journal of Tropical Medicine and Hygiene* **2020**, *103* (2), 778–784. DOI: 10.4269/ajtmh.19-0653.
(19) Burrows, J. N.; Duparc, S.; Gutteridge, W. E.; Hooft van Huijsduijnen, R.; Kaszubska, W.; Macintyre, F.; Mazzuri, S.; Mohrle, J. J.; Wells, T. N. C. New developments in anti-malarial target candidate and product profiles. *Malar J* **2017**, *16* (1), 26. DOI: 10.1186/s12936-016-1675-x From NLM Medline.
(20) Witkowski, B.; Amaratunga, C.; Khim, N.; Sreng, S.; Chim, P.; Kim, S.; Lim, P.; Mao, S.; Sopha, C.; Sam, B.; et al. Novel phenotypic assays for the detection of artemisinin-resistant Plasmodium falciparum malaria in Cambodia: in-vitro and ex-vivo drug-response studies. *Lancet Infect Dis* **2013**, *13* (12), 1043–1049. DOI: 10.1016/S1473-3099(13)70252-4 From NLM Medline.
(21) Patra, A. T.; Hingamire, T.; Belekar, M. A.; Xiong, A.; Subramanian, G.; Bozdech, Z.; Preiser, P.; Shanmugam, D.; Chandramohanadas, R. Whole-Cell Phenotypic Screening of Medicines for Malaria Venture Pathogen Box Identifies Specific Inhibitors of Plasmodium falciparum Late-Stage Development and Egress. *Antimicrob Agents Chemother* **2020**, *64* (5). DOI: 10.1128/aac.01802-19 From NLM.
(22) Delves, M. J.; Miguel-Blanco, C.; Matthews, H.; Molina, I.; Ruecker, A.; Yahiya, S.; Straschil, U.; Abraham, M.; León, M. L.; Fischer, O. J.; et al. A high throughput screen for next-generation leads targeting malaria parasite transmission. *Nature Communications* **2018**, *9* (1), 3805. DOI: 10.1038/s41467-018-05777-2.
(23) Appetecchia, F.; Fabbrizi, E.; Fiorentino, F.; Consalvi, S.; Biava, M.; Poce, G.; Rotili, D. Transmission-Blocking Strategies for Malaria Eradication: Recent Advances in Small-Molecule Drug Development. *Pharmaceuticals (Basel)* **2024**, *17* (7). DOI: 10.3390/ph17070962 From NLM.
(24) Joice, R.; Nilsson, S. K.; Montgomery, J.; Dankwa, S.; Egan, E.; Morahan, B.; Seydel, K. B.; Bertuccini, L.; Alano, P.; Williamson, K. C.; et al. Plasmodium falciparum transmission stages accumulate in the human bone marrow. *Sci Transl Med* **2014**, *6* (244), 244re245. DOI: 10.1126/scitranslmed.3008882 From NLM.
(25) Yang, T.; Ottilie, S.; Istvan, E. S.; Godinez-Macias, K. P.; Lukens, A. K.; Baragana, B.; Campo, B.; Walpole, C.; Niles, J. C.; Chibale, K.; et al. MalDA, Accelerating Malaria Drug Discovery. *Trends Parasitol* **2021**, *37* (6), 493–507. DOI: 10.1016/j.pt.2021.01.009 From NLM Medline.
(26) Auparakkitanon, S.; Wilairat, P. Ring stage dormancy of Plasmodium falciparum tolerant to artemisinin and its analogues – A genetically regulated "Sleeping Beauty". *International Journal*

for Parasitology: Drugs and Drug Resistance **2023**, *21*, 61–64. DOI: https://doi.org/10.1016/j.ijpddr.2023.01.002.
(27) Tripathi, J.; Stoklasa, M.; Nayak, S.; En Low, K.; Qian Hui Lee, E.; Duong Tien, Q. H.; Renia, L.; Malleret, B.; Bozdech, Z. The artemisinin-induced dormant stages of Plasmodium falciparum exhibit hallmarks of cellular quiescence/senescence and drug resilience. *Nat Commun* **2024**, *15* (1), 7485. DOI: 10.1038/s41467-024-51846-0 From NLM Medline.
(28) Oyegbade, S. A.; Mameh, E. O.; Balogun, D. O.; Aririguzoh, V. O.; Akinduti, P. A. Emerging Plasmodium falciparum K13 gene mutation to artemisinin-based combination therapies and partner drugs among malaria-infected population in sub-Saharan Africa. *Parasites Hosts Dis* **2025**, *63* (2), 109–122. DOI: 10.3347/PHD.24053 From NLM Medline.
(29) Noedl, H.; Se, Y.; Schaecher, K.; Smith, B. L.; Socheat, D.; Fukuda, M. M. Evidence of artemisinin-resistant malaria in western Cambodia. *N Engl J Med* **2008**, *359* (24), 2619–2620. DOI: 10.1056/NEJMc0805011 From NLM.
(30) Paloque, L.; Ramadani, A. P.; Mercereau-Puijalon, O.; Augereau, J. M.; Benoit-Vical, F. Plasmodium falciparum: multifaceted resistance to artemisinins. *Malar J* **2016**, *15*, 149. DOI: 10.1186/s12936-016-1206-9 From NLM Medline.
(31) Teuscher, F.; Gatton, M. L.; Chen, N.; Peters, J.; Kyle, D. E.; Cheng, Q. Artemisinin-induced dormancy in plasmodium falciparum: duration, recovery rates, and implications in treatment failure. *J Infect Dis* **2010**, *202* (9), 1362–1368. DOI: 10.1086/656476 From NLM Medline.
(32) Stepniewska, K.; Allen, E. N.; Humphreys, G. S.; Poirot, E.; Craig, E.; Kennon, K.; Yilma, D.; Bousema, T.; Guerin, P. J.; White, N. J.; et al. Safety of single-dose primaquine as a Plasmodium falciparum gametocytocide: a systematic review and meta-analysis of individual patient data. *BMC Med* **2022**, *20* (1), 350. DOI: 10.1186/s12916-022-02504-z From NLM.
(33) Woodward, R. B.; Doering, W. E. The Total Synthesis of Quinine. *Journal of the American Chemical Society* **1945**, *67* (5), 860–874. DOI: 10.1021/ja01221a051.
(34) Kaufman, T. S.; Ruveda, E. A. The quest for quinine: those who won the battles and those who won the war. *Angew Chem Int Ed Engl* **2005**, *44* (6), 854–885. DOI: 10.1002/anie.200400663 From NLM Medline.
(35) Achan, J.; Talisuna, A. O.; Erhart, A.; Yeka, A.; Tibenderana, J. K.; Baliraine, F. N.; Rosenthal, P. J.; D'Alessandro, U. Quinine, an old anti-malarial drug in a modern world: role in the treatment of malaria. *Malar J* **2011**, *10*, 144. DOI: 10.1186/1475-2875-10-144 From NLM Medline.
(36) Wellems, T. E.; Plowe, C. V. Chloroquine-resistant malaria. *J Infect Dis* **2001**, *184* (6), 770–776. DOI: 10.1086/322858 From NLM Medline.
(37) Rasmussen, C.; Alonso, P.; Ringwald, P. Current and emerging strategies to combat antimalarial resistance. *Expert Rev Anti Infect Ther* **2022**, *20* (3), 353–372. DOI: 10.1080/14787210.2021.1962291 From NLM Medline.
(38) Triglia, T.; Menting, J. G.; Wilson, C.; Cowman, A. F. Mutations in dihydropteroate synthase are responsible for sulfone and sulfonamide resistance in Plasmodium falciparum. *Proc Natl Acad Sci U S A* **1997**, *94* (25), 13944–13949. DOI: 10.1073/pnas.94.25.13944 From NLM Medline.
(39) Aubouy, A.; Jafari, S.; Huart, V.; Migot-Nabias, F.; Mayombo, J.; Durand, R.; Bakary, M.; Le Bras, J.; Deloron, P. DHFR and DHPS genotypes of Plasmodium falciparum isolates from Gabon correlate with in vitro activity of pyrimethamine and cycloguanil, but not with

sulfadoxine-pyrimethamine treatment efficacy. *J Antimicrob Chemother* **2003**, *52* (1), 43–49. DOI: 10.1093/jac/dkg294 From NLM Medline.
(40) Peterson, D. S.; Walliker, D.; Wellems, T. E. Evidence that a point mutation in dihydrofolate reductase-thymidylate synthase confers resistance to pyrimethamine in falciparum malaria. *Proc Natl Acad Sci U S A* **1988**, *85* (23), 9114–9118. DOI: 10.1073/pnas.85.23.9114 From NLM Medline.
(41) Eastman, R. T.; Fidock, D. A. Artemisinin-based combination therapies: a vital tool in efforts to eliminate malaria. *Nat Rev Microbiol* **2009**, *7* (12), 864–874. DOI: 10.1038/nrmicro2239 From NLM.
(42) Thellier, M.; Gemegah, A. A. J.; Tantaoui, I. Global Fight against Malaria: Goals and Achievements 1900-2022. *J Clin Med* **2024**, *13* (19). DOI: 10.3390/jcm13195680 From NLM PubMed-not-MEDLINE.
(43) Wang, J.; Zhang, C. J.; Chia, W. N.; Loh, C. C.; Li, Z.; Lee, Y. M.; He, Y.; Yuan, L. X.; Lim, T. K.; Liu, M.; et al. Haem-activated promiscuous targeting of artemisinin in Plasmodium falciparum. *Nat Commun* **2015**, *6*, 10111. DOI: 10.1038/ncomms10111 From NLM.
(44) Klonis, N.; Crespo-Ortiz, M. P.; Bottova, I.; Abu-Bakar, N.; Kenny, S.; Rosenthal, P. J.; Tilley, L. Artemisinin activity against Plasmodium falciparum requires hemoglobin uptake and digestion. *Proc Natl Acad Sci U S A* **2011**, *108* (28), 11405–11410. DOI: 10.1073/pnas.1104063108 From NLM Medline.
(45) Murithi, J. M.; Owen, E. S.; Istvan, E. S.; Lee, M. C. S.; Ottilie, S.; Chibale, K.; Goldberg, D. E.; Winzeler, E. A.; Llinas, M.; Fidock, D. A.; et al. Combining Stage Specificity and Metabolomic Profiling to Advance Antimalarial Drug Discovery. *Cell Chem Biol* **2020**, *27* (2), 158–171 e153. DOI: 10.1016/j.chembiol.2019.11.009.
(46) Hanboonkunupakarn, B.; Tarning, J.; Pukrittayakamee, S.; Chotivanich, K. Artemisinin resistance and malaria elimination: Where are we now? *Front Pharmacol* **2022**, *13*, 876282. DOI: 10.3389/fphar.2022.876282 From NLM PubMed-not-MEDLINE.
(47) Rosenthal, M. R.; Ng, C. L. Plasmodium falciparum Artemisinin Resistance: The Effect of Heme, Protein Damage, and Parasite Cell Stress Response. *ACS Infect Dis* **2020**, *6* (7), 1599–1614. DOI: 10.1021/acsinfecdis.9b00527 From NLM.
(48) Rahman, A.; Tamseel, S.; Dutta, S.; Khan, N.; Faaiz, M.; Rastogi, H.; Nath, J. R.; Haldar, K.; Chowdhury, P.; Ashish; et al. Artemisinin-resistant Plasmodium falciparum Kelch13 mutant proteins display reduced heme-binding affinity and decreased artemisinin activation. *Communications Biology* **2024**, *7* (1), 1499. DOI: 10.1038/s42003-024-07178-2.
(49) Mok, S.; Ashley, E. A.; Ferreira, P. E.; Zhu, L.; Lin, Z.; Yeo, T.; Chotivanich, K.; Imwong, M.; Pukrittayakamee, S.; Dhorda, M.; et al. Drug resistance. Population transcriptomics of human malaria parasites reveals the mechanism of artemisinin resistance. *Science* **2015**, *347* (6220), 431–435. DOI: 10.1126/science.1260403 From NLM Medline.
(50) Ward, K. E.; Fidock, D. A.; Bridgford, J. L. Plasmodium falciparum resistance to artemisinin-based combination therapies. *Curr Opin Microbiol* **2022**, *69*, 102193. DOI: 10.1016/j.mib.2022.102193 From NLM.
(51) Birnbaum, J.; Flemming, S.; Reichard, N.; Soares, A. B.; Mesén-Ramírez, P.; Jonscher, E.; Bergmann, B.; Spielmann, T. A genetic system to study Plasmodium falciparum protein function. *Nature Methods* **2017**, *14* (4), 450–456. DOI: 10.1038/nmeth.4223.
(52) Waring, M. J.; Arrowsmith, J.; Leach, A. R.; Leeson, P. D.; Mandrell, S.; Owen, R. M.; Pairaudeau, G.; Pennie, W. D.; Pickett, S. D.; Wang, J.; et al. An analysis of the attrition of drug

candidates from four major pharmaceutical companies. *Nat Rev Drug Discov* **2015**, *14* (7), 475–486. DOI: 10.1038/nrd4609 From NLM Medline.
(53) DiMasi, J. A.; Grabowski, H. G.; Hansen, R. W. Innovation in the pharmaceutical industry: New estimates of R&D costs. *J Health Econ* **2016**, *47*, 20–33. DOI: 10.1016/j.jhealeco.2016.01.012 From NLM.
(54) Paul, S. M.; Mytelka, D. S.; Dunwiddie, C. T.; Persinger, C. C.; Munos, B. H.; Lindborg, S. R.; Schacht, A. L. How to improve R&D productivity: the pharmaceutical industry's grand challenge. *Nature Reviews Drug Discovery* **2010**, *9* (3), 203–214. DOI: 10.1038/nrd3078.
(55) Keseru, G. M.; Makara, G. M. The influence of lead discovery strategies on the properties of drug candidates. *Nat Rev Drug Discov* **2009**, *8* (3), 203–212. DOI: 10.1038/nrd2796 From NLM Medline.
(56) Leeson, P. D.; Springthorpe, B. The influence of drug-like concepts on decision-making in medicinal chemistry. *Nat Rev Drug Discov* **2007**, *6* (11), 881–890. DOI: 10.1038/nrd2445 From NLM Medline.
(57) Katsuno, K.; Burrows, J. N.; Duncan, K.; Hooft van Huijsduijnen, R.; Kaneko, T.; Kita, K.; Mowbray, C. E.; Schmatz, D.; Warner, P.; Slingsby, B. T. Hit and lead criteria in drug discovery for infectious diseases of the developing world. *Nat Rev Drug Discov* **2015**, *14* (11), 751–758. DOI: 10.1038/nrd4683 From NLM Medline.
(58) Hughes, J. P.; Rees, S.; Kalindjian, S. B.; Philpott, K. L. Principles of early drug discovery. *Br J Pharmacol* **2011**, *162* (6), 1239–1249. DOI: 10.1111/j.1476-5381.2010.01127.x From NLM.
(59) Lipinski, C. A. Lead- and drug-like compounds: the rule-of-five revolution. *Drug Discovery Today: Technologies* **2004**, *1* (4), 337–341. DOI: https://doi.org/10.1016/j.ddtec.2004.11.007.
(60) Pammolli, F.; Magazzini, L.; Riccaboni, M. The productivity crisis in pharmaceutical R&D. *Nature Reviews Drug Discovery* **2011**, *10* (6), 428–438. DOI: 10.1038/nrd3405.
(61) Okombo, J.; Fidock, D. A. Towards next-generation treatment options to combat Plasmodium falciparum malaria. *Nature Reviews Microbiology* **2025**, *23* (3), 178–191. DOI: 10.1038/s41579-024-01099-x.
(62) Burrows, J. N.; Hooft van Huijsduijnen, R.; Möhrle, J. J.; Oeuvray, C.; Wells, T. N. C. Designing the next generation of medicines for malaria control and eradication. *Malaria Journal* **2013**, *12* (1), 187. DOI: 10.1186/1475-2875-12-187.
(63) Corey, V. C.; Lukens, A. K.; Istvan, E. S.; Lee, M. C. S.; Franco, V.; Magistrado, P.; Coburn-Flynn, O.; Sakata-Kato, T.; Fuchs, O.; Gnädig, N. F.; et al. A broad analysis of resistance development in the malaria parasite. *Nature Communications* **2016**, *7* (1), 11901. DOI: 10.1038/ncomms11901.
(64) Forte, B.; Ottilie, S.; Plater, A.; Campo, B.; Dechering, K. J.; Gamo, F. J.; Goldberg, D. E.; Istvan, E. S.; Lee, M.; Lukens, A. K.; et al. Prioritization of Molecular Targets for Antimalarial Drug Discovery. *ACS Infectious Diseases* **2021**, *7* (10), 2764–2776. DOI: 10.1021/acsinfecdis.1c00322.
(65) Gamo, F.-J.; Sanz, L. M.; Vidal, J.; de Cozar, C.; Alvarez, E.; Lavandera, J.-L.; Vanderwall, D. E.; Green, D. V. S.; Kumar, V.; Hasan, S.; et al. Thousands of chemical starting points for antimalarial lead identification. *Nature* **2010**, *465* (7296), 305–310. DOI: 10.1038/nature09107.
(66) Yipsirimetee, A.; Chiewpoo, P.; Tripura, R.; Lek, D.; Day, N. P. J.; Dondorp, A. M.; Pukrittayakamee, S.; White, N. J.; Chotivanich, K. Assessment In Vitro of the Antimalarial and Transmission-Blocking Activities of Cipargamin and Ganaplacide in Artemisinin-Resistant

Plasmodium falciparum. *Antimicrob Agents Chemother* **2022**, *66* (3), e0148121. DOI: 10.1128/aac.01481-21 From NLM.
(67) Baragaña, B.; Hallyburton, I.; Lee, M. C. S.; Norcross, N. R.; Grimaldi, R.; Otto, T. D.; Proto, W. R.; Blagborough, A. M.; Meister, S.; Wirjanata, G.; et al. A novel multiple-stage antimalarial agent that inhibits protein synthesis. *Nature* **2015**, *522* (7556), 315–320. DOI: 10.1038/nature14451.
(68) Siqueira-Neto, J. L.; Wicht, K. J.; Chibale, K.; Burrows, J. N.; Fidock, D. A.; Winzeler, E. A. Antimalarial drug discovery: progress and approaches. *Nat Rev Drug Discov* **2023**, *22* (10), 807–826. DOI: 10.1038/s41573-023-00772-9 From NLM.
(69) Cowell, A. N.; Winzeler, E. A. The genomic architecture of antimalarial drug resistance. *Brief Funct Genomics* **2019**, *18* (5), 314–328. DOI: 10.1093/bfgp/elz008 From NLM.
(70) Carolino, K.; Winzeler, E. A. The antimalarial resistome – finding new drug targets and their modes of action. *Current Opinion in Microbiology* **2020**, *57*, 49–55. DOI: https://doi.org/10.1016/j.mib.2020.06.004.
(71) Dziekan, J. M.; Wirjanata, G.; Dai, L.; Go, K. D.; Yu, H.; Lim, Y. T.; Chen, L.; Wang, L. C.; Puspita, B.; Prabhu, N.; et al. Cellular thermal shift assay for the identification of drug–target interactions in the Plasmodium falciparum proteome. *Nature Protocols* **2020**, *15* (6), 1881–1921. DOI: 10.1038/s41596-020-0310-z.
(72) Giannangelo, C.; Challis, M. P.; Siddiqui, G.; Edgar, R.; Malcolm, T. R.; Webb, C. T.; Drinkwater, N.; Vinh, N.; Macraild, C.; Counihan, N.; et al. Chemoproteomics validates selective targeting of Plasmodium M1 alanyl aminopeptidase as an antimalarial strategy. *eLife* **2024**, *13*, RP92990. DOI: 10.7554/eLife.92990.
(73) Broichhagen, J.; Kilian, N. Chemical Biology Tools To Investigate Malaria Parasites. *Chembiochem* **2021**, *22* (13), 2219–2236. DOI: 10.1002/cbic.202000882 From NLM Medline.
(74) Iacobucci, I.; Monaco, V.; Hovasse, A.; Dupouy, B.; Keumoe, R.; Cichocki, B.; Elhabiri, M.; Meunier, B.; Strub, J. M.; Monti, M.; et al. Proteomic Profiling of Antimalarial Plasmodione Using 3-Benz(o)ylmenadione Affinity-Based Probes. *Chembiochem* **2024**, *25* (15), e202400187. DOI: 10.1002/cbic.202400187 From NLM.
(75) Lindblom, J. C. R.; Zhang, X.; Lehane, A. M. A pH Fingerprint Assay to Identify Inhibitors of Multiple Validated and Potential Antimalarial Drug Targets. *ACS Infectious Diseases* **2024**, *10* (4), 1185–1200. DOI: 10.1021/acsinfecdis.3c00588.
(76) Mathew, J.; Ding, S.; Kunz, K. A.; Stacy, E. E.; Butler, J. H.; Haney, R. S.; Merino, E. F.; Butschek, G. J.; Rizopoulos, Z.; Totrov, M.; et al. Malaria Box-Inspired Discovery of N-Aminoalkyl-beta-carboline-3-carboxamides, a Novel Orally Active Class of Antimalarials. *ACS Med Chem Lett* **2022**, *13* (3), 365–370. DOI: 10.1021/acsmedchemlett.1c00663.
(77) Mathew, J.; Zhou, B.; Haney, R. S.; Kunz, K. A.; Do Amaral, L. S.; Roy Chowdhury, R.; Butler, J. H.; Li, H.; Chakraborty, A. J.; Tabassum, A.; et al. beta-Carboline-3-carboxamide Antimalarials: Structure-Activity Relationship, ADME-Tox Studies, and Resistance Profiling. *ACS Infect Dis* **2024**, *10* (11), 3951–3962. DOI: 10.1021/acsinfecdis.4c00653 From NLM Medline.
(78) Balevic, S. J.; Raja, S. M.; Randell, R.; Deye, G. A.; Conrad, T.; Nakamura, A.; Peyton, D. H.; Shotwell, S.; Liebman, K.; Cohen-Wolkowiez, M.; et al. Adverse Reactions in a Phase 1 Trial of the Anti-Malarial DM1157: An Example of Pharmacokinetic Modeling and Simulation Guiding Clinical Trial Decisions. *Infect Dis Ther* **2022**, *11* (2), 841–852. DOI: 10.1007/s40121-022-00605-z From NLM.

(79) Fisher, N.; Abd Majid, R.; Antoine, T.; Al-Helal, M.; Warman, A. J.; Johnson, D. J.; Lawrenson, A. S.; Ranson, H.; O'Neill, P. M.; Ward, S. A.; et al. Cytochrome b mutation Y268S conferring atovaquone resistance phenotype in malaria parasite results in reduced parasite bc1 catalytic turnover and protein expression. *J Biol Chem* **2012**, *287* (13), 9731–9741. DOI: 10.1074/jbc.M111.324319 From NLM.
(80) White, N. J. Cardiotoxicity of antimalarial drugs. *Lancet Infect Dis* **2007**, *7* (8), 549–558. DOI: 10.1016/s1473-3099(07)70187-1 From NLM.
(81) Behrens, H. M.; Schmidt, S.; Henshall, I. G.; López-Barona, P.; Peigney, D.; Sabitzki, R.; May, J.; Maïga-Ascofaré, O.; Spielmann, T. Impact of different mutations on Kelch13 protein levels, ART resistance, and fitness cost in Plasmodium falciparum parasites. *mBio* **2024**, *15* (6), e0198123. DOI: 10.1128/mbio.01981-23 From NLM.
(82) Mbengue, A.; Bhattacharjee, S.; Pandharkar, T.; Liu, H.; Estiu, G.; Stahelin, R. V.; Rizk, S. S.; Njimoh, D. L.; Ryan, Y.; Chotivanich, K.; et al. A molecular mechanism of artemisinin resistance in Plasmodium falciparum malaria. *Nature* **2015**, *520* (7549), 683–687. DOI: 10.1038/nature14412 From NLM.
(83) Yang, T.; Yeoh, L. M.; Tutor, M. V.; Dixon, M. W.; McMillan, P. J.; Xie, S. C.; Bridgford, J. L.; Gillett, D. L.; Duffy, M. F.; Ralph, S. A.; et al. Decreased K13 Abundance Reduces Hemoglobin Catabolism and Proteotoxic Stress, Underpinning Artemisinin Resistance. *Cell Reports* **2019**, *29* (9), 2917–2928.e2915. DOI: 10.1016/j.celrep.2019.10.095 (accessed 2025/09/05).
(84) Theodoridis, L.; Carvalho, T. G. Antimalarial drug resistance and drug discovery: learning from the past to innovate the future. *Int J Parasitol Drugs Drug Resist* **2025**, *28*, 100602. DOI: 10.1016/j.ijpddr.2025.100602 From NLM Publisher.
(85) Carrasquilla, M.; Drammeh, N. F.; Rawat, M.; Sanderson, T.; Zenonos, Z.; Rayner, J. C.; Lee, M. C. S. Barcoding Genetically Distinct Plasmodium falciparum Strains for Comparative Assessment of Fitness and Antimalarial Drug Resistance. *mBio* **2022**, *13* (5), e0093722. DOI: 10.1128/mbio.00937-22 From NLM Medline.

CHAPTER 2

CHARACTERIZATION OF β-CARBOLINE DERIVATIVES REVEALS A HIGH BARRIER TO REISTANCE AND POTENT ACTIVITY AGAINST RING-STAGE AND DHA-INDUCED DORMANT *PLASMODIUM FALCIPARUM*

Haney, R.S., Butler, J.H., Wardlaw, L.A., Merino, E.F., Mendiola, V., Cooper, C.A., Mathew, J., Tumwebaze, P.K., Rosenthal, P.J., Cooper, R.A., Kyle, D.E., Rizopoulous, Z., Baud., D., Brand, S., Totrov, M., Carlier, P.R., Cassera, M.B. 2025. Accepted by ACS Infectious Disease.

Reprinted here with permission of publisher.

Abstract

Malaria, caused by *Plasmodium falciparum*, remains a major global health challenge, with an estimated 263 million new infections and 597,000 deaths annually. Increasing resistance to current antimalarial drugs underscores the urgent need for new therapeutics that target novel pathways in the parasite. We previously reported a novel class of β-carboline antimalarials, exemplified by PRC1584, which demonstrated a favorable oral pharmacokinetic profile, *in vivo* efficacy in *P. berghei*-infected mice, and no cross-resistance with other antimalarials in various *P. falciparum* strains. In this study, we demonstrate that PRC1584 exhibits a high resistance barrier and retains potent activity against fresh Ugandan *P. falciparum* isolates. PRC1584, along with its more potent analogue PRC1697, demonstrated strong *in vitro* potency against both actively proliferating ring stages and dihydroartemisinin-induced dormant stages. Additionally, our study demonstrated that the PfKelch13-C580Y mutation was associated with increased susceptibility to PRC1584, whereas the PfKelch13-R539T and Pfcoronin-R100K-E107V mutations were not associated with this effect. These findings underscore the therapeutic potential of this new "irresistible" compound class, support a possible novel mechanism of action, and suggest the future development of novel ACTs active against resistant parasites by targeting DHA-dormancy, an essential survival mechanism of *P. falciparum*.

Keywords: malaria, β-carbolines, collateral drug sensitivity, dormancy, kelch-13, irresistible

Malaria is a deadly disease caused by parasites of the genus *Plasmodium*, with *Plasmodium falciparum* being the deadliest of the human-infecting species. In 2023, an estimated 263 million malaria cases and 597,000 deaths were reported worldwide[1]. Despite considerable progress over the last two decades in the fight against malaria, the current trend indicates a standstill. Chemotherapy remains a cornerstone of malaria control alongside vector management, new vaccines, diagnosis, and prompt access to treatment[1]. However, declining clinical efficacy and rising resistance affect all currently used antimalarial drug classes, including artemisinin-based combination therapies (ACTs)[2], which pair fast-acting artemisinin derivatives with slower-acting antimalarial drugs and remain the first-line treatment for malaria[3].

Artemisinin partial resistance (ART-R) first emerged in the Greater Mekong subregion of Southeast Asia in 2008[4] and has since also emerged in Africa[5]. Clinically, ART-R is defined by a delay in parasite clearance following the initiation of an ACT regimen[1], and it is associated with reduced susceptibility in the early ring stages of the *P. falciparum* intraerythrocytic life cycle. This phenotype is assessed *in vitro* by the ring-stage survival assay ($RSA_{0\text{-}3\ h}$), which measures survival of early ring-stage parasites (0-3 h post-invasion) at 72 hours post incubation with 700 nM dihydroartemisinin (DHA) for 6 h. This assay identifies resistant parasites with a survival rate over 1%, compared to untreated controls[6]. Resistance to artemisinin is linked to single nucleotide polymorphisms (SNPs) in *pfkelch13* gene, which encodes Kelch13 protein (K13)[3]. Although the exact function of PfKelch13 remains unclear, it is known that it is involved in hemoglobin uptake and endocytosis[7], regulation of phosphatidylinositol-3-phosphate vesicles enriched with proteins involved in proteostasis[8], unfolded protein response (UPR), and redox stress mitigation[9]. Notably, many SNPs have been reported but the PfKelch13-C580Y and

R539T mutations are among the validated mutations strongly linked to ART-R [3], displaying elevated survival rates in the $RSA_{0\text{-}3\ h}$ assay[3, 10].

One survival mechanism in DHA-exposed parasites, regardless of their genetic background, is the temporary arrest of growth during the ring stage, known as dormancy[11, 12]. This is a phenomenon in which subpopulations of parasites, termed persisters, shutdown energy-related processes, and cease growth and proliferation[9]. Phenotypically, dormancy is characterized as small (pyknotic) parasites with condensed nuclei and a reduced cytoplasm. This dormancy allows parasites to tolerate treatment, increasing the risk of clinical failure as they can later resume proliferation, a process known as recrudescence[13]. A recent study showed that DHA-induced dormant parasites exhibit characteristics of cellular quiescence and senescence, meaning they temporarily halt growth and metabolic activity while maintaining viability[14]. This work also showed dormancy requires a five-day maturation process during which gene expression gradually shifts from a ring-like state to a unique pattern different from that observed in the intraerythrocytic asexual and sexual stages. This slow transcriptional shift contrasts with the quick morphological change to pyknotic forms that occurs within 24 hours, with parasites acquiring an irregular cellular ultrastructure, indicative of distinct biological characteristics. Therefore, the ability of malaria parasites to enter dormancy adds complexity to the challenge of developing novel antimalarials targeting the ring stage to the reduce pathogenesis and block transmission.

During ACT treatment, the artemisinin component has a short duration of efficacy resulting in rapid parasite clearance; the partner drug, which acts more slowly, has much longer duration of pharmacologically active concentrations[15]. With the spread of ART-R, having an effective partner drug that eliminates dormant parasites or remains in the bloodstream long

enough to kill parasites as they exit their DHA-induced dormant state to prevent recrudescence is crucial for the success of new ACTs[16].

We recently identified a new class of β-carboline antimalarials, exemplified by PRC1584, which demonstrated a favorable oral pharmacokinetic profile, *in vivo* efficacy in *Plasmodium berghei*-infected mice, and low cross-resistance with other antimalarials in both susceptible and drug-resistant *P. falciparum* strains[17]. Structure-activity relationship studies[18] revealed a preference for a 3,4-dichloro- or 3,4,5-trichlorophenyl ring, with the most potent analog, PRC1697 ($^{Dd2}EC_{50}$ = 54 ± 8 nM), exhibiting twice the potency of PRC1584 ($^{Dd2}EC_{50}$ = 108 ± 7 nM). Barcoded cross-resistance profiling confirmed no cross-resistance against 32 resistance mutations in the Dd2 background and 10 in the 3D7 background, strongly suggesting that compounds within this scaffold possess a novel mechanism of antimalarial action[18].

In this report, we describe a comprehensive evaluation of PRC1584 across key points of the parasite life cycle and its inability to select resistant parasites *in vitro*. Importantly, we demonstrate that PRC1584 is effective against both ring stages and DHA-induced dormant forms of *P. falciparum* parasites, regardless of their sensitivity or resistance to DHA. Together, these findings underscore the therapeutic potential of this "irresistible" β-carboline class of antimalarials that may act through a novel mechanism of action. The distinctive properties of this class provide opportunities for the advancement of innovative new combinations, including potentially future ACTs, particularly in the setting of ART-R, by specifically targeting DHA-induced dormancy, a critical survival strategy of *P. falciparum*.

Results

Activity of PRC1584 across the *Plasmodium falciparum* life cycle. In our first study, we identified PRC1584 ($^{Dd2}EC_{50}$ = 108 ± 7 nM) as the most potent analog among the new class of β-carbolines against asexual intraerythrocytic stages of *P. falciparum* (Figure 2.1A)[17]. Based on the promising activity of this early lead compound, we next tested PRC1584 against transmission and liver stages.

Potential transmission blocking activity was assessed by measuring the stage-specific action of PRC1584 against immature and mature *P. falciparum* gametocytes (MMV, University of Pretoria). Gametocytes were induced from the PfNF54-*pfs16*-GFP-luc reporter line. Drug assays began on day 5 with gametocytes at stage II/III (immature), and on day 13 with gametocytes at stage V (mature). In each case, parasites were exposed to PRC1584 at varying concentrations for 48 h. Micromolar activity was observed against immature (EC_{50} = 4.62 ± 0.09 μM) and mature gametocytes (EC_{50} = 8.0 ± 0.3 μM) (Figure 2.1B).

To further assess the potential for β-carbolines to block transmission, the viability of mature stage V gametocytes was evaluated by their ability to develop into male and female gametes (MMV, Imperial College London). Since mature stage V gametocytes exhibit sex-specific sensitivity to antimalarials, both sexes should be studied to better characterize compound transmission-blocking activity.[19] Therefore, compounds were incubated with mature stage V gametocytes for 48 h before inducing gamete formation by reducing the temperature and adding xanthurenic acid. Approximately 25 minutes post-induction, male gamete exflagellation was recorded and quantified using automated microscopy. Samples were then incubated at 26°C for an additional 24 hours, after which female gamete formation was assessed by live staining using a fluorophore-conjugated αPfs25 antibody specific for female gametes and quantified by

automated microscopy. PRC1584 exhibited similar potency against male (EC_{50} = 1.3 µM) and female gametes (EC_{50} = 2.5 µM, Figure 2.1C).

Finally, we assessed the potential of PRC1584 in inhibiting liver stage development of *P. berghei*. No inhibition was seen at concentrations up to 5 µM, with activity, but also toxicity to HepG2 cells observed at 10 µM (Figure 2.1D). Collectively, these results demonstrate that PRC1584 displays significant *in vitro* potency primarily during the asexual intraerythrocytic cycle, while exhibiting limited activity against gametocytes and liver-stage parasites.

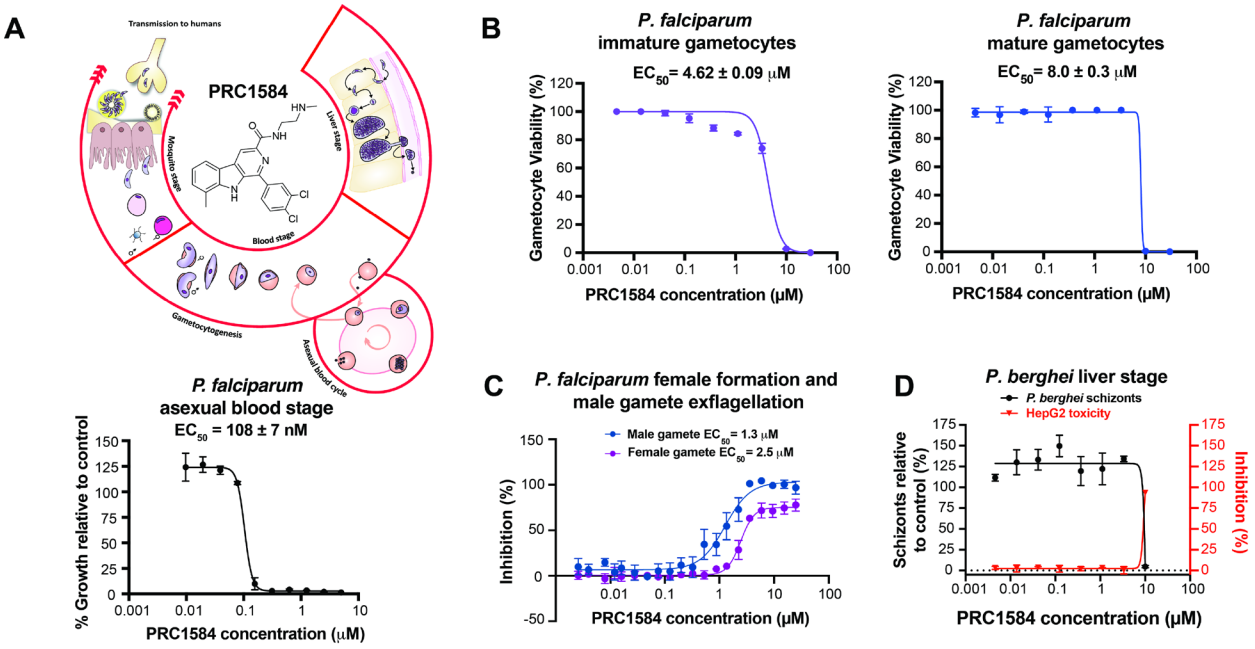

Figure 2.1. Antiplasmodial activity of PRC1584 throughout the *Plasmodium* parasite life cycle. **A)** Schematic representation of the *P. falciparum* life cycle and chemical structure of PRC1584. Dose-dependent activity of PRC1584 against *P. falciparum* Dd2 strain. **B)** Dose-dependent activity of PRC1584 against immature (stage II/III) and mature (stage V) *P. falciparum* gametocytes following 48 h of exposure. Data represent mean ± SEM from three independent biological replicates, each performed in technical triplicate. **C)** Assessment of the ability of *P. falciparum* stage V gametocytes to undergo gametogenesis after 48 h of dose-dependent exposure to PRC1584. Data represent mean from one biological replicate performed in technical triplicate. **D)** Dose-dependent activity of PRC1584 on *P. berghei* schizont development and HepG2 cell viability. Data represent mean from two biological replicates performed in technical duplicates. All x-axes are shown on a logarithmic scale.

PRC1584 retains potency against field isolates. We previously established that PRC1584 is not subject to known resistance mechanisms of several antimalarials, including chloroquine,

mefloquine, quinine, pyrimethamine, cycloguanil, sulfadoxine, KAE609, and dihydroartemisinin[17]. This lack of cross-reactivity was further confirmed using the Antimalarial Resistome Barcode Sequencing (AReBar) pooled-screening assay[18]. To determine whether resistance to PRC1584 is already present in parasites circulating in Africa, *ex vivo* sensitivity to PRC1584 was evaluated in fresh clinical isolates of *P. falciparum* obtained in Tororo, Uganda. At the time of these assays isolates in Tororo were generally susceptible to most standard antimalarial drugs (chloroquine, monodesethylamodiaquine, piperaquine, pyronaridine, lumefantrine, mefloquine, and DHA) but resistant to pyrimethamine[20].

Table S2.1. Summary of the *in vitro* potencies (EC_{50} values; nM) of PRC1584, PRC1967, and PRC1664 across various wild-type strains and mutants at different exposure times

	PRC1584			**PRC1697**			**PRC1664**			**DHA**		
	6 h (early ring)	**8 h (early ring)**	**72 h**	**6 h (early ring)**	**8 h (early ring)**	**72 h**	**6 h (early ring)**	**8 h (early ring)**	**72 h**	**6 h (early ring)**	**8 h (early ring)**	**72 h**
3D7		740 ± 60	67 ± 5									3.0 ± 0.3
Dd2*			182 ± 18							10 ± 0.4		4.3
Dd2-R539T	1950 ± 610		188 ± 17							11 ± 2		4.2
Dd2**	1630 ± 170	696 ± 62	114 ± 9			54 ± 8			211 ± 41		3.0 ± 0.2	2.02 ± 0.02
4G-K13-C580Y		211 ± 55	66 ± 35								7.7 ± 1.1	3.9 ± 0.2
W2			100 ± 8									4.7 ± 1.3
NF54	987 ± 64	476 ± 16	140 ± 15		102 ± 2	59 ± 5		1364	256	17.± 3	10 ± 2	7 ± 1
NF54-K13-C580Y	394 ± 51	200 ± 56	94 ± 13		70 ± 13	38 ± 4		675	182	17 ± 4	6 ± 2	5 ± 1

Pikine	530	753	77 ± 7		159	55				6	20	6 ± 1
Pikine-Pfcoronin-R100K-E107V	534	604	73 ± 6		116	37				23	20	6 ± 0.5

Assays comparing EC50 values across different parasite lines were performed concurrently.
(*) EC50 value obtained concomitant with that of Dd2-R539T.
(**) EC50 value obtained concomitant with that of 4G-K13-C580Y.
Gray cells indicate that EC50 values were not determined.
The mean and standard error of the mean (SEM) are presented for experiments conducted with two or more independent biological replicates.

The mean EC_{50} value for PRC1584 was found to be 70 nM, with a range of 26 to 177 nM (n = 31), which is consistent with potencies observed in laboratory strains (Figure 2.2, Table S2.1). The mean EC_{50} for DHA in these isolates was 1.8 nM, with a range of 0.5 - 4.4 nM while for chloroquine it was 17.2 nM with a range of 6.9 - 27 nM. Although these *ex vivo* results exhibited a 7-fold variation, which may be attributed to the complexity involved in assessing polyclonal isolates, all values remained within the low nanomolar range, suggesting that field isolates are consistently highly sensitive to PRC1584.

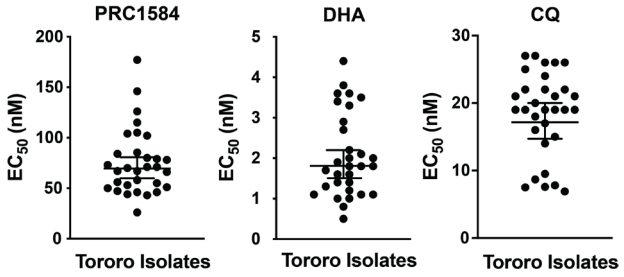

Figure 2.2 *Ex vivo* sensitivity to PRC1584 in fresh clinical isolates of *P. falciparum* obtained from Uganda (n = 31). Dose-response curves and EC_{50} values for PRC1584 (70 nM), DHA (1.8 nM) and chloroquine (CQ, 17.2 nM) were determined using a 72-hour SYBR Green I growth inhibition assay. Data points represent individual isolates; horizontal bars indicate mean EC_{50} values, and error bars represent the standard error of the mean (SEM).

PRC1584 is refractory to resistance selection *in vitro*. To gain further insight into the molecular targets or pathways that drive the significant antiplasmodial activity of PRC1584

against the asexual intraerythrocytic stages, we carried out multiple resistance selection protocols with the drug-sensitive *P. falciparum* 3D7 strain (Figure S2.1)[21-23].

Initially, a single step of resistance selection was performed by subjecting flasks containing an inoculum of 1 x 10^9 parasites to PRC1584 at a concentration of five times the EC_{50} value ($^{3D7\text{-clone}}EC_{50}$ = 67 ± 5 nM; Figure S2.2) for 14 days. In parallel, a flask treated with an equal volume of DMSO was used as the reference control. After the drug pressure was removed, cultures were monitored for 60 days.

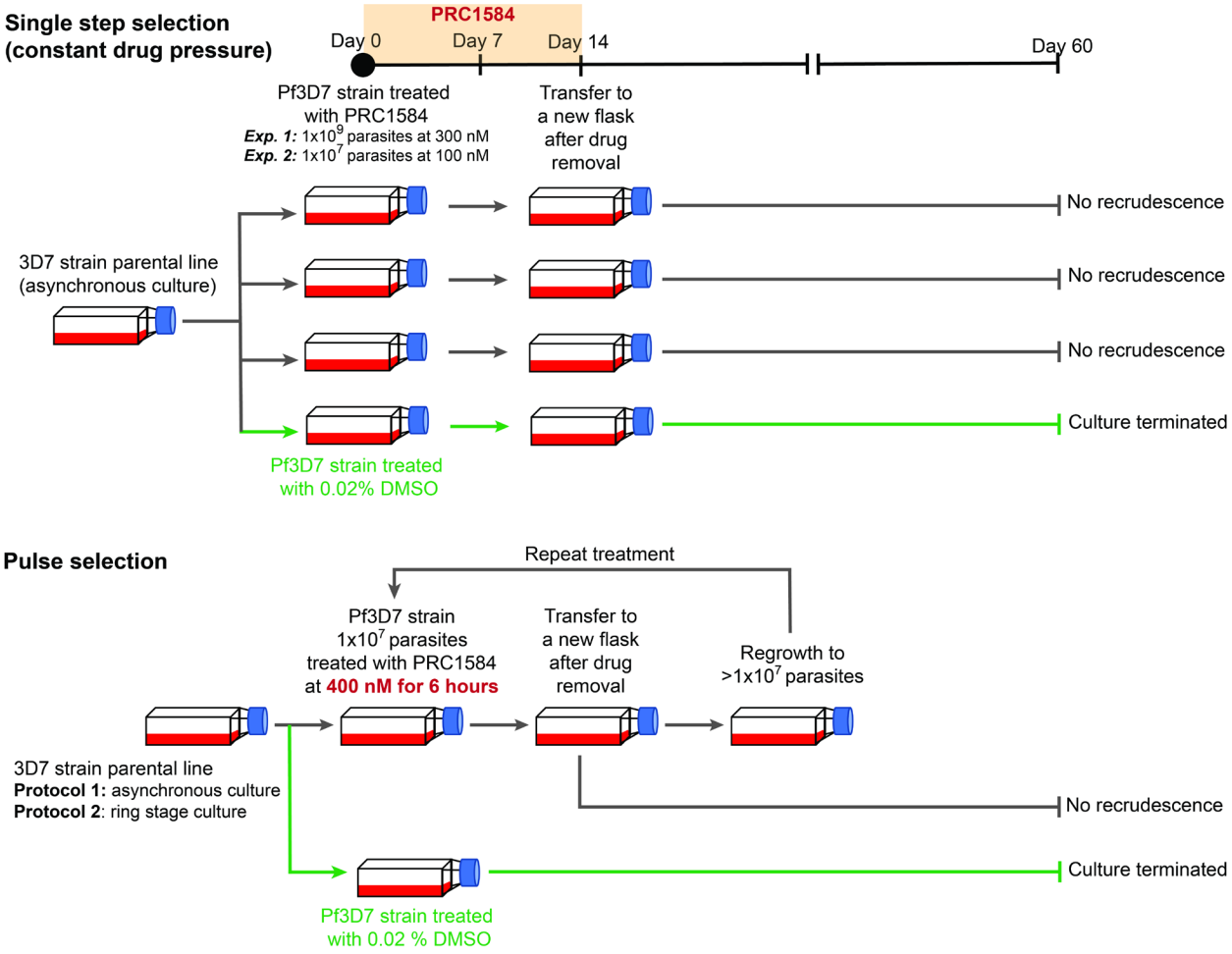

Figure S2.1. A schematic representation of the *in vitro* resistance selection methodologies employed is shown. Specific details regarding each approach are outlined in the methods section below.

A second single-step of resistance selection was performed using an inoculum of 1 x 10^7 parasites and a concentration of 100 nM for 14 days (Figure S2.2). After removing drug pressure, cultures were monitored for 60 days. In both conditions, parasite clearance occurred within the first four days, and no parasite recrudescence was observed. From these experiments, the minimum inoculum of resistance (MIR) was determined to be > 9 (i.e., >10^9 infected red blood cells).

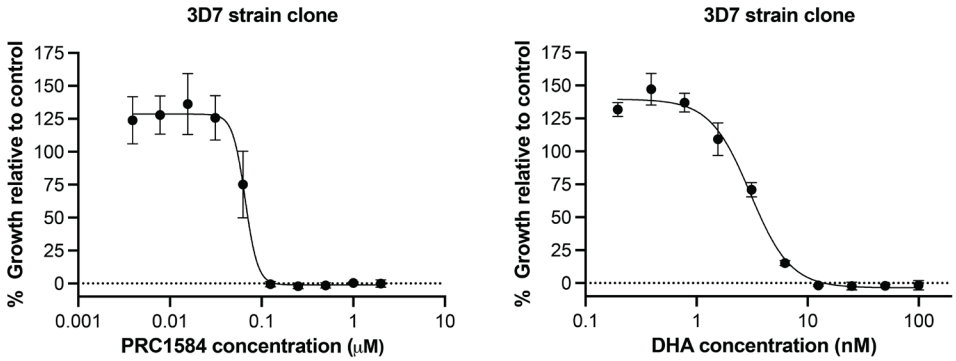

Figure S2.2 Dose-response curves for PRC1584 and DHA in the 3D7 strain clone (72 hours continuous exposure). Dose-dependent response curves for PRC1584 and DHA (control) were obtained using the *P. falciparum* 3D7 strain clone employed in resistance selection experiments. Data represent the mean from two independent biological replicates; each performed in technical duplicates. All x-axes are displayed in logarithmic scale.

These findings were further validated using the *P. falciparum* Dd2-B2 clone (EC_{50} = 69 nM and EC_{90} = 136 nM). Parasites were subjected to constant drug pressure for 60 days at three times the EC_{90} (408 nM). Parasite clearance occurred within the first four days, and no recrudescence was observed over 60 days. In contrast, with the control DSM265 tested in parallel at five times the EC_{50} value of 57 nM, 68/96 wells yielded recrudescent parasites (Log_{10} MIR = 5.45).

We also attempted resistance selection by pulsing parasites for six hours with eight times the 72 hours EC_{50} value of PRC1584 (400 nM), followed by drug removal to allow parasites to recover before repeating the pulse (Figure S2.1B)[23]. This approach involves exposing parasites to

elevated concentrations of the drug for a short period of time, resulting in the elimination of most parasites, followed by a drug-free period to enable the population recovery. The process of alternating drug exposure is continued until the parasites no longer responded to the treatment. The pulse-exposure method was performed with both highly synchronous rings (12-16 h post-invasion) and asynchronous cultures. Parasites re-emerged during each of the four drug pulse cycles over a 30-day period, but all cultures died after the fourth cycle, preventing further *in vitro* assessments of PRC1584 potency. Across all conditions tested, including prolonged drug pressure and repeated pulsed exposure, no parasites were recovered. These findings provide evidence that PRC1584 exhibits a high barrier for resistance.

PRC1584 is most active against late ring and early trophozoite stages. Our assessment across the *P. falciparum* life cycle revealed that PRC1584 exhibits significant activity primarily during the asexual intraerythrocytic cycle. To determine if PRC1584 targets specific stages within this cycle, we performed the asexual blood stage specificity inhibition assay described by Murithi and colleagues[24]. This assay also enables the identification of potential mechanisms of action for new antimalarial drugs by comparing their susceptibility profiles to those of established antimalarials. As shown in Figure 2.3, PRC1584 displayed enhanced potency against parasites in the late ring and early trophozoite stages. Strikingly, an 8-hour exposure during the early trophozoite stage yielded an $^{3D7}EC_{50}^{8h}$ value of 192 ± 52 nM, slightly greater than the EC_{50} value observed with continuous 72-hour exposure ($^{3D7}EC_{50}^{72h}$ = 108 ± 7 nM) (Figure 2.3C). Microscopy assessments of Giemsa-stained thin blood smears confirmed this stage-specific profile (Figure 2.3A). Interestingly, despite the biphasic dose-dependent curve shown in the 24–32 h window (Figure 2.3B), when parasites transition from late trophozoite stages to schizont stages, PRC1584-treated parasites remained arrested in the late trophozoite stage (Figure 2.3A).

Moreover, the stage-specific dose-response profile of PRC1584 did not match the stage-specificity profile of any of the 36 clinical or experimental antimalarials reported by Murithi and colleagues[24], suggesting that this compound class may act through a distinct and potentially novel mechanism.

The Kelch 13-C580Y mutation increases susceptibility to PRC1584 and its analogs. We previously reported that PRC1584 remained equipotent against the *P. falciparum* 4G strain, which has reduced susceptibility to artemisinin, using a 72-hour continuous exposure assay[17].

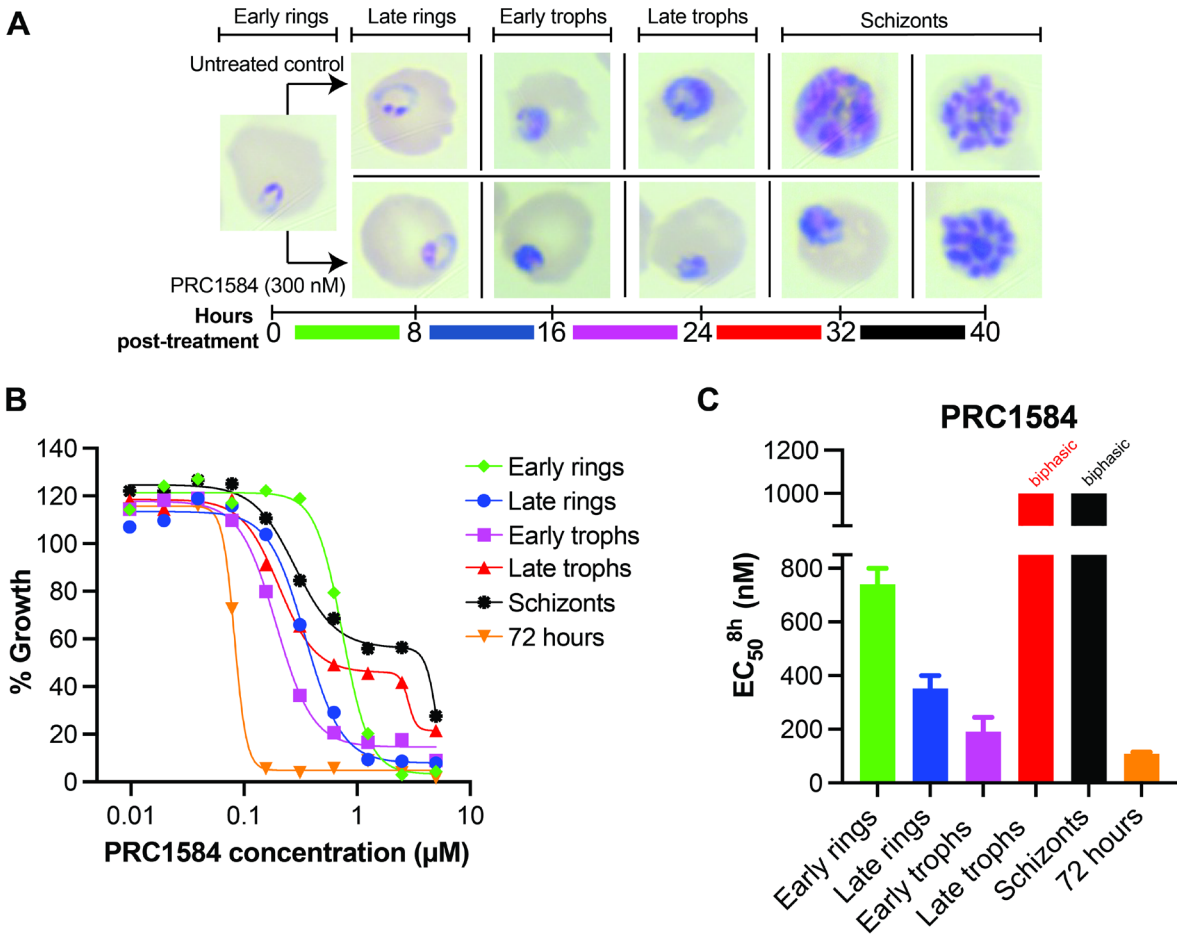

Figure 2.3. Stage specificity inhibition profile for PRC1584. **A)** Schematic of the intraerythrocytic life cycle of *P. falciparum* used for drug susceptibility assessment. Timeline represents 8-hour treatment windows. Giemsa-stained images were captured at the treatment initiation (0 h) and after an 8-hour drug exposure at the time of treatment removal, comparing untreated controls (top row) with parasites exposed to 300 nM PRC1584 (bottom row). **B)** Dose-

response curves of *P. falciparum* (3D7 strain) exposed for 8 h at defined developmental stages (early ring, late ring, early trophozoite (trophs), late trophozoites, and schizont). A 72-hour continuous exposure curve was performed in parallel as a control. The x-axis for the growth-inhibition curves is displayed on a logarithmic scale. **C)** Bar plots showing the EC_{50}^{8h} values when parasites were exposed only during the indicated stage as shown in panel A, with error bars displaying the SEM based on three biological replicates conducted in technical duplicate.

However, previous studies have established that ART-R is associated with reduced susceptibility specifically in the ring stage[25, 26].

To better evaluate the susceptibility of the ring-stage to PRC1584, we performed the stage specificity assay described above, comparing the *P. falciparum* Dd2 (DHA-susceptible) strain with the 4G strain carrying the PfKelch13-C580Y mutation, which confers ART-R [27]. Strikingly, PRC1584 was significantly more potent against the 4G strain than the Dd2 strain ($^{Dd2\text{-}PRC1584}EC_{50}^{8h}$ = 696 ± 62 nM vs. $^{4G\text{-}PRC1584}EC_{50}^{8h}$ = 211 ± 55 nM; Figure 2.4A, S3A). As expected, DHA was significantly less potent against the 4G strain compared to the Dd2 strain ($^{Dd2\text{-}DHA}EC_{50}^{8h}$ = 3.0 ± 0.2 nM vs. $^{4G\text{-}DHA}EC_{50}^{8h}$ = 7.7 ± 1.1 nM, Figure 2.4A). This unexpected collateral drug sensitivity was confirmed by comparing the susceptibility of PRC1584 in the NF54 wildtype strain and NF54-K13-C580Y line, expressing K13 wildtype (WT) or C580Y mutation, respectively[28] ($^{NF54\text{-}WT\text{-}PRC1584}EC_{50}^{8h}$ = 476 ± 16 nM vs. $^{NF54\text{-}K13\text{-}C580Y\text{-}PRC1584}EC_{50}^{8h}$ = 200 ± 56 nM; Figure 2.4B, S3B). The EC_{50} value for DHA was slightly but not significantly decreased in the NF54-K13-C580Y line compared to the NF54-WT ($^{NF54\text{-}WT\text{-}DHA}EC_{50}^{8h}$ = 10 ± 2 nM vs. $^{NF54\text{-}K13\text{-}C580Y\text{-}DHA}EC_{50}^{8h}$ = 6 ± 2 nM; Figure 2.4B). In addition, the potency of PRC1584 after 8-hour exposure was slightly higher against the NF54-WT strain compared to Dd2 ($^{NF54\text{-}WT\text{-}PRC1584}EC_{50}^{8h}$ = 476 ± 16 nM vs. $^{Dd2\text{-}PRC1584}EC_{50}^{8h}$ = 696 ± 62 nM), likely due to differences in genetic background. Importantly, PRC1584 maintained strong potency against both 4G and NF54-K13-C580Y strains after an 8-hour exposure (Figure 2.4A-B). Time dependent effects were also observed, as 6-hour exposure to PRC1584 led to increased EC_{50} values against both

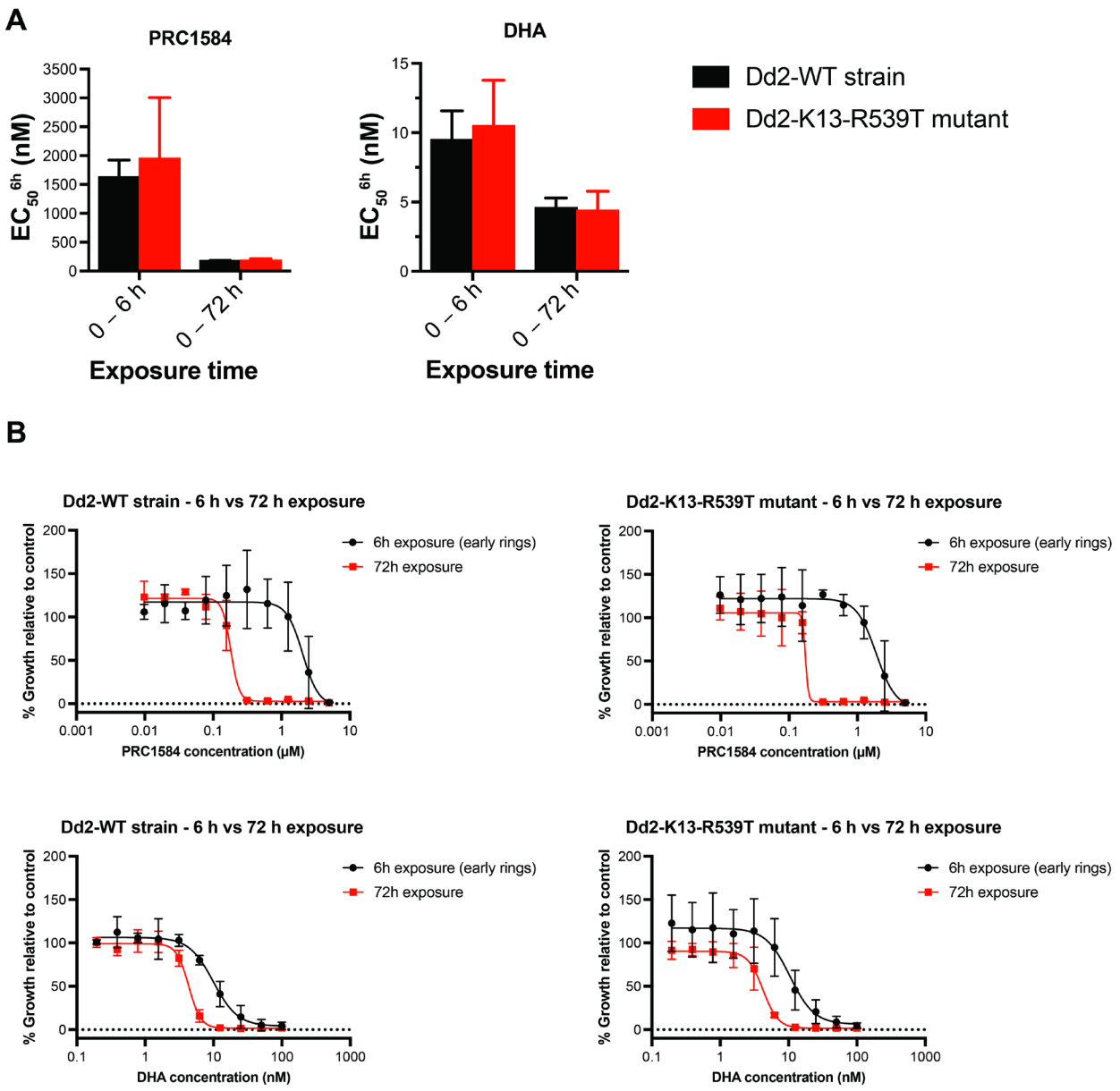

Figure S2.5. The Kelch-13 R539T mutation does not confer collateral drug sensitivity to PRC1584. **A)** EC_{50} values for PRC1584 (left) and DHA (right) after 6 hours (0–6 h, early rings) or continuous 72-hour exposure in Dd2-WT (black bars) and Dd2-K13-R539T mutant (red bars) strains. Increased sensitivity to PRC1584 in the PfK13-R539T mutant was not observed. **B)** Corresponding dose-dependent response curves for Dd2-WT strain and Dd2-K13-R539T mutant parasites exposed for 6 hours (black lines) or 72 hours (red lines) to PRC1584. The data represent the mean ± SEM from two to three biological replicates, each performed in technical triplicates. All x-axes are shown on a logarithmic scale.

the WT strain and PfK13-C580Y line. Nevertheless, the PfK13-C580Y mutant continued to exhibit greater sensitivity to PRC1584 ($^{\text{NF54-WT-PRC1584}}EC_{50}^{6h}$ = 987 ± 64 nM vs. $^{\text{NF54-K13-C580Y-PRC1584}}EC_{50}^{6h}$ = 394 ± 51 nM; Figure S2.4, Table S2.1).

To test whether this effect extended to other K13 mutations, we assessed PRC1584 against the Dd2-K13- R539T mutant, another DHA-resistant line. No differences were observed between the Dd2-WT and Dd2-K13-R539T after 6-hours of exposure ($^{\text{Dd2-WT-PRC1584}}EC_{50}^{6h}$ = 1630 ± 170 nM vs. $^{\text{Dd2-K13-R539T-PRC1584}}EC_{50}^{6h}$ = 1950 ± 610 nM; Figure S2.5, Table S2.1). We also evaluated PRC1584 against parasites carrying *Pfcoronin* mutations (Pikine-Pfcoronin-R100K-E107V), which also appear to mediate resistance to DHA[29].

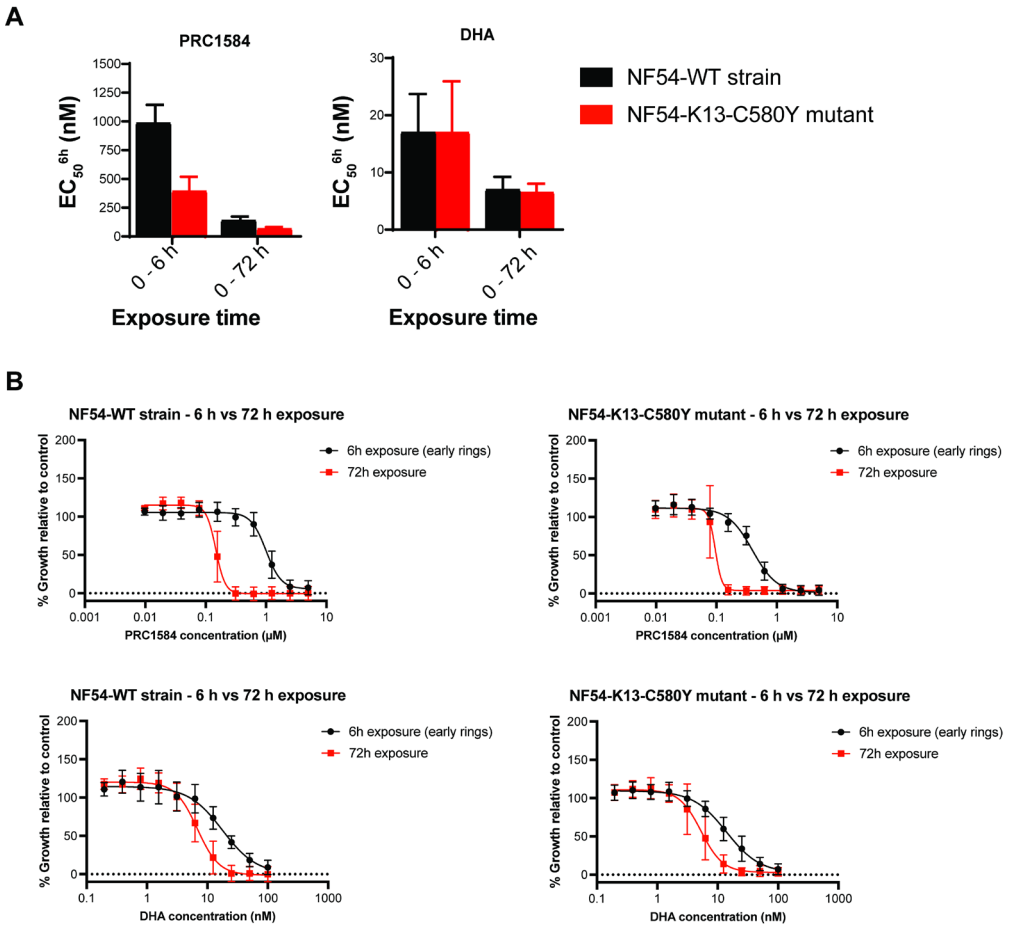

Figure S2.4. Collateral drug sensitivity to PRC1584 after 6-hour versus 72-hour exposure in PfK13-C580Y mutant. **A)** EC_{50} values for PRC1584 (left) and DHA (right) after 6 hours of exposure (0-6 h, early rings) or continuous 72-

hour exposure in NF54-WT (black bars) and NF54-K13-C580Y mutant (red bars) strains. **B)** Dose-dependent response curves for PRC1584 (top) and DHA (bottom) comparing 6-hour exposure (black lines) and 72-hour continuous exposure (red lines) in NF54-WT (left) and NF54-K13-C580Y mutant (right) strains. Data represent the mean ± SEM from six independent biological replicates, each performed in technical triplicates. X-axes are shown on a logarithmic scale.

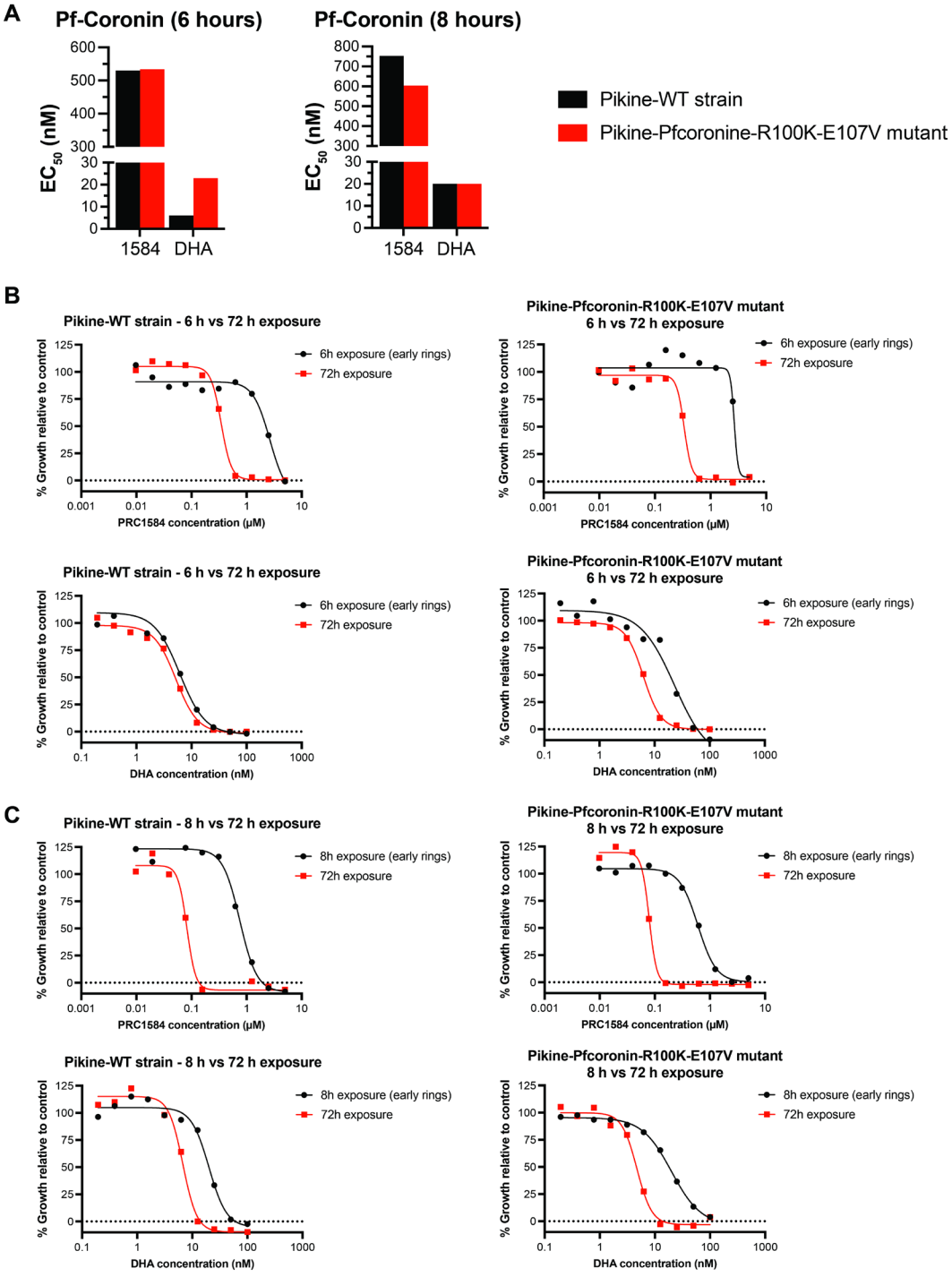

Figure S2.6. Dose-dependent response curves for Pikine-WT strain and Pikine-Pfcoronin-R100K-E107V mutant line after 6-hour and 8-hour exposure to PRC1584. **A)** EC_{50} values for PRC1584 and DHA after 6 or 8 hours of exposure (early rings) in Pikine-WT (black bars) and Pikine-Pfcoronin-R100K-E107V mutant (red bars) lines. **B)** Dose-response curves for Pikine-WT (left) and Pikine-Pfcoronin-R100K-E107V mutant (right) parasites after 6 hours of exposure (black lines) compared with 72 hours of continuous exposure (red lines) to PRC1584 (top row) or DHA (bottom row). **B)** Dose-response curves corresponding to the 8 hours of exposure to PRC1584 and DHA (control). The data represent the mean from one biological replicate performed in technical triplicates. All x-axes are shown on a logarithmic scale.

The Pikine-Pfcoronin-R100K-E107V mutant line exhibited similar susceptibility to PRC1584 as the parental Pikine strain after 6 and 8 h of exposure ($^{\text{Pikine-WT-PRC1584}}EC_{50}^{6h}$ = 530 nM vs. $^{\text{Pikine-Pfcoronin-R100K-E107V-PRC1584}}EC_{50}^{6h}$ = 534 nM; $^{\text{Pikine-WT-PRC1584}}EC_{50}^{8h}$ = 753 nM vs. $^{\text{Pikine-Pfcoronin-R100K-E107V-PRC1584}}EC_{50}^{8h}$ = 604 nM; Figure S2.6). These data suggest that the PfK13-C580Y mutation specifically contributes to increased potency for PRC1584.

We further examined whether collateral drug sensitivity extends to other β-carboline analogs recently reported in this series, specifically PRC1697 and PRC1664 (Figure 2.4B)[18]. Both analogs showed a similar profile of increased potency in the NF54-K13-C580Y mutant compared to NF54-WT ($^{\text{NF54-WT-PRC1697}}EC_{50}^{8h}$ = 102 ± 2 nM vs. $^{\text{NF54-K13-C580Y-PRC1697}}EC_{50}^{8h}$ = 70 ± 13 nM; $^{\text{NF54-WT-PRC1664}}EC_{50}^{8h}$ = 1364 nM vs. $^{\text{NF54-K13-C580Y-PRC1664}}EC_{50}^{8h}$ = 675 nM; Figure 2.4B). Consistent with our previous findings using the Dd2 strain[18], PRC1697 demonstrated greater potency than PRC1584 in both the WT and mutant parasites following 72 h of continuous exposure ($^{\text{NF54-WT-PRC1697}}EC_{50}^{72h}$ = 59 ± 5 nM vs. $^{\text{NF54-WT-PRC1584}}EC_{50}^{72h}$ = 140 ± 15 nM; $^{\text{NF54-K13-C580Y-PRC1697}}EC_{50}^{72h}$ = 38 ± 4 nM vs. $^{\text{NF54-K13-C580Y-PRC1584}}EC_{50}^{72h}$ = 94 ± 13 nM; Figure 2.4B, Table S2.1). Notably, PRC1697 demonstrated approximately 5-fold higher potency than PRC1584 following an 8-hour exposure in the NF54-WT strain and exhibited 3-fold greater potency against the NF54-K13-C580Y mutant. Collectively, these findings demonstrate that the PfK13-C580Y mutation confers a distinctive collateral sensitivity profile by increasing

susceptibility to PRC1584 and its analogs, further supporting a specific association with the C580Y mutation independent of reduced DHA sensitivity.

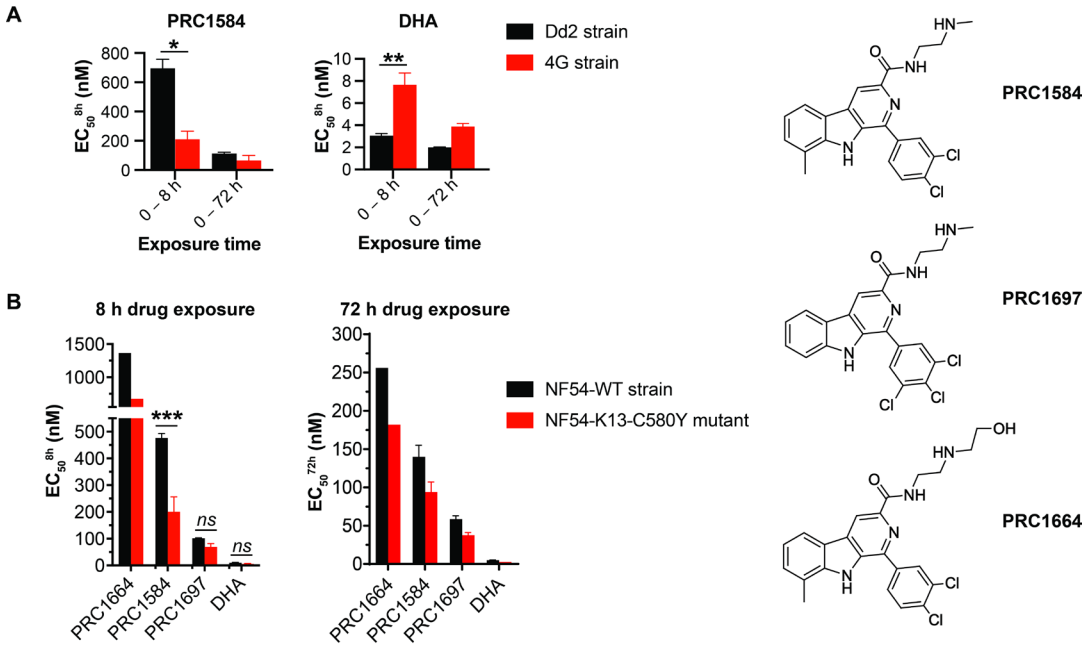

Figure 2.4. Collateral drug sensitivity in the presence of the PfK13-C580Y mutation assessed by the stage-specificity profiling assay. **A)** Early ring stage parasites for both susceptible (Dd2) and resistant (4G) strains were exposed to PRC1584 and DHA in a dose-dependent manner for 8 h. A dose-dependent curve for 72-hour continuous exposure was used as a control. Data represents the mean and SEM based on two to three independent biological replicates performed in technical triplicates. **B)** A similar stage-specificity assay, as described in A, was performed with NF54-WT and NF54-K13-C580Y strains. Data represent one or two biological replicates performed in technical duplicates. Statistical comparisons were performed using the two-sample student's t-test. *p $<10^{-5}$; **p $<2x10^{-5}$; ***p $<10^{-4}$; *ns,* not significant. Sensitivity to PRC1697 increased but the change was not statistically significant. Dose-response curves are shown in the supplementary materials (Figure S3).

Effects of PRC1584 and its analogs on ring-stage parasite morphology. As shown in Figure 2.3, PRC1584 affects ring stages within 8 h of exposure. To further investigate whether these effects persist beyond the initial treatment window, we examined the morphological development of the ring stages after drug removal. Highly synchronous ring-stage cultures were treated with either 500

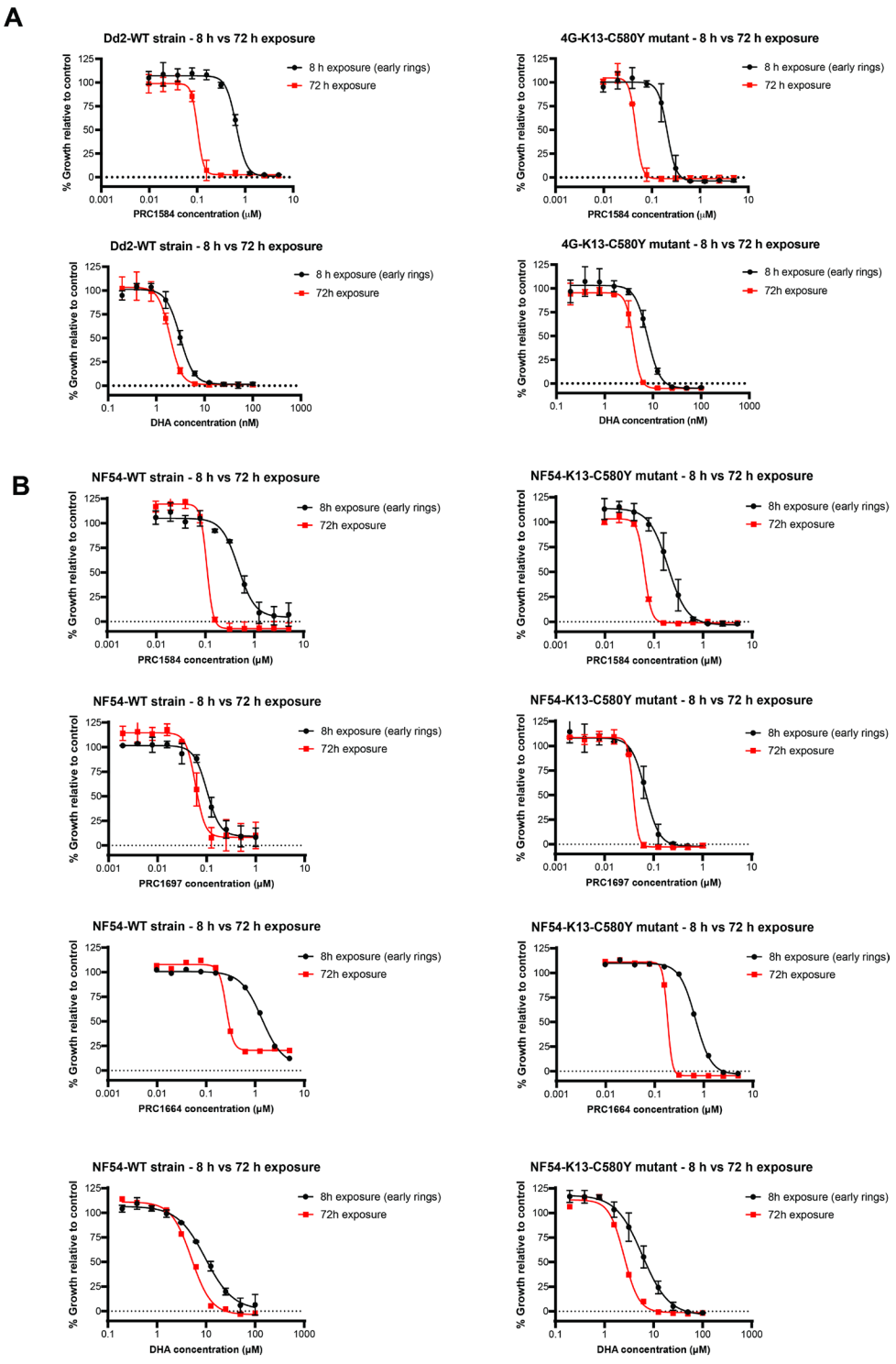

Figure S2.3. Dose-response curves for Kelch 13 WT and C580Y mutant strains after 8-hour versus 72-hour exposure. **A)** Dose-dependent response curves for the Dd2-WT strain (left) and the 4G-K13-C580Y mutant (right) after 8 hours of exposure (black line) or continuous 72-hour exposure (red lines) to PRC1584 (top row) and DHA (bottom row). **B)** Dose-dependent response curves for NF54-WT strain and NF54-K13-C580Y mutant after 8 hours or 72 hours of exposure to PRC1584 (top row), PRC1697 (second row), and PRC1664 (third row), and DHA (bottom row). These data were used to calculate EC_{50} values shown in Figure 2.4. Curves represent the mean from one to three biological replicates; each performed in technical triplicates. All x-axes are displayed in logarithmic scale.

nM PRC1584, PRC1697, PRC1664 or 700 nM DHA for 8 h, after which treatments were removed, and cultures were maintained in drug-free media. A concentration of 500 nM, corresponding to the 8-hour EC_{50} value of PRC1584 in NF54-WT, was selected to **a**llow direct potency comparisons across analogs (Figure 2.4B). Giemsa-stained thin blood smears were prepared from both treated and untreated controls every 24 hours for three consecutive days and analyzed by light microscopy. As shown in Figure 2.5, parasites treated with PRC1584 and PRC1697 exhibited a dormant-like morphology comparable to that observed following DHA exposure, characterized by small parasites with condensed chromatin and reduced cytoplasm. In contrast, consistent with its higher 8-hour EC_{50} (Figure 2.4B), a subpopulation of parasites treated with PRC1664 progressed normally through the intraerythrocytic cycle. Based on the dormant-like morphology identified following short-term exposure, we subsequently investigated whether ring-stage parasites treated with PRC1584 could resume growth over time.

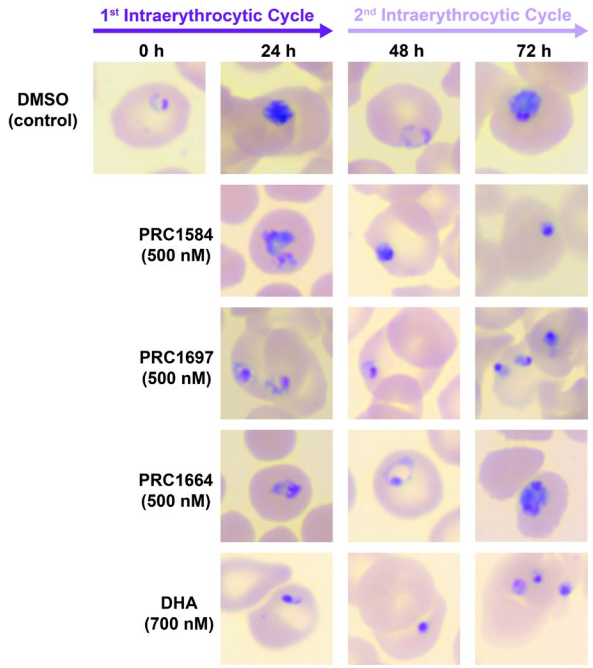

Figure 2.5. Effect of PRC1584 and its analogs on the morphology of ring-stage parasites. Highly synchronous (6-8 h post-invasion) NF54-WT ring-stage cultures were treated with 500 nM PRC1584, PRC1697, PRC1664 or 700 nM

DHA for 8 h. Following drug removal, cultures were maintained in drug-free media and monitored over three days by Giemsa-stained thin blood smears and light microscopy. Parasites treated with PRC1584 and PRC1697 displayed dormant-like morphology, characterized by condensed chromatin and reduced cytoplasm, similar to DHA-treated parasites.

PRC1584 and its potent analog PRC1697 are active against ring stages. It is well established that short exposure to DHA induces a dormant state in *P. falciparum* rings, with cultures typically recrudescing 3 to 4 days after DHA treatment is removed[30]. To be effective, novel antimalarials should eliminate ring-stage parasites before they enter dormancy or progress to transmissible gametocyte stages. To determine whether parasites exhibiting PRC1584- and PRC1697-induced dormant-like morphology could also recrudesce, we performed ring recrudescence assays following 8 h of exposure to PRC1584 and its analogs (Figure 2.6A). A concentration of 500 nM, corresponding to the 8-hour EC_{50} value of PRC1584 in NF54-WT, was selected to allow direct potency comparisons across analogs (Figure 2.6A). As expected, after an 8-hour treatment with 700 nM DHA followed by washout, recrudescence occurred after 3 to 5 days in the NF54-WT strain (DHA-sensitive) and within 1 to 4 days in the NF54-K13-C580Y line (DHA-resistant) (Figure 2.6B-C, S7). In contrast, cultures treated with 500 nM PRC1584 showed markedly delayed or no recrudescence within 17 to 30 days post-treatment in both lines. The variation between experiments was expected, as the concentration used was around the 8-hour EC_{50} value for NF54-WT strain and twice for the mutant line (Figure 2.6A). Similar results were observed in the Dd2 and 4G strains, in which higher concentrations prevented recrudescence (Figure S2.8). Notably, no recrudescence was observed in cultures treated with 500 nM PRC1697, regardless of the presence of the PfK13 mutation (Figure 2.6B-C). Consistent with its higher 8-hour EC_{50} value of 1364 nM for NF54-WT and 675 nM for NF54-K13-C580Y line (Figure 2.4B; Table S2.1), parasites exposed to 500 nM PRC1664 resumed growth

immediately post-treatment in the NF54-WT strain, whereas a slight delay was observed in NF54-K13-C580Y. Collectively, these findings indicate that an 8 h exposure to PRC1584 or PRC1697 efficiently eliminates ring-stage P. falciparum parasites, thereby preventing recrudescence beyond the 72 h period observed in DHA-treated cultures.

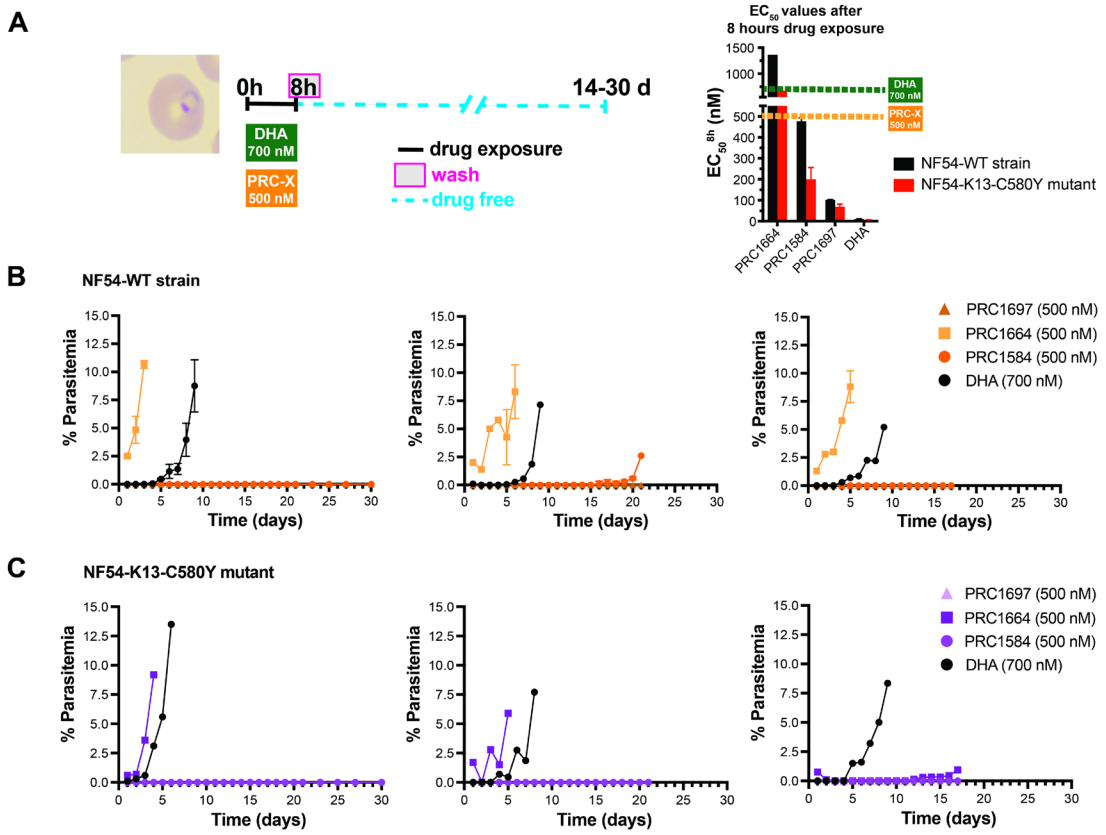

Figure 2.6. Ring-stage recrudescence following short-term drug exposure. **A)** Schematic of the experimental design used to monitor recovery following 8 h of drug exposure in highly synchronous ring-stage cultures (6-8 h post-invasion), as detailed in the materials and methods section. Graph depicts the 8-hour EC_{50} values as shown in Figure 2.4B. Giemsa-stained thin blood smears were prepared daily to assess parasite morphology and viability. **B)** Recrudescence outcomes for NF54-WT (DHA-sensitive) cultures following treatment with PRC1584, PRC1697, PRC1664, or DHA (control). **C)** Recrudescence outcomes for NF54-K13-C580Y (DHA-resistant) cultures under the same treatment conditions. Each panel shows data from a separate experiment, which was independently evaluated by two microscopists under blinded conditions.

PRC1584 and its potent analog PRC1697 are active against DHA-induced dormant parasites. There is increasing evidence suggesting that activity against artemisinin derivative-

induced dormant rings should be considered the "gold standard" for evaluating potential partner drugs[14, 16, 31, 32]. This property could enable the future development of novel ACTs even in the

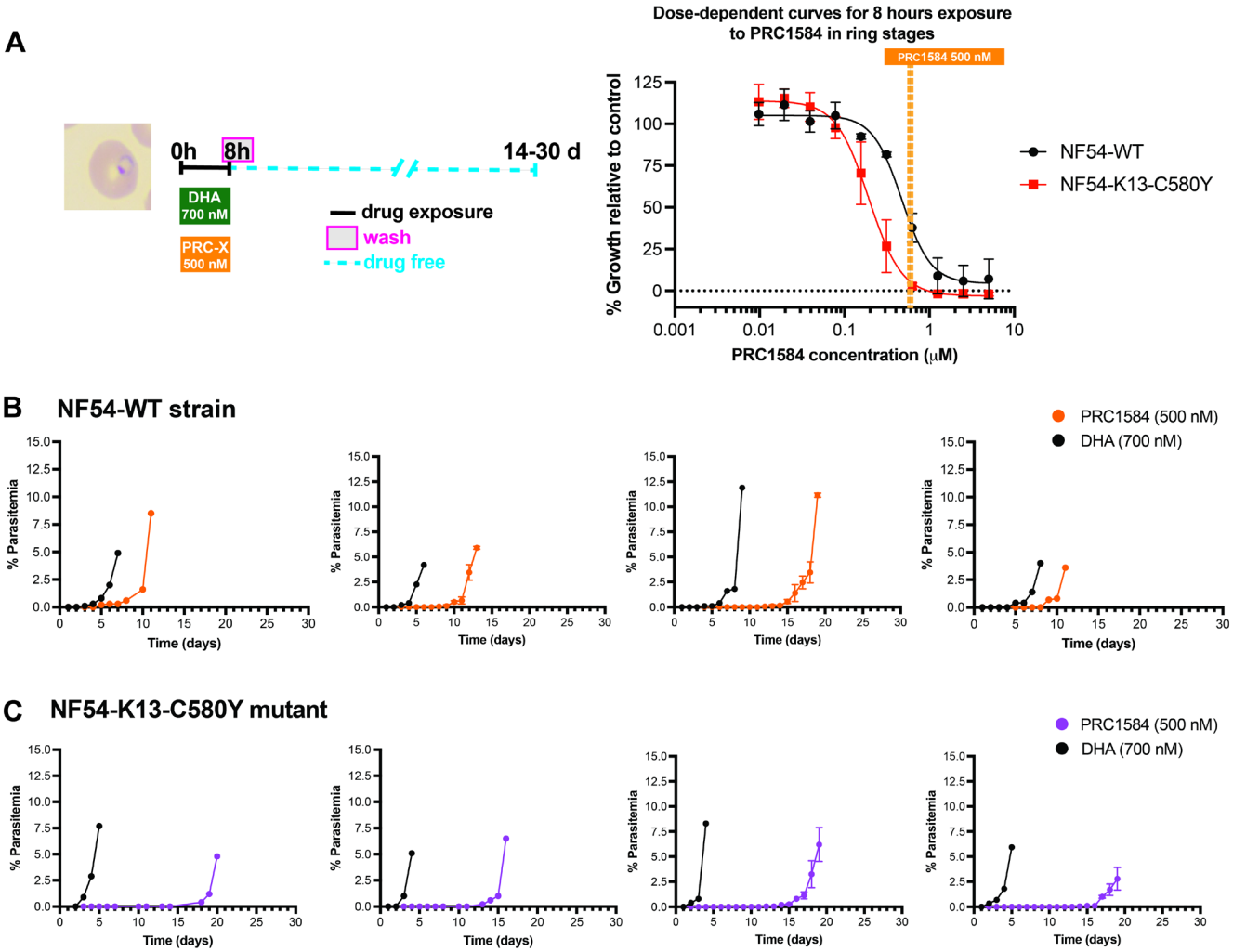

Figure S2.7. Initial ring stage recrudescence assays of parasites exposed to PRC1584 performed before PRC1664 and PRC1697 were designed and synthesized. **A)** Schematic of the experimental design used to monitor parasite recovery following 8 hours of drug exposure in highly synchronous ring-stage cultures (6-8 h post-invasion). After 8 hours of treatment with 500 nM PRC1584 or 700 nM DHA, cultures were washed and maintained in drug-free medium. Giemsa-stained thin blood smears were prepared daily to track parasite morphology and growth. X-axis is shown on a logarithmic scale for the dose-dependent curves obtained after 8 hours of exposure to PRC1584. **B)** Recrudescence profiles for NF54-WT (DHA-sensitive) cultures treated with PRC1584 (orange) or DHA (black). **C)** Recrudescence profiles for NF54-K13-C580Y (DHA-resistant) cultures under the same treatment conditions (PRC1584, purple; DHA, black). Each panel shows data from a separate experiment, which was independently evaluated by two microscopists under blinded conditions.

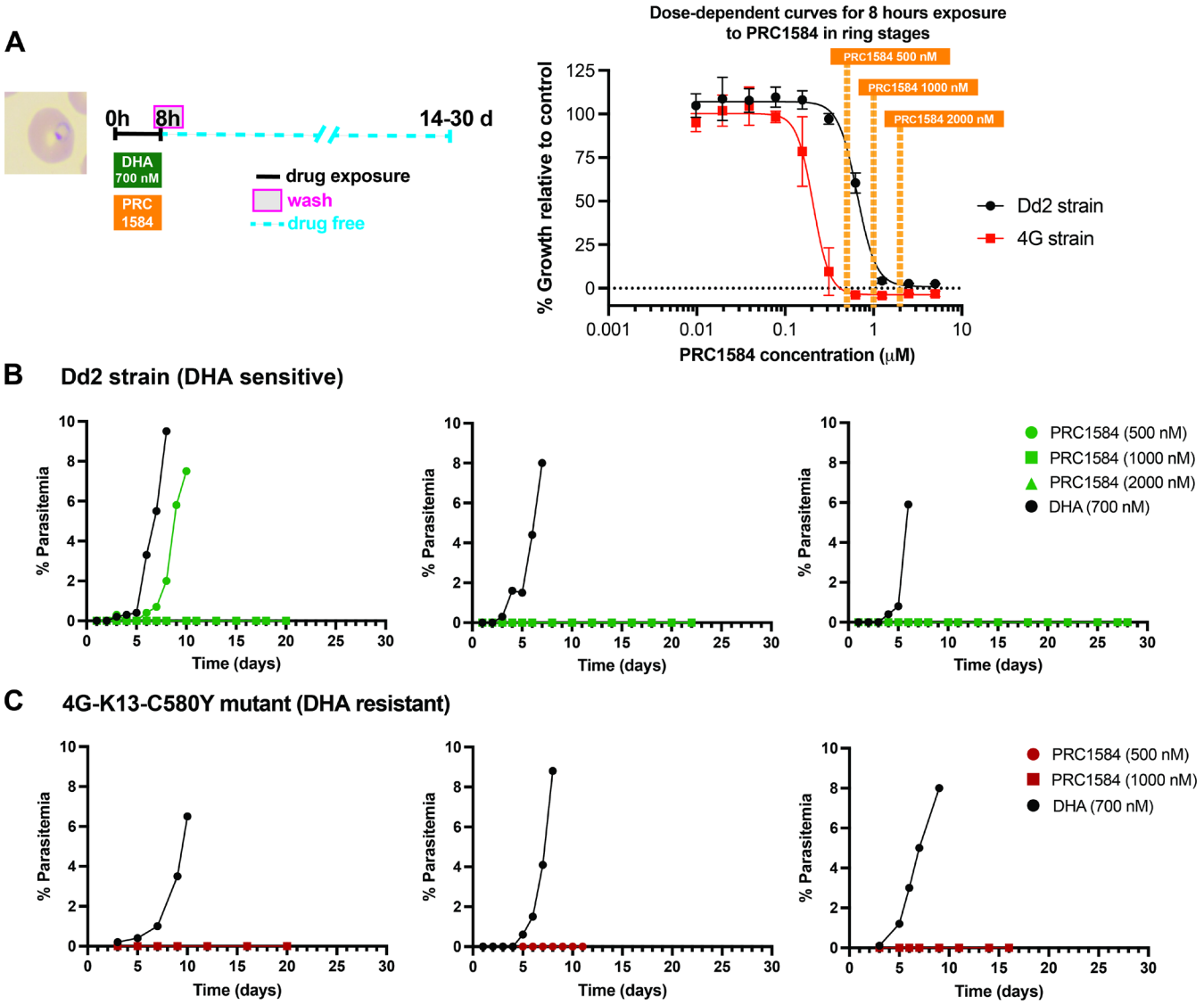

Figure S2.8. Ring-stage recrudescence assays with varying concentrations of PRC1584. **A)** Schematic of the experimental design used to monitor recovery of parasite after 8 hours of drug exposure at different concentrations in highly synchronous ring-stage cultures (6-8 h post-invasion). After drug removal, cultures were maintained in drug-free medium and monitored daily by Giemsa-stained thin blood smears. X-axis is shown on a logarithmic scale for the dose-dependent curves obtained after 8 hours of exposure to PRC1584. **B)** Recrudescence profiles for the Dd2 strain (K13-WT, DHA-sensitive) following treatment with PRC1584 at 500 nM (green circles), 1000 nM (green squares), or 2000 nM (green triangles) compared to DHA at 700 nM (black circles). **C)** Recrudescence profiles for the 4G-K13-C580Y mutant strain (DHA-resistant) following treatment with PRC1584 at 500 nM (red circles) or 1000 nM (red squares) compared to DHA at 700 nM (black circles). Each panel represents an independent experiment, with parasitemia plotted as % infected erythrocytes over time after treatment.

context of ART-R as well as the advancement of new combinations. To assess whether these β-carbolines display activity against DHA-induced dormant parasites, we treated highly synchronous ring cultures (6-8 h post-invasion) with 700 nM DHA for 8 h. Following

incubation, drug was removed and incubated in drug-free media for 16 h to ensure that parasites displayed morphological dormancy, at which time these parasites were treated with either PRC1584, PRC1697, PRC1664 or DMSO (Figure 2.7A). Based on previous studies showing that many antimalarials only delayed recrudescence[12, 16, 32], indicating partial toxicity to persisters, we selected a concentration of 1000 nM (approximately twice the 8-hour EC_{50} value for PRC1584 in NF54-WT) for these experiments. Following an initial 8-hour exposure to 700 nM DHA (DHA/DMSO), recrudescence occurred at similar time points in both the NF54-WT strain and the PfK13-C580Y mutant line, consistent with earlier observations (Figure 2.7B-C, S9). Remarkably, when DHA-induced dormant parasites were subsequently treated with PRC1584 or PRC1697, no proliferating parasites were detected for up to 20 days. These findings indicate that both PRC1584 and PRC1697 effectively eliminate DHA-induced dormant parasites regardless of DHA-sensitivity (Figure 2.7B-C). In contrast, treatment with 1000 nM PRC1664 delayed recrudescence by only several days, suggesting partial toxicity to persisters. Furthermore, delayed recrudescence was observed in W2 (artemisinin susceptible) and 4G strains following treatment with PRC1664 or PRC1584, suggesting that factors unique to each strain may affect the compounds' efficacy against persisters (Figure S2.10).

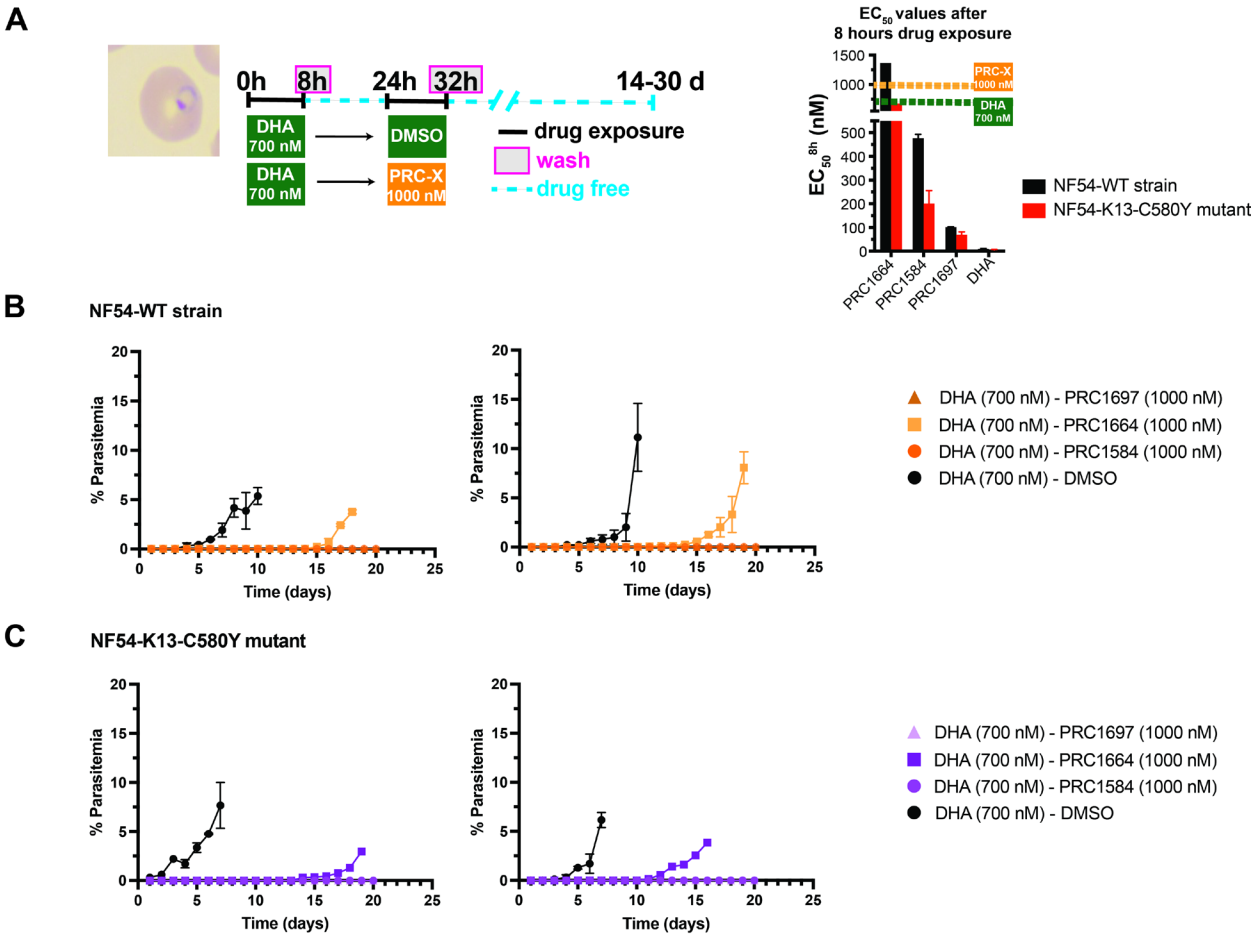

Figure 2.7. Effect of PRC1584 and related analogs on DHA-induced dormant parasites. **A)** Schematic of the experimental design used to monitor recovery following 8 h of drug exposure in DHA-induced dormant *P. falciparum* parasites, as detailed in the materials and methods. Graph depicts the 8-hour EC_{50} values as shown in Figure 2.4B. Giemsa-stained thin blood smears were prepared daily to assess the parasite morphology and viability. **B)** Effects of PRC1584 and its analogs (PRC1697 and PRC1664) on DHA-induced dormant parasites in the NF54-WT strain (DHA-sensitive). **C)** Recrudescence outcomes for NF54-K13-C580Y (DHA-resistant) cultures under the same treatment conditions. Each panel shows data from a separate experiment, which was independently evaluated by two microscopists under blinded conditions.

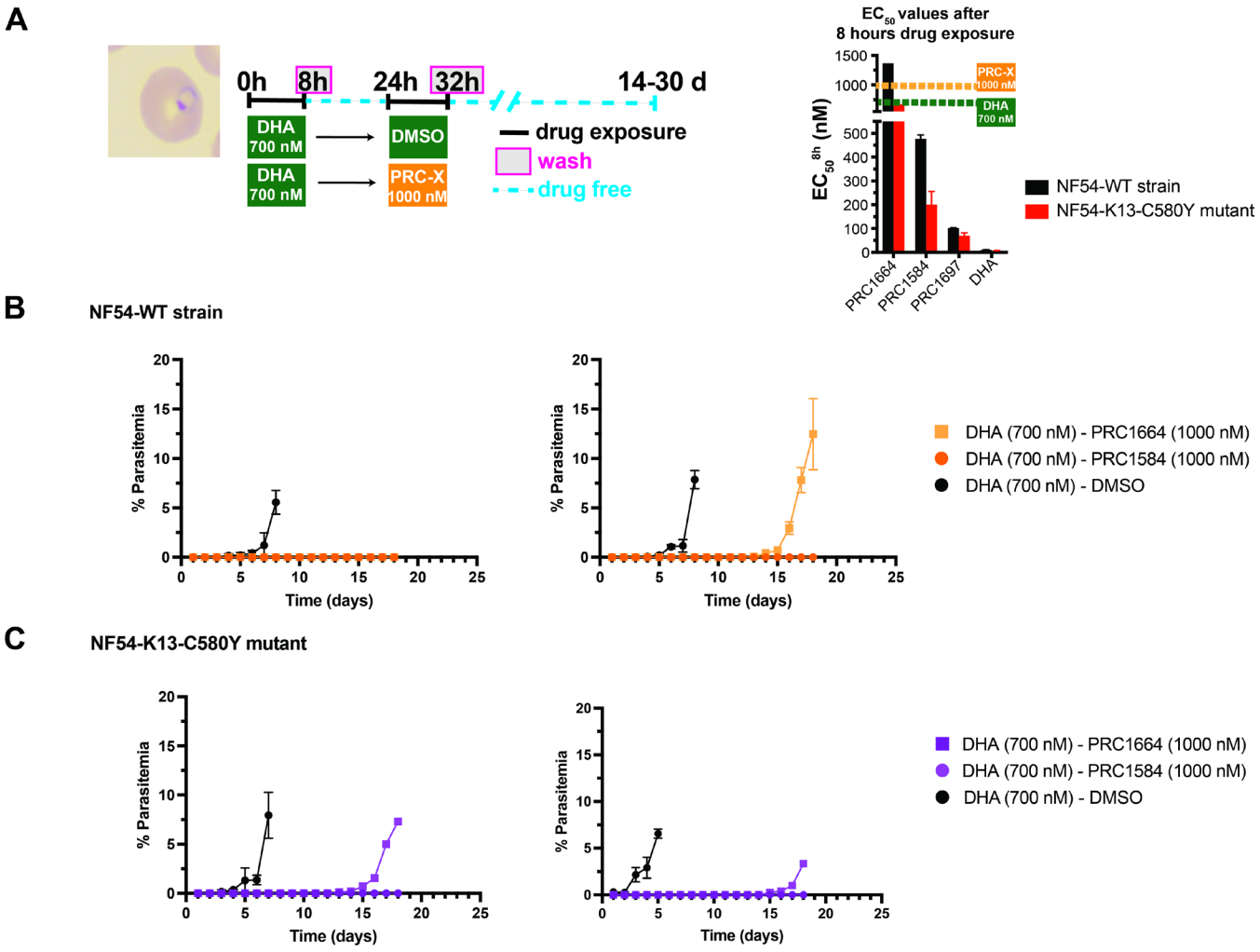

Figure S2.9. Effect of PRC1584 and PRC1664 on DHA-induced dormant parasites. **A)** Schematic of the experimental design used to monitor parasite recovery following 8 hours of drug exposure in DHA-induced dormant cultures. Highly synchronous ring stage parasites (6-8 h post-invasion) were first treated with 700 nM DHA for 8 hours (0–8 h), washed, and 16 hours after DHA treatment was removed, parasites were treated with 1000 nM of PRC1584 or PRC1664, or DMSO as control. Cultures were subsequently maintained in drug-free medium. Graph depicts the 8-hours EC_{50} values as shown in Figure 2.4B. **B)** Recrudescence profiles for the NF54-WT strain (DHA-sensitive) cultures treated with DHA followed by PRC1664 (orange squares), PRC1584 (orange circles), or DMSO (black circles). **C)** Recrudescence profiles for the NF54-K13-C580Y strain (DHA-resistant) cultures under the same treatment conditions (PRC1664, purple squares; PRC1584, purple diamonds; DMSO, black circles). Each panel shows data from a separate experiment, which was independently evaluated by two microscopists under blinded conditions.

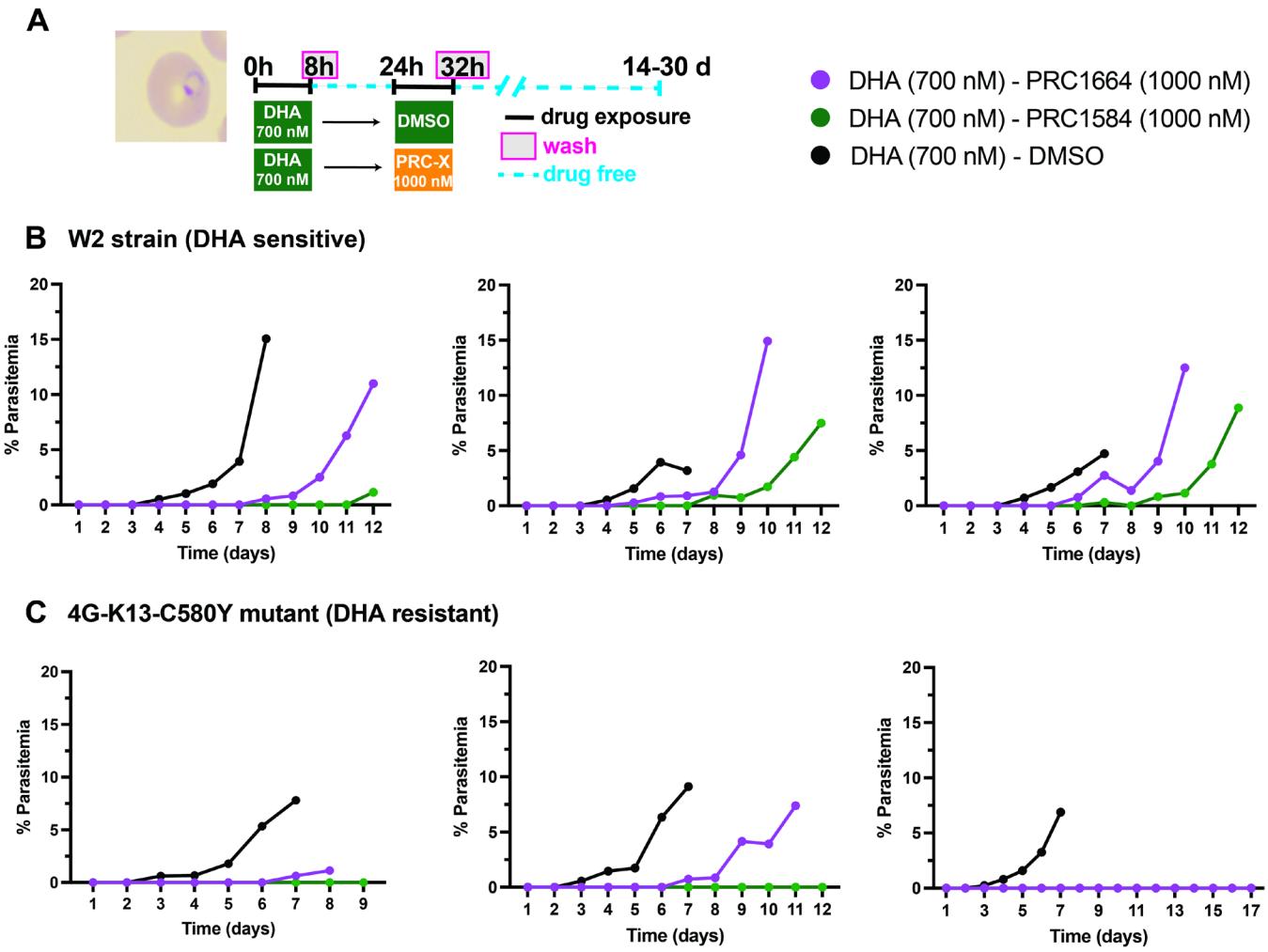

Figure S2.10. Initial studies evaluating the effect of PRC1584 and PRC1664 on DHA-induced dormant parasites in W2 strain (DHA-sensitive) and 4G-K13-C580Y mutant strain (DHA-resistant). **A)** Schematic of the experimental design used to monitor parasite recovery following 8 hours of drug exposure in DHA-induced dormant cultures. Highly synchronous ring stage parasites (6-8 h post-invasion) were first treated with 700 nM DHA for 8 hours (0–8 h), washed, and 16 hours after DHA treatment was removed, parasites were treated with 1000 nM of PRC1584 or PRC1664, or DMSO as control. Cultures were subsequently maintained in drug-free medium. **B)** Recrudescence profiles for the W2 strain (DHA-sensitive) after treatment with DHA followed by PRC1664 (purple), PRC1584 (green), or DMSO (black). **C)** Recrudescence profiles for the 4G-K13-C580Y mutant strain (DHA-resistant) under the same treatment conditions (PRC1664, purple; PRC1584, green; DMSO, black). Each panel represents an independent experiment, with parasitemia plotted as % infected erythrocytes over time after treatment.

Discussion

Malaria remains a significant global health issue, with increasing drug resistance, including ART-R, threatening current control efforts. A major challenge lies in the parasite's capacity to survive treatment by entering a dormant state; artemisinin derivatives facilitate this

dormancy and fail to fully eliminate it. A recent review described how temporary growth arrest in *P. falciparum* ring-stage parasites, a non-genetic survival mechanism, contributes to ART-R, underscoring the need for therapeutic strategies that can target growth-arrested ring stages, which may underlie treatment failure and persistent infection[33]. Recent studies describing improved methods for isolating and characterizing *P. falciparum* blood-stage dormant parasites induced by DHA further underscore the importance of effectively studying and targeting these forms[31]. Dormant parasites exhibit hallmarks of cellular quiescence/senescence and significant drug resilience, providing insights into their capacity to evade current treatments, and reinforcing the need for compounds capable of eliminating these populations[14]. Recognizing that drugs may show differential activity against proliferating ring stages versus quiescent or dormant parasites has led to the development of specialized assays to specifically identify compounds effective against these drug-resilient forms[12, 32].

In this study, we provide a comprehensive characterization of a novel β-carboline class of antimalarials, focusing on PRC1584 and the more potent analog PRC1697[17, 18]. These compounds exhibited compelling activity against both proliferating ring stages and DHA-induced dormant parasites. Our findings show that PRC1584 and PRC1697 exhibit robust activity primarily against the asexual intraerythrocytic stages of *P. falciparum* (Figure 2.1), with EC_{50} values in the 60-200 nM range after 72 h of drug exposure across various strains with diverse resistance profiles (Table S2.1)[17, 18]. Additionally, PRC1584 showed micromolar activity against gametocytes and gamete formation, but had low activity against *P. berghei* liver schizonts (Figure 2.1), positioning this class as a target candidate profile 1 (TCP-1) compound[34].

Refractoriness to resistance selection is a highly desirable characteristic for any new antimalarial[34], and a particularly valuable feature of PRC1584 is its remarkable resistance

barrier. Rigorous *in vitro* resistance selection experiments employing various constant drug pressure and pulsed-treatment protocols, consistently failed to yield resistant parasites, with a MIR greater than 10^9 infected red blood cells, qualifying this compound as "irresistible"[35]. Furthermore, PRC1584 retained potent activity against a diverse panel of fresh *P. falciparum* clinical isolates from Uganda, with a mean EC_{50} value of 70 nM (range 26 to 177 nM), consistent with its activity against laboratory strains (Table S2.1). Combined with previous findings confirming no cross-resistance with existing known mechanisms of resistance, these data underscore the potential utility of this scaffold in endemic regions with prevalent multidrug-resistant parasites[1, 3, 5].

Detailed stage-specific assays revealed a monophasic survival profile, with the greatest activity during late ring and early trophozoite stages. Remarkably, an 8-hour exposure to PRC1584 during the early trophozoite stage yielded an EC_{50} value approaching that of a continuous 72-hour exposure (Figure 2.3; Table S2.1). Moreover, PRC1697 demonstrated even greater potency against early rings (Figure 2.4), again approaching the 72-hour EC_{50} value (Table S2.1). Morphological assessments confirmed that PRC1584 arrested parasites at the early trophozoite stage and PRC1697 at late rings, preventing further development (Figure 2.5), with minimum effect on late trophozoite and schizont stages (Figure 2.3A). Biphasic survival curves observed in later stages (Figure 2.3B) suggest that PRC1584 may act on two distinct molecular targets that may be either functionally related or independent. The molecular target(s) of this class appear to be vital for biological processes during rings and early trophozoite stages, with lower activity in late trophozoites and schizonts, in which a second target may be active, leading to the biphasic response observed. Importantly, the unique asexual blood stage-specific profile of PRC1584 did not match that of any stage-specific profiles of the 36 clinical or experimental

antimalarials profiled by Murithi and colleagues[24], suggesting a distinct, potentially novel mechanism of action. The refractoriness to resistance of this class is a major plus for clinical development, but it comes with the disadvantage of preventing ready determination of the mechanism of action[35]. Currently, we are conducting chemoproteomics studies aimed at identifying potential molecular targets of this novel class.

An especially compelling and therapeutically significant finding is the unique collateral sensitivity observed in the PfKelch13-C580Y background (Figure 2.4). ART-R, characterized by delayed clearance and reduced drug susceptibility in ring stages, is associated with mutations in the *pfkelch13* gene, with C580Y being the most prevalent mutation in Southeast Asia[3, 10]. Strikingly, the C580Y mutation conferred significantly increased susceptibility to PRC1584 (Figure 2.4), with approximately 3-fold lower EC_{50} values in the 4G strain (PfKelch13-C580Y) compared to the Dd2 strain (PfKelch13-WT). This collateral sensitivity was confirmed in an isogenic NF54 background and was not observed with other PfKelch13 (R539T) or Pfcoronin (R100K-E107V) mutations, suggesting a specific association with the C580Y mutation independent of reduced DHA sensitivity. A collateral drug sensitivity phenomenon has been described in *P. falciparum* before, especially in the context of multidrug resistance protein 1 (PfMDR1)[36]. We recently reported the PfMDR1-G293V mutation as a key mediator of stereospecific resistance to the tetrahydro-β-carboline antimalarial PRC1590, while simultaneously conferring collateral sensitivity to other antimalarials[37]. Such findings highlight opportunities for drug cycling and combination therapies.

Beyond their activity against actively proliferating ring stage parasites, PRC1584 and PRC1697 were highly active against DHA-induced dormant parasites. It is well established that short exposure to DHA induces a dormant state in *P. falciparum* rings, with cultures typically

recrudescing 3 to 4 days after DHA treatment removal[30]. A recent study has shown that this dormant state displays hallmarks of cellular quiescence/senescence and drug resilience, with a unique transcriptional profile without resemblance to that of any normal parasite stages[14]. Our morphological assessments initially revealed that parasites treated with PRC1584 and PRC1697 displayed dormant-like features comparable to those observed following DHA exposure (Figure 2.5), characterized by small parasites with condensed chromatin and reduced cytoplasm. However, we conducted ring-stage recrudescence assays and under this assay's conditions, exposure to 700 nM DHA for 8 h typically resulted in parasite re-emergence in culture within days (Figure 2.6), while exposure to 500 nM PRC1584 for only 8 h either significantly delayed or completely prevented recrudescence for up to 30 days, regardless of DHA sensitivity. The variation between experiments was expected, as the concentration used was around the 8-hour EC_{50} value for the NF54-WT strain and twice that for the mutant line (Figure 2.6A). This ability to prevent recrudescence from ring stages underscores the therapeutic potential of PRC1584 and PRC1697. Targeting early ring stages is a highly desirable attribute for antimalarials, as these forms may progress to either asexual or sexual (transmission) blood stages, or alternatively enter dormancy under adverse conditions[33]. Furthermore, identification of dormant parasite forms triggered by drug exposure during the asexual intraerythrocytic life cycle has recently gained attention, and its molecular characteristics are only beginning to be understood[14]. Therefore, further research is necessary to determine at the molecular level whether PRC1584 and its analogs induce dormancy equivalent to that associated with artemisinins.

Currently, there are no treatments available that specifically target the dormant blood stages of *P. falciparum*. Notably, when specifically tested against DHA-induced dormant parasites, both PRC1584 and PRC1697 completely eliminated parasites, with no recrudescence

observed for up to 20 days irrespective of DHA sensitivity (Figure 2.7). In contrast, PRC1664 only delayed recrudescence, thus showing partial toxicity to persisters. Given that parasite growth typically resumes within 3 to 5 days following DHA withdrawal, and β-carboline analogs were administered for only 8 h starting 16 h post-DHA treatment (Figure 2.7A), the observed lack of recrudescence is unlikely to be attributable solely to effects on the proliferating ring-stage parasites. Presumably the mechanism by which the novel compounds kill DHA-induced dormant parasites is related to their toxicity to proliferating ring stages, and thus the lower asexual blood stage potency of PRC1664 relative to PRC1584 and PRC1697 may come into play. It is also possible that differences in lipophilicity may affect the ability of compounds to accumulate in DHA-induced dormant parasites. As expected from the ethanolamine group present in PRC1664, it is less lipophilic than PRC1584 and PRC1697 (calculated Log D values of 3.3, 3.5, and 4.1 respectively, CDD Vault, Collaborative Drug Discovery). This capability to kill asexual blood stage dormant forms is a major advantage and positions this class as an ideal candidate for inclusion in future artemisinin-based combination therapies. Nevertheless, confirmation of the ability of PRC1584 and PRC1697 to clear dormant parasites *in vivo* in relevant animal models is essential. In addition, our findings align with the growing body of research demonstrating the importance of targeting dormant stages, highlight the utility of specialized approaches for identifying such active compounds, and reinforce the crucial need to better characterize dormant parasites[16, 31, 32].

Interestingly, the spiroindolone KAE609, which targets PfATP4, does not induce dormant-like parasites but prevents recrudescence of DHA-induced dormant parasites[38]. Differently from PRC1584, KAE609 does not affect ring stages but is effective against early trophozoites and later developmental stages[24]. Thus, our data suggest that PRC1584 operates via

a different mechanism than KAE609. Likewise, imidazolopiperazines such as GNF179 effectively kill both ring stages and DHA-induced dormant parasites in wild-type and K13-mediated artemisinin resistant *P. falciparum* strains[39]. However, imidazolopiperazines may act through mechanisms different from those of PRC1584, as they are cidal against schizonts whereas PRC1584 does not prevent merozoite formation (Figure 2.3A). Therefore, it is likely that this class of β-carboline acts against distinct molecular targets in proliferating ring-stage parasites compared to those in DHA-induced dormant parasites.

In summary, our study highlights a novel β-carboline class with a high barrier to resistance, potent activity against ring stages, and the ability to eliminate DHA-induced dormant parasites. These attributes directly address critical challenges in malaria chemotherapy[34]. In addition, the unique collateral sensitivity to PfKelch13-C580Y mutation offers a strategic advantage, providing a potential therapeutic avenue to combat artemisinin resistance. Importantly, the proven capacity of these compounds to eradicate DHA-induced dormant parasites underscores their promise as optimal partner drugs for next-generation ACTs. Continued research to identify specific molecular targets and refine this scaffold will be crucial to achieving this goal.

Materials and Methods

Chemicals. Dihydroartemisinin was obtained from Sigma-Aldrich (St. Louis, MO). PRC1584, PRC1697 and PRC1664 were synthesized and purified, as previously described[17, 18]. All compounds were reconstituted at 10 mM in DMSO.

***Plasmodium falciparum* cultures.** The *P. falciparum* strain Dd2 (MRA-150), 3D7 (MRA-102)

and NF54 (MRA-1000) were obtained from MR4 (ATCC, Manassas, VA; BEI Resources, NIAID, NIH). The *P. falciparum* 4G strain containing the PfK13-C580Y mutation was kindly supplied by Dennis Kyle[27]. The *P. falciparum* NF54-PfK13-C580Y and Dd2-PfK13-R539T lines were kindly supplied by David Fidock[28]. The *P. falciparum* Pikine-Pfcoronin-R100K-E107V mutant line and the parental Pikine strain were kindly supplied by Dyann Wirth[29]. All *P. falciparum* strains were maintained in O^+ positive human erythrocytes (Grifols, Memphis, TN, USA) at 5% hematocrit in RPMI 1640 media (Thermo Fisher Scientific, Waltham, MA) containing 2 g/L glucose, 5.94 g/L HEPES, 2.3 g/L sodium bicarbonate, 5 g/L Albumax I, and 50 mg/L hypoxanthine. All reagents were obtained from Sigma-Aldrich (St. Louis, MO). Media was supplemented with 20 mg/L of gentamicin (Thermo Fisher Scientific, Waltham, MA). Parasite cultures were maintained at 37°C under reduced oxygen conditions (5% CO_2, 5% O_2, and 90% N_2) with shaking. Highly synchronous ring stage cultures (>98%) were obtained through two consecutive 5% sorbitol treatments (Sigma-Aldrich, St. Louis, MO) performed 6 hours apart.

***In vitro* selection of drug resistance.** Resistance selection for PRC1584 was assessed using both single-step and pulse methods as outlined in Figure S2.1[23, 37, 40]. For the single step selection, inoculums of 1 x 10^7 and 1 x 10^9 asynchronous parasites from newly cloned *P. falciparum* 3D7 strain were subjected to continuous drug pressure at twice and five times the 72 hours EC_{50} value (67 ± 5 nM), respectively. Each condition was performed in three independent cultures. For the first 7 days, media containing PRC1584 was replaced daily, then every other day until day 14. A parallel control culture was maintained under identical conditions with an equal volume of DMSO. After 14 days, drug pressure was removed, and cultures were monitored daily by Giemsa-stained smears with media changes every other day for 60 days. Fresh blood (50 µL)

was added weekly to sustain culture viability.

For the pulse method (Figure S2.1), three independent inoculums of 1 x 10^7 asynchronous or ring stage parasites from the same 3D7 clone were briefly pulsed with eight times the EC_{50} value of PRC1584 (400 nM) for 6 hours. Cultures were washed thrice with drug-free media and transferred to a new flask. Parasites were allowed to recover to 1 x 10^7 parasites and pulsed again with 400 nM PRC1584. Cultures underwent four cycles of recovery and re-exposure; however, parasites ultimately failed to recrudesce after the fourth pulse.

***P. falciparum* morphological assessments.** Ring stage NF54-WT strain parasite cultures (>98%) were synchronized by two consecutive 5% sorbitol treatment (Sigma-Aldrich, St. Louis, MO), administered 6 hours apart, 48 hours prior to the initiation of the experiment. All cultures were maintained at 37°C under reduced oxygen conditions (5% CO_2, 5% O_2, and 90% N_2) with continuous shaking. To evaluate morphological alterations following drug treatment, compounds were applied at specified concentrations and durations detailed in each figure legend. Thin blood smears were prepared at designated time points, fixed with 100% methanol (Sigma-Aldrich, St. Louis, MO, USA), and stained for 15 minutes using a 20% Giemsa solution (Sigma-Aldrich; diluted in deionized water). Following smear preparation, parasites were immediately gassed and returned to 37°C with shaking. Morphological growth phenotypes were assessed in biological duplicates.

HepG2 and liver stage assays. HepG2 cells (*Homo sapiens* hepatoblastoma, ATCC) were maintained in collagen-coated T-75 flasks with sugar-free DMEM (Gibco), supplemented with 10% FBS (Corning), 25 mM glucose (Millipore-Sigma), 1 mM sodium pyruvate (Corning), 5

μg/mL penicillin, 5 μg/mL streptomycin, 10 μg/mL neomycin, and 2 mM L-glutamine (Gibco). Cultures were incubated at 37°C in a humidified atmosphere containing 5% CO_2. Cells were detached using TrypLE (Gibco) once cultures reached 60–90% confluence. Cell density was determined via trypan blue exclusion with a hemocytometer. Subsequently, 17,500 cells per well were dispensed into collagen-coated 384-well plates (Greiner Bio-One) using a Biomek NX^P automated workstation (Beckman Coulter), 24 hours prior to sporozoite infection.

Luciferase-expressing *P. berghei* ANKA strain GFP-Lucama1-eef1a (line 1052cl1) was obtained from the Sporocore at the University of Georgia, as previously described[41]. Sporozoites were isolated according to established protocols, utilizing bicarbonate-free RPMI (KD Medical) as the collection buffer[42]. HepG2 cells were infected with 2,000 sporozoites per well. At three hours post-infection, 40 nL of each compound dilution was transferred from dose–response source plates to assay plates using a pin tool (V&P Scientific) mounted on a Biomek NX^P, achieving a final test concentration of 1x in media. The plates were incubated for 44 hours at 37°C in a humidified atmosphere containing 5% CO_2. After incubation, plates were fixed with 4% paraformaldehyde (Thermo Scientific) in PBS for 20 minutes. Following fixation, the plates were washed twice by adding and removing 20 μL of PBS per well. Plates were stained with 50 ng/mL mouse monoclonal antibody 13.3 (anti-GAPDH) sourced from The European Malaria Reagent Repository (http://www.malariaresearch.eu) diluted in a permeabilization and blocking buffer containing 0.3% Triton X and 1% BSA, and incubated overnight at 4°C. After three PBS washes, plates were treated with 2 μg/mL goat anti-mouse AlexaFluor 488 (Invitrogen), diluted in stain buffer, and incubated overnight at 4°C. Subsequently, three PBS washes were performed before counterstaining with 10 μg/mL Hoechst 33342 (Invitrogen) at room temperature for 30 minutes, followed by two additional washes. Imaging was conducted using an ImageXpress

Micro Confocal high content system (Molecular Devices). Schizont number and area were normalized using positive (MMV390048) and negative (DMSO) controls, and hepatocyte nuclei counts were used as an indicator of toxicity.

Determination of the Minimum Inoculum for Resistance (MIR) for PRC1584 based on continuous drug pressure selection. This assay was conducted at Columbia University under a contract with Medicines for Malaria Venture. The EC_{50} and EC_{90} was first experimentally determined in duplicate in the *P. falciparum* Dd2-B2 clone. Continuous drug pressure selection was set up using 2 x 10^5 Dd2-B2 parasites in each well of a 96-well plate at a concentration of 3 x EC_{90} (408.3 nM). Parasites cleared within the first 4 days. Drug pressure was maintained at 3 x EC_{90} over 60 days, and cultures were screened three times weekly by flow cytometry and smearing. Wells were considered positive for recrudescence when the overall parasitemia reached 0.3%, and parasites were seen on a blood smear. No recrudescence was observed over the course of this selection. The study was run alongside a DSM265 (57.5 nM) control, which yielded 68 recrudescent wells out of 96 (MIR 2.8 x 10^5, Log10 MIR 5.45).

***P. falciparum* male/female gamete formation assay.** This assay was conducted at Imperial College London under a contract with Medicines for Malaria Venture. This assay assesses the viability of mature stage V gametocytes as reported by their ability to undergo onward development and form gametes[19, 43-45]. Compounds were incubated in a dose-dependent manner with mature stage V gametocytes for 48 hours in 384 well plates before gamete formation was triggered by a drop in temperature and addition of xanthurenic acid. Twenty-five minutes post-triggering gamete formation, male gamete exflagellation was recorded and quantified by

automated microscopy. The plates were then incubated at 26°C for a further 24 hours and the female gamete formation of the same samples was assessed by live staining using a fluorophore-conjugated αPfs25 antibody specific for female gametes and quantified by automated microscopy. Gamete formation was expressed as a percent inhibition, taking into consideration DMSO-negative control wells and 10 mM methylene blue-positive control wells, with methylene blue being a potent inhibitor of the functional viability of male and female stage V gametocytes as previously reported[19]. This assay identifies compounds that either directly kill the male/female gametocyte, or "sterilize" the male/female gametocyte thus preventing gamete formation or interfere with the process of gamete formation itself.

Stage-specific gametocytocidal activity. This assay was conducted at the University of Pretoria under a contract with Medicines for Malaria Venture. Gametocytes were robustly induced from the PfNF54-pfs16-GFP-luc reporter line. Drug assays were initiated on immature gametocytes on day 5-6 (QC: >30% conversion, gametocytemia >3%, viable by hydroethidine staining, >90% stage II/III distribution) or on mature gametocytes on day 13 (QC: gametocytemia ~3%, >95% mature stage V gametocytes, functional gamete formation)[46]. For immature and mature gametocytes, compounds were evaluated with 48 hours drug pressure (2% gametocytemia, 1.5% hematocrit) at 37ºC under hypoxic conditions (90% N_2, 5% O_2, and 5% CO_2). After 48 hours, luciferase activity was measured in 20 µL parasite lysates by adding 50 µL luciferin substrate (Promega Luciferase Assay System) at room temperature. Bioluminescence detection was conducted with an integration constant of 10 seconds using the GloMax® Multi Detection System, operated with Instinct® Software. Dose-response experiments include 9 points of two-fold dilution per curve, a negative control (vehicle). Methylene blue at 5 mM (immature

gametocyte inhibition: 97 ± 5%; mature gametocyte inhibition: 93 ± 2%) and MMV390048 at 5 mM (immature gametocyte inhibition: 98 ± 1%; mature gametocyte inhibition: 97 ± 1%) were used as positive controls. The EC_{50} values were determined with a non-linear curve fitting normalized to maximum and minimum inhibition (DMSO control wells), using GraphPad Prism (GraphPad Software, Inc.). The assays were conducted in three biological replicates, each with technical triplicates.

***P. falciparum* Growth Inhibition Assay.** Dose-dependent growth inhibition with the reported compounds was evaluated using a 10-point dilution series and the *in vitro* SYBR Green I assay as a readout. Synchronous ring-stage parasites (1% starting parasitemia and 1% hematocrit) were cultured in 96-well half-area dark plates and continuously exposed to each compound for 72 h at 37 °C under reduced oxygen conditions (5% CO_2, 5% O_2, and 90% N_2). After 72 h, parasite growth was assessed by the SYBR Green I assay as previously described[47]. SYBR Green I was excited at 485 nm and its emission was measured at 535 nm using a Cytation5 plate reader (Agilent Bio Tek). Parasite growth was normalized to that of untreated control parasites and calculated as a percentage. The background was determined by using uninfected red blood cells (RBCs).

Dose-dependent assays were performed in at least two biological replicates and two technical replicates. Reported values represent the mean of biological replicates with the standard error of the mean (SEM). Initial concentrations were optimized after compound screening to ensure the EC_{50} value fell within the tested range. DMSO concentrations were maintained at ≤0.02% in all assays. Data were fitted using a four-parameter logistic dose-response curve, and half-maximal effective concentration (EC_{50}) values were calculated using

GraphPad Prism (GraphPad Software, Inc.). Assays comparing EC_{50} values across different parasite lines were performed concurrently.

Dose-dependent Stage Specificity Assays. Stage-specific assays were performed as previously described[24] with slight modifications[37]. Parasites of the *P. falciparum* 3D7 strain were synchronized in the ring stage 48 h prior to the assay by two rounds of 5% sorbitol treatment (Sigma-Aldrich, St. Louis, MO) with a 6 h interval between treatments. After parasites completed one life cycle and reinvaded RBCs, an additional sorbitol treatment was performed on the day of the assay to obtain highly synchronous early rings. Synchronized infected RBCs were plated in five 96-well plates and sequentially exposed to compounds for 8-hour windows starting at the following developmental stages: early rings (0-8 h), late rings (8-16 h), early trophozoites (16-24 h), late trophozoites (24-32 h), and schizonts (32-40 h). After each exposure window, compounds were removed by three rounds of washing with pre-warmed RPMI to avoid growth delays, and infected RBCs were transferred to a new plate. Plates were incubated under standard culture conditions, and parasite growth was assessed 72 h after the start of the assay using the SYBR Green I assay as described above. A 72-hour continuous exposure dose-response curve was included in parallel as control. Dose-response data were fitted using a four-parameter logistic dose-response curve or, where appropriate, a biphasic dose-response, and EC_{50} values were calculated using GraphPad Prism (GraphPad Software, Inc.). Assays were performed in at least two independent biological replicates, each with two to four technical replicates.

A similar experimental design was used to determine the EC_{50} values in ring stages following 6- or 8-hour exposure periods in a dose-dependent manner using different strains and mutants. Assays comparing EC_{50} values across different parasite lines were performed

concurrently. These assays were performed in one or two independent biological replicates, each with two to four technical replicates.

Modified Recrudescence and DHA-induced Dormancy Survival Assays. Recrudescence was monitored in bulk cultures as previously described[12], with slight modifications (Figures 6A, 7A). Parasites were synchronized twice with 5% sorbitol, with a 6 h interval between treatments. Thirty-six hours after the final synchronization, 5 mL cultures of early ring stages (0-6 h post-invasion) were adjusted to 3% parasitemia and 5% hematocrit and treated with DHA (700 nM), PRC1584, PRC1697, or PRC1664 (500 nM) for 8 h at 37°C with shaking under reduced oxygen conditions (5% CO_2, 5% O_2, and 90% N_2). Following incubation, parasites were washed three times with pre-warmed complete RPMI media and transferred to new flasks containing drug-free media. Thin blood smears were prepared every 24 h over a 15-30 day period, fixed with 100% methanol (Sigma-Aldrich, St. Louis, MO, USA), and stained with 20% Giemsa for 15 min (Sigma-Aldrich; diluted in deionized water). After smear preparation, cultures were immediately gassed and returned to 37°C with shaking. Media was replaced every other day, and 50 µL of fresh blood was added weekly. Recrudescence was assessed by light microscopy, scoring the proportion of viable parasites with a normal morphology following drug removal. For each condition, 10,000 erythrocytes were independently evaluated by two microscopists under blinded conditions, and the results were reported as percentages.

The effect of PRC analogs on DHA-induced dormant parasites was assessed as previously described[12], with slight modifications. Bulk cultures were synchronized and treated with 700 nM DHA for 8 h as described above. At 24 h post-treatment, parasites were treated with 1 µM of PRC1584, PRC1697, PRC1664, or DMSO (mock) for 8 h. Final DMSO

concentrations did not exceed 0.02%. After incubation, parasites were washed three times with pre-warmed complete RPMI media and transferred to new flasks containing drug-free media. Recrudescence was monitored by light microscopy as described above for up to 30 days.

***Ex vivo* EC_{50} Values against *P. falciparum* Field Isolates in Uganda.** The activity of PRC1584 was tested against fresh clinical *P. falciparum* isolates using a 72-hour growth inhibition assay with parasite DNA detection by SYBR Green I as previously described[47, 48]. These isolates were collected in June and July 2018, from patients living in the Tororo and Busia Districts, Uganda, who were newly diagnosed with *P. falciparum* malaria before antimalarial treatment was administered. The studies were approved by the Uganda National Council of Science and Technology, the Makerere University Research and Ethics Committee (SBS-REC 341), and the University of California San Francisco Committee on Human Research (16-19084).

Author Contributions

The overall study was designed by R.S.H, E.F.M., D.K., M.T., P.R.C., and M.B.C. Experiments and data analyses were conducted by R.S.H, J.H.B., L.A.W. V.M., and C.A.C. Related β-carboline compounds were synthesized and prepared by J.M., and P.R.C. Tests against fresh clinical *P. falciparum* isolates in Uganda were performed by P.K.T., P.J.R and R.A.C. Studies supported by Medicines for Malaria Venture were coordinated by Z.R., D.B. and S.B. Funding for this work was acquired by M.T., P.R.C., and M.B.C. The original draft was written by R.S.H. and edited by E.F.M., P.J.R., M.T., P.R.C., and M.B.C. All authors have read and agreed to the published version of this manuscript.

Acknowledgments

M.B.C., P.R.C., and M.T. thank the National Institutes of Health (AI157445) for financial support. We also thank the National Institutes of Health T32-AI060546 for providing financial support to R.S.H. and J.H.B., as well as R25GM109435 for supporting. We are grateful to Medicines for Malaria Venture for funding the assays described in this study. Our appreciation extends to David Fidock, Imran Ullah, Dyann Wirth, and MR4 (BEI Resources) for generously supplying the cell lines used in this research. We also thank Brett Reynolds for his assistance with microscopy experiments, and Jeremy Burrows for insightful comments on this manuscript prior to submission.

References

(1) Organization, W. H. *World malaria report 2024: addressing inequity in the global malaria response.* ; 2024.
(2) van der Pluijm, R. W.; Imwong, M.; Chau, N. H.; Hoa, N. T.; Thuy-Nhien, N. T.; Thanh, N. V.; Jittamala, P.; Hanboonkunupakarn, B.; Chutasmit, K.; Saelow, C.; et al. Determinants of dihydroartemisinin-piperaquine treatment failure in Plasmodium falciparum malaria in Cambodia, Thailand, and Vietnam: a prospective clinical, pharmacological, and genetic study. *Lancet Infect Dis* **2019**, *19* (9), 952–961. DOI: 10.1016/S1473-3099(19)30391-3 From NLM Medline.
(3) Ariey, F.; Witkowski, B.; Amaratunga, C.; Beghain, J.; Langlois, A. C.; Khim, N.; Kim, S.; Duru, V.; Bouchier, C.; Ma, L.; et al. A molecular marker of artemisinin-resistant Plasmodium falciparum malaria. *Nature* **2014**, *505* (7481), 50–55. DOI: 10.1038/nature12876 From NLM.
(4) Noedl, H.; Se, Y.; Schaecher, K.; Smith, B. L.; Socheat, D.; Fukuda, M. M. Evidence of artemisinin-resistant malaria in western Cambodia. *N Engl J Med* **2008**, *359* (24), 2619–2620. DOI: 10.1056/NEJMc0805011 From NLM.
(5) Rosenthal, P. J.; Asua, V.; Conrad, M. D. Emergence, transmission dynamics and mechanisms of artemisinin partial resistance in malaria parasites in Africa. *Nature Reviews Microbiology* **2024**, *22* (6), 373–384. DOI: 10.1038/s41579-024-01008-2.
(6) Witkowski, B.; Amaratunga, C.; Khim, N.; Sreng, S.; Chim, P.; Kim, S.; Lim, P.; Mao, S.; Sopha, C.; Sam, B.; et al. Novel phenotypic assays for the detection of artemisinin-resistant Plasmodium falciparum malaria in Cambodia: in-vitro and ex-vivo drug-response studies. *Lancet Infect Dis* **2013**, *13* (12), 1043–1049. DOI: 10.1016/S1473-3099(13)70252-4 From NLM Medline.
(7) Birnbaum, J.; Scharf, S.; Schmidt, S.; Jonscher, E.; Hoeijmakers, W. A. M.; Flemming, S.; Toenhake, C. G.; Schmitt, M.; Sabitzki, R.; Bergmann, B.; et al. A Kelch13-defined endocytosis pathway mediates artemisinin resistance in malaria parasites. *Science* **2020**, *367* (6473), 51–59. DOI: 10.1126/science.aax4735 From NLM.
(8) Bhattacharjee, S.; Coppens, I.; Mbengue, A.; Suresh, N.; Ghorbal, M.; Slouka, Z.; Safeukui, I.; Tang, H. Y.; Speicher, D. W.; Stahelin, R. V.; et al. Remodeling of the malaria parasite and host human red cell by vesicle amplification that induces artemisinin resistance. *Blood* **2018**, *131* (11), 1234–1247. DOI: 10.1182/blood-2017-11-814665 From NLM Medline.
(9) Mok, S.; Stokes, B. H.; Gnadig, N. F.; Ross, L. S.; Yeo, T.; Amaratunga, C.; Allman, E.; Solyakov, L.; Bottrill, A. R.; Tripathi, J.; et al. Artemisinin-resistant K13 mutations rewire Plasmodium falciparum's intra-erythrocytic metabolic program to enhance survival. *Nat Commun* **2021**, *12* (1), 530. DOI: 10.1038/s41467-020-20805-w.
(10) Ashley, E. A.; Dhorda, M.; Fairhurst, R. M.; Amaratunga, C.; Lim, P.; Suon, S.; Sreng, S.; Anderson, J. M.; Mao, S.; Sam, B.; et al. Spread of artemisinin resistance in Plasmodium falciparum malaria. *N Engl J Med* **2014**, *371* (5), 411–423. DOI: 10.1056/NEJMoa1314981 From NLM Medline.
(11) Witkowski, B.; Lelièvre, J.; Barragán, M. J.; Laurent, V.; Su, X. Z.; Berry, A.; Benoit-Vical, F. Increased tolerance to artemisinin in Plasmodium falciparum is mediated by a quiescence mechanism. *Antimicrob Agents Chemother* **2010**, *54* (5), 1872–1877. DOI: 10.1128/aac.01636-09 From NLM.
(12) Teuscher, F.; Gatton, M. L.; Chen, N.; Peters, J.; Kyle, D. E.; Cheng, Q. Artemisinin-induced dormancy in plasmodium falciparum: duration, recovery rates, and implications in treatment failure. *J Infect Dis* **2010**, *202* (9), 1362–1368. DOI: 10.1086/656476 From NLM Medline.

(13) Cheng, Q.; Kyle, D. E.; Gatton, M. L. Artemisinin resistance in Plasmodium falciparum: A process linked to dormancy? *International Journal for Parasitology: Drugs and Drug Resistance* **2012**, *2*, 249–255. DOI: https://doi.org/10.1016/j.ijpddr.2012.01.001.
(14) Tripathi, J.; Stoklasa, M.; Nayak, S.; En Low, K.; Qian Hui Lee, E.; Duong Tien, Q. H.; Renia, L.; Malleret, B.; Bozdech, Z. The artemisinin-induced dormant stages of Plasmodium falciparum exhibit hallmarks of cellular quiescence/senescence and drug resilience. *Nat Commun* **2024**, *15* (1), 7485. DOI: 10.1038/s41467-024-51846-0 From NLM Medline.
(15) Nosten, F.; White, N. J. Artemisinin-based combination treatment of falciparum malaria. *Am J Trop Med Hyg* **2007**, *77* (6 Suppl), 181–192. From NLM Medline.
(16) Reyser, T.; Paloque, L.; Ouji, M.; Nguyen, M.; Menard, S.; Witkowski, B.; Augereau, J. M.; Benoit-Vical, F. Identification of compounds active against quiescent artemisinin-resistant Plasmodium falciparum parasites via the quiescent-stage survival assay (QSA). *J Antimicrob Chemother* **2020**, *75* (10), 2826–2834. DOI: 10.1093/jac/dkaa250 From NLM Medline.
(17) Mathew, J.; Ding, S.; Kunz, K. A.; Stacy, E. E.; Butler, J. H.; Haney, R. S.; Merino, E. F.; Butschek, G. J.; Rizopoulos, Z.; Totrov, M.; et al. Malaria Box-Inspired Discovery of N-Aminoalkyl-beta-carboline-3-carboxamides, a Novel Orally Active Class of Antimalarials. *ACS Med Chem Lett* **2022**, *13* (3), 365–370. DOI: 10.1021/acsmedchemlett.1c00663.
(18) Mathew, J.; Zhou, B.; Haney, R. S.; Kunz, K. A.; Do Amaral, L. S.; Roy Chowdhury, R.; Butler, J. H.; Li, H.; Chakraborty, A. J.; Tabassum, A.; et al. beta-Carboline-3-carboxamide Antimalarials: Structure-Activity Relationship, ADME-Tox Studies, and Resistance Profiling. *ACS Infect Dis* **2024**, *10* (11), 3951–3962. DOI: 10.1021/acsinfecdis.4c00653 From NLM Medline.
(19) Ruecker, A.; Mathias, D. K.; Straschil, U.; Churcher, T. S.; Dinglasan, R. R.; Leroy, D.; Sinden, R. E.; Delves, M. J. A male and female gametocyte functional viability assay to identify biologically relevant malaria transmission-blocking drugs. *Antimicrob Agents Chemother* **2014**, *58* (12), 7292–7302. DOI: 10.1128/AAC.03666-14 From NLM Medline.
(20) Okitwi, M.; Orena, S.; Tumwebaze, P. K.; Katairo, T.; Taremwa, Y.; Byaruhanga, O.; Tukwasibwe, S.; Nsobya, S. L.; Legac, J.; Bailey, J. A.; et al. Changes in susceptibility of Plasmodium falciparum to antimalarial drugs in Uganda over time: 2019-2024. *Nat Commun* **2025**, *16* (1), 7353. DOI: 10.1038/s41467-025-62810-x From NLM Medline.
(21) Carolino, K.; Winzeler, E. A. The antimalarial resistome - finding new drug targets and their modes of action. *Curr Opin Microbiol* **2020**, *57*, 49–55. DOI: 10.1016/j.mib.2020.06.004 From NLM Medline.
(22) Cowell, A. N.; Istvan, E. S.; Lukens, A. K.; Gomez-Lorenzo, M. G.; Vanaerschot, M.; Sakata-Kato, T.; Flannery, E. L.; Magistrado, P.; Owen, E.; Abraham, M.; et al. Mapping the malaria parasite druggable genome by using in vitro evolution and chemogenomics. *Science* **2018**, *359* (6372), 191–199. DOI: 10.1126/science.aan4472 From NLM Medline.
(23) Ng, C. L.; Fidock, D. A. Plasmodium falciparum In Vitro Drug Resistance Selections and Gene Editing. *Methods Mol Biol* **2019**, *2013*, 123–140. DOI: 10.1007/978-1-4939-9550-9_9 From NLM Medline.
(24) Murithi, J. M.; Owen, E. S.; Istvan, E. S.; Lee, M. C. S.; Ottilie, S.; Chibale, K.; Goldberg, D. E.; Winzeler, E. A.; Llinas, M.; Fidock, D. A.; et al. Combining Stage Specificity and Metabolomic Profiling to Advance Antimalarial Drug Discovery. *Cell Chem Biol* **2020**, *27* (2), 158–171 e153. DOI: 10.1016/j.chembiol.2019.11.009.
(25) Klonis, N.; Crespo-Ortiz, M. P.; Bottova, I.; Abu-Bakar, N.; Kenny, S.; Rosenthal, P. J.; Tilley, L. Artemisinin activity against Plasmodium falciparum requires hemoglobin uptake and digestion.

Proc Natl Acad Sci U S A **2011**, *108* (28), 11405–11410. DOI: 10.1073/pnas.1104063108 From NLM Medline.
(26) Witkowski, B.; Khim, N.; Chim, P.; Kim, S.; Ke, S.; Kloeung, N.; Chy, S.; Duong, S.; Leang, R.; Ringwald, P.; et al. Reduced artemisinin susceptibility of Plasmodium falciparum ring stages in western Cambodia. *Antimicrob Agents Chemother* **2013**, *57* (2), 914–923. DOI: 10.1128/AAC.01868-12 From NLM Medline.
(27) Hott, A.; Casandra, D.; Sparks, K. N.; Morton, L. C.; Castanares, G. G.; Rutter, A.; Kyle, D. E. Artemisinin-resistant Plasmodium falciparum parasites exhibit altered patterns of development in infected erythrocytes. *Antimicrob Agents Chemother* **2015**, *59* (6), 3156–3167. DOI: 10.1128/aac.00197-15 From NLM.
(28) Gnadig, N. F.; Stokes, B. H.; Edwards, R. L.; Kalantarov, G. F.; Heimsch, K. C.; Kuderjavy, M.; Crane, A.; Lee, M. C. S.; Straimer, J.; Becker, K.; et al. Insights into the intracellular localization, protein associations and artemisinin resistance properties of Plasmodium falciparum K13. *PLoS Pathog* **2020**, *16* (4), e1008482. DOI: 10.1371/journal.ppat.1008482 From NLM Medline.
(29) Demas, A. R.; Sharma, A. I.; Wong, W.; Early, A. M.; Redmond, S.; Bopp, S.; Neafsey, D. E.; Volkman, S. K.; Hartl, D. L.; Wirth, D. F. Mutations in Plasmodium falciparum actin-binding protein coronin confer reduced artemisinin susceptibility. *Proc Natl Acad Sci U S A* **2018**, *115* (50), 12799–12804. DOI: 10.1073/pnas.1812317115 From NLM Medline.
(30) Wellems, T. E.; Sa, J. M.; Su, X. Z.; Connelly, S. V.; Ellis, A. C. 'Artemisinin Resistance': Something New or Old? Something of a Misnomer? *Trends Parasitol* **2020**, *36* (9), 735–744. DOI: 10.1016/j.pt.2020.05.013 From NLM Medline.
(31) Kiboi, D.; Sa, J. M.; Nayak, A.; Micchelli, C. E.; Amin, S. N.; Burbelo, A. G.; Abielmona, S. A.; Xi, B.; Mulei, L. A.; Onchieku, N. M.; et al. Isolation and characterization of Plasmodium falciparum blood-stage persisters by improved selection protocols using dihydroartemisinin alone. *Antimicrob Agents Chemother* **2025**, *69* (3), e0005324. DOI: 10.1128/aac.00053-24 From NLM Medline.
(32) Reyser, T.; Paloque, L.; Nguyen, M.; Augereau, J. M.; Fuchter, M. J.; Lopez, M.; Arimondo, P. B.; Hassell-Hart, S.; Spencer, J.; Di Stefano, L.; et al. Epidrugs as Promising Tools to Eliminate Plasmodium falciparum Artemisinin-Resistant and Quiescent Parasites. *Pharmaceutics* **2023**, *15* (10). DOI: 10.3390/pharmaceutics15102440 From NLM PubMed-not-MEDLINE.
(33) Platon, L.; Menard, D. Plasmodium falciparum ring-stage plasticity and drug resistance. *Trends Parasitol* **2024**, *40* (2), 118–130. DOI: 10.1016/j.pt.2023.11.007 From NLM Medline.
(34) Burrows, J. N.; Duparc, S.; Gutteridge, W. E.; Hooft van Huijsduijnen, R.; Kaszubska, W.; Macintyre, F.; Mazzuri, S.; Mohrle, J. J.; Wells, T. N. C. New developments in anti-malarial target candidate and product profiles. *Malar J* **2017**, *16* (1), 26. DOI: 10.1186/s12936-016-1675-x From NLM Medline.
(35) Yang, T.; Ottilie, S.; Istvan, E. S.; Godinez-Macias, K. P.; Lukens, A. K.; Baragana, B.; Campo, B.; Walpole, C.; Niles, J. C.; Chibale, K.; et al. MalDA, Accelerating Malaria Drug Discovery. *Trends Parasitol* **2021**, *37* (6), 493–507. DOI: 10.1016/j.pt.2021.01.009 From NLM Medline.
(36) Shafik, S. H.; Richards, S. N.; Corry, B.; Martin, R. E. Mechanistic basis for multidrug resistance and collateral drug sensitivity conferred to the malaria parasite by polymorphisms in PfMDR1 and PfCRT. *PLoS Biol* **2022**, *20* (5), e3001616. DOI: 10.1371/journal.pbio.3001616 From NLM Medline.

(37) Bremers, E. K.; Butler, J. H.; Do Amaral, L. S.; Merino, E. F.; Almolhim, H.; Zhou, B.; Baptista, R. P.; Totrov, M.; Carlier, P. R.; Cassera, M. B. Stereospecific Resistance to N2-Acyl Tetrahydro-beta-carboline Antimalarials Is Mediated by a PfMDR1 Mutation That Confers Collateral Drug Sensitivity. *ACS Infect Dis* **2025**, *11* (2), 529–542. DOI: 10.1021/acsinfecdis.4c01001 From NLM Medline.
(38) Chavchich, M.; Van Breda, K.; Rowcliffe, K.; Diagana, T. T.; Edstein, M. D. The Spiroindolone KAE609 Does Not Induce Dormant Ring Stages in Plasmodium falciparum Parasites. *Antimicrob Agents Chemother* **2016**, *60* (9), 5167–5174. DOI: 10.1128/AAC.02838-15 From NLM Medline.
(39) Dembele, L.; Gupta, D. K.; Lim, M. Y.; Ang, X.; Selva, J. J.; Chotivanich, K.; Nguon, C.; Dondorp, A. M.; Bonamy, G. M. C.; Diagana, T. T.; et al. Imidazolopiperazines Kill both Rings and Dormant Rings in Wild-Type and K13 Artemisinin-Resistant Plasmodium falciparum In Vitro. *Antimicrob Agents Chemother* **2018**, *62* (5). DOI: 10.1128/AAC.02235-17 From NLM Medline.
(40) Butler, J. H.; Baptista, R. P.; Valenciano, A. L.; Zhou, B.; Kissinger, J. C.; Tumwebaze, P. K.; Rosenthal, P. J.; Cooper, R. A.; Yue, J. M.; Cassera, M. B. Resistance to Some But Not Other Dimeric Lindenane Sesquiterpenoid Esters Is Mediated by Mutations in a Plasmodium falciparum Esterase. *ACS Infect Dis* **2020**, *6* (11), 2994–3003. DOI: 10.1021/acsinfecdis.0c00487 From NLM Medline.
(41) Maher, S. P.; Vantaux, A.; Cooper, C. A.; Chasen, N. M.; Cheng, W. T.; Joyner, C. J.; Manetsch, R.; Witkowski, B.; Kyle, D. A Phenotypic Screen for the Liver Stages of Plasmodium vivax. *Bio Protoc* **2021**, *11* (23), e4253. DOI: 10.21769/BioProtoc.4253 From NLM PubMed-not-MEDLINE.
(42) Nguyen, G. B.; Cooper, C. A.; McWhorter, O.; Sharma, R.; Elliot, A.; Ruberto, A.; Freitas, R.; Pathak, A. K.; Kyle, D. E.; Maher, S. P. Screening the Global Health Priority Box against Plasmodium berghei liver stage parasites using an inexpensive luciferase detection protocol. *Malar J* **2024**, *23* (1), 357. DOI: 10.1186/s12936-024-05155-y From NLM Medline.
(43) Delves, M. J.; Miguel-Blanco, C.; Matthews, H.; Molina, I.; Ruecker, A.; Yahiya, S.; Straschil, U.; Abraham, M.; Leon, M. L.; Fischer, O. J.; et al. A high throughput screen for next-generation leads targeting malaria parasite transmission. *Nat Commun* **2018**, *9* (1), 3805. DOI: 10.1038/s41467-018-05777-2 From NLM Medline.
(44) Delves, M. J.; Ruecker, A.; Straschil, U.; Lelievre, J.; Marques, S.; Lopez-Barragan, M. J.; Herreros, E.; Sinden, R. E. Male and female Plasmodium falciparum mature gametocytes show different responses to antimalarial drugs. *Antimicrob Agents Chemother* **2013**, *57* (7), 3268–3274. DOI: 10.1128/AAC.00325-13 From NLM Medline.
(45) Delves, M. J.; Straschil, U.; Ruecker, A.; Miguel-Blanco, C.; Marques, S.; Dufour, A. C.; Baum, J.; Sinden, R. E. Routine in vitro culture of P. falciparum gametocytes to evaluate novel transmission-blocking interventions. *Nat Protoc* **2016**, *11* (9), 1668–1680. DOI: 10.1038/nprot.2016.096 From NLM Medline.
(46) Reader, J.; van der Watt, M. E.; Birkholtz, L. M. Streamlined and Robust Stage-Specific Profiling of Gametocytocidal Compounds Against Plasmodium falciparum. *Front Cell Infect Microbiol* **2022**, *12*, 926460. DOI: 10.3389/fcimb.2022.926460 From NLM Medline.
(47) Smilkstein, M.; Sriwilaijaroen, N.; Kelly, J. X.; Wilairat, P.; Riscoe, M. Simple and inexpensive fluorescence-based technique for high-throughput antimalarial drug screening. *Antimicrob Agents Chemother* **2004**, *48* (5), 1803–1806. DOI: 10.1128/aac.48.5.1803-1806.2004.

(48) Rasmussen, S. A.; Ceja, F. G.; Conrad, M. D.; Tumwebaze, P. K.; Byaruhanga, O.; Katairo, T.; Nsobya, S. L.; Rosenthal, P. J.; Cooper, R. A. Changing Antimalarial Drug Sensitivities in Uganda. *Antimicrob Agents Chemother* **2017**, *61* (12). DOI: 10.1128/AAC.01516-17.

CHAPTER 3

DISRUPTING HEMOGLOBIN UPTAKE: PRC1584's MECHANISM OF ACTION AND IMPLICATIONS FOR OVERCOMING ARTEMISININ RESITANCE

Haney, R.S., Mccord, H.T., Carlier, P.R., Cassera, M.B. To be submitted to a peer-reviewed journal.

Abstract

Our prior results demonstrated that PRC1584 exhibited greater potency in the PfKelch13-C580Y lines compared to the wild type following brief exposure periods. Because Kelch13 localizes to the cytostomal collar that mediates host-cytosol uptake, we have investigated the digestive vesicle formation and function as a potential mechanism of action of PRC1584. To address this hypothesis, we used the hemoglobin fractionation assay that separates hemoglobin, free heme, and hemozoin crystals, and transmission electron microscopy (TEM) to assess the cytostome-derived digestive vesicles and hemozoin content, in addition to a stepwise chemoproteomic probe strategy to identify possible molecular targets. In parasites in late ring-early trophozoite subjected to a 5 hours pulse, PRC1584 lowered the free heme:hemozoin ratio and reduced the total heme (free heme + hemozoin) content, consistent with reduced cargo delivery to the digestive vacuole rather than blocking hemozoin formation. By contrast, chloroquine increased the free heme:hemozoin ratio while leaving the total-heme unchanged compared to control, aligning with inhibition at hemozoin formation. Strikingly, parasites treated under the same conditions with PRC1584 also displayed defective cytostomes, fewer cytostome-derived digestive vesicles, and a marked loss of hemozoin crystals, including a higher fraction of parasites completely lacking vesicles/crystals as assessed by TEM. Altogether, these findings further support the biochemical observations and suggest that this class may disrupt hemoglobin uptake and metabolism as part of, or as a consequence of its MOA. Furthermore, to enable molecular target identification, we first developed a linker-only intermediate (PRC1859) to verify that a modification was tolerated that showed modest potency loss and preserved genotype selectivity, followed by the introduction of a diazirine–azide (PRC1860) which maintained the the collateral drug sensitivity in the PfK13-C580Y mutant. The probe also showed specific

labeling by western blot, establishing a quantitative engagement assay for downstream enrichment and mass spectrometry analysis for future studies to identify molecular target(s) candidate for target deconvolution.

Introduction

Malaria remains one of the most devastating infectious diseases, causing over 600,000 deaths annually, predominantly due to *Plasmodium falciparum*[1]. Artemisinin-based combination therapies (ACTs) have been the cornerstone of global malaria control, yet the emergence and spread of artemisinin partial resistance and partner-drug resistance are eroding their effectiveness [2, 3]. Sustained progress in malaria control will depend on the discovery and development of novel compounds with new mechanisms of action (MOA). Importantly, defining MOA early in the drug discovery process improves target product profile (TPP) alignment, resistance-risk prediction, and rational combination design[4, 5]. A persistent challenge in antimalarial discovery is that phenotypic screens yield potent hits without direct insight into molecular targets. Parasite responses to drug pressure often vary by developmental stage, complicating mechanistic interpretation[6]. For example, compounds that induce quiescence or growth arrest in ring stages may act through distinct biochemical pathways. This underscores the need to resolve MOA not only at the molecular level but also at the cellular process level to assess the relevance of this mechanism at each developmental stage.

Hemoglobin metabolism is a central process in *P. falciparum* to obtain amino acids and a validated druggable target. Once merozoites invade erythrocytes, parasites ingest large quantities of hemoglobin through a non-selective endocytic process that involves the invagination of both the parasitophorous vacuole membrane and parasite plasma membrane, leading to the creation of a cytostome. The collar at the cytostome is a specialized pore-like structure at the interface of the parasite plasma and parasitophorous vacuolar membranes, required to constrict and pinch off the invagination containing hemoglobin to form digestive vesicles. During the ring stage, hemoglobin digestion begins at these digestive vesicles that will merge at the trophozoite stage to

form a central digestive vacuole (DV)[7]. However, how the cytostome contents are transported to the parasite's DV remains to be experimentally confirmed[8]. In addition, free heme released during proteolysis is detoxified by crystallization into hemozoin (Figure 3.1)[9-11]. The importance of hemoglobin digestion for parasite growth was first demonstrated by Rosenthal and colleagues in the 1990s, who identified key proteases mediating hemoglobin degradation[12]. More recently, Tutor and colleagues presented compelling evidence indicating that the Kelch13 protein (K13) is localized at the collar of the cytostome and plays a direct role in hemoglobin uptake. Their findings revealed that alterations in K13 protein levels lead to abnormal cytostomes and a decrease in hemoglobin catabolism[13]. These changes while impairing the parasite's ability to properly process and utilize essential nutrients from its host, also allow it to survive artemisinin treatment since hematin is required for drug activation. As a result, the cytostome serves as a pivotal mediator linking nutrient acquisition with both parasite survival and tolerance to artemisinin.

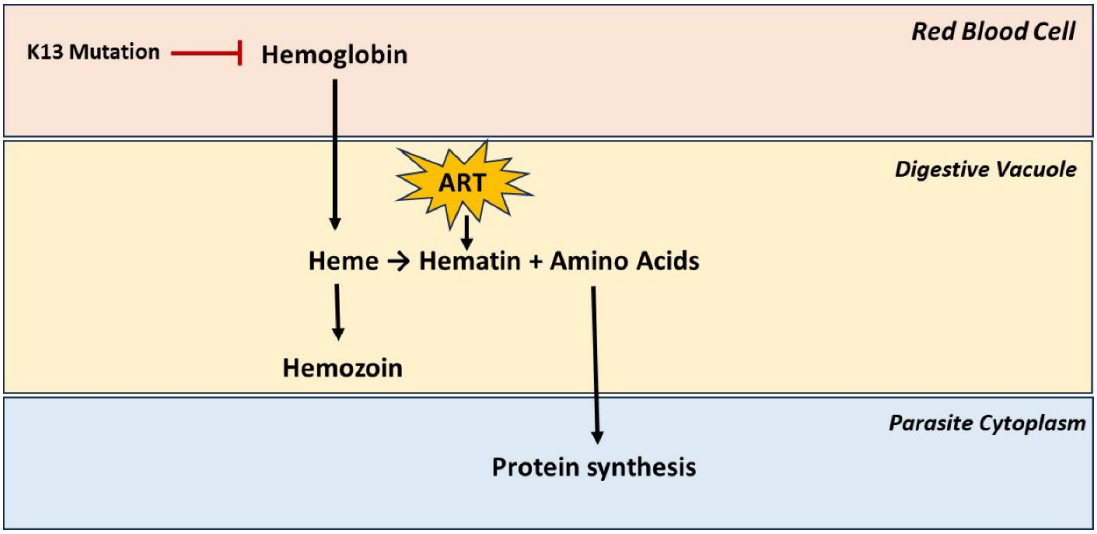

Figure 3.1 Hemoglobin Digestion and Artemisinin Activation. Schematic of hemoglobin uptake and digestion in *Plasmodium falciparum*. Host hemoglobin is internalized via cytostomal endocytosis and trafficked to the parasite food vacuole, where it undergoes proteolytic degradation by multiple parasite proteases. This process releases free heme, which is rapidly oxidized to hematin. Artemisinin and related endoperoxides require hematin (or ferrous heme)

for drug activation, linking hemoglobin catabolism directly to drug efficacy. To avoid heme toxicity, the parasite detoxifies hematin by crystallizing it into inert hemozoin. Mutations in the K13 protein disrupt hemoglobin uptake, thereby reducing hematin availability for artemisinin activation and contributing to partial drug resistance.

The K13 protein has emerged as one of the most consequential factors in modern malaria biology. Identified in 2014 as the molecular marker underlying delayed clearance of artemisinin-treated infections in Southeast Asia[14], K13 propeller mutations such as C580Y, R539T, and Y493H are now used globally by the World Health Organization as surveillance markers for artemisinin resistance[2, 3]. The importance of K13 is thus twofold: it is not only a clinically validated marker of drug resistance but also a protein essential for parasite survival[15]. Although its precise molecular functions were unclear at the time of its discovery, subsequent work established that K13 localizes to endocytic structures at the parasite plasma membrane [13, 16, 17]. Birnbaum and colleagues demonstrated that K13 defines a specialized endocytosis pathway, directly linking the protein to hemoglobin uptake and vesicle trafficking[17]. When K13 is mutated or depleted, parasites display malformed cytostomes, reduced hemoglobin ingestion, and altered flux of host material to the digestive vacuole[18, 19]. These defects not only compromise hemoglobin catabolism but also rewire parasite stress responses, particularly in early ring stages, enabling survival after short artemisinin exposures[20, 21].

The centrality of K13 therefore extends beyond artemisinin resistance. It represents a gatekeeper of hemoglobin endocytosis and a nexus between nutrient acquisition and drug susceptibility. This dual role makes K13 both a global health surveillance marker and a mechanistic clue for novel drug discovery. The collateral sensitivity we observed in PRC1584 treated *P. falciparum* C580Y mutants highlights this duality: mutations that reduces artemisinin potency simultaneously increase the PRC1584 *in vitro* potency, suggesting that PRC1584 may exploit vulnerabilities in the cellular pathways that K13 governs. As reported in Chapter 2, PRC1584 demonstrated potent inhibition of asexual blood-stage *P. falciparum* parasites, with

low nanomolar EC_{50} values in the 72-h growth inhibition assays. In side-by-side comparisons, the C580Y mutant line displayed lower EC_{50} values than its wild-type counterpart, indicating increased susceptibility under continuous exposure (Figure 3.2). We next evaluated the effect of short drug exposures using a 8-h washout assay. PRC1584 retained strong activity under this format, consistent with a rapid onset of action. In these assays, the PfK13-C580Y line again showed heightened susceptibility relative to wild type, with significantly reduced parasite survival following drug removal (Figure 3.2). RSAs further confirmed this trend, as well as the quiescence survival assays (QSAs): while both strains exhibited a growth-arrest phenotype following drug exposure, recrudescence occurred more slowly and less frequently in the C580Y background and prevented recrudescence of DHA-induced dormant parasites (Chapter 2). Importantly, this collateral sensitivity effect was specific to the PfK13-C580Y mutation. When PRC1584 was tested against parasites carrying the R539T mutation in K13, no significant difference in susceptibility was observed compared to wild type (Chapter 2). This indicates that collateral sensitivity is not a universal feature of K13 mutations, but rather a mutation-specific phenomenon associated with PfK13-C580Y. The uniqueness of this phenotype elevates its significance: while C580Y is the most globally prevalent K13 mutation associated with artemisinin resistance, it simultaneously creates a weakness that PRC1584 can exploit.

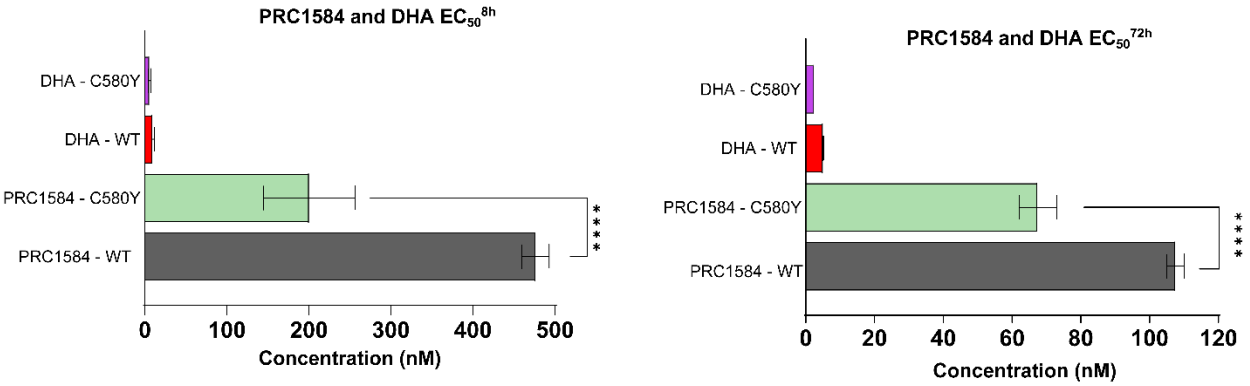

Figure 3.2 Comparison of short- and long-exposure activity of PRC1584 and DHA.
Mean EC_{50} ± SEM for 8 h pulse (washout) and 72 h continuous exposure. Under the 8 h pulse, PRC1584 was significantly more potent in the NF54 K13-C580Y line than NF54 wild-type**,** consistent with collateral sensitivity;

DHA showed high potency although decreased activity in the NF54 K13-C580Y line was not observed after 8 hours exposure. Data are n = 2 biological replicates; EC_{50} values compared by extra-sum-of-squares F-test (Holm–Šídák–corrected).

PRC1584 is a β-carboline scaffold compound with low nanomolar potency across multiple *P. falciparum* strains, and oral efficacy in rodent malaria models[22]. Our previous work demonstrated that PRC1584 exerts its strongest effects during the late ring to early trophozoite stages, coinciding with peak hemoglobin metabolism, and induces a morphological quiescent/pyknotic phenotype reminiscent of DHA exposure (Chapter 2). As mentioned above, parasites carrying the K13-C580Y mutation, which typically confer resistance to DHA, exhibit collateral sensitivity to PRC1584. This inverse relationship suggests that PRC1584's MOA may intersect with K13 cellular functions. Based on these observations, we hypothesize that PRC1584 disrupts hemoglobin uptake by perturbing cytostome formation or function, potentially through interactions with K13 or its protein partners. This chapter integrates multiple lines of evidence obtained through hemoglobin fractionation assays and electron microscopy with the previous stage-specific survival analyses, to evaluate this hypothesis. In doing so, we aimed to establish whether PRC1584 represents a novel class of antimalarials acting through the cytostome–hemoglobin uptake cellular system.

Results and Discussion

Reduced K13 protein levels in C580Y mutants

To investigate whether differences in PRC1584 susceptibility correlated with changes in K13 protein abundance, we compared K13 protein levels between NF54 wild-type and NF54 C580Y parasites. Lysates were prepared from late ring/early trophozoite stage cultures, the window in which PRC1584 shows peak stage-specific activity and analyzed by Western blot using an anti-K13 antibody (E9 mAb)[21]. K13 protein was readily detected in NF54 wild-type parasites (Figure 3.3). In contrast, K13 signal intensity was markedly reduced in NF54 C580Y mutant, consistent with prior reports that this mutation destabilizes the protein[18, 21, 23]. Quantification of normalized band intensities confirmed a statistically significant reduction in K13 abundance in the C580Y background relative to wild type ($p < 0.004$) (Figure 3.3). These findings establish that the C580Y mutation decreases steady-state K13 protein levels in the NF54 C580Y strain.

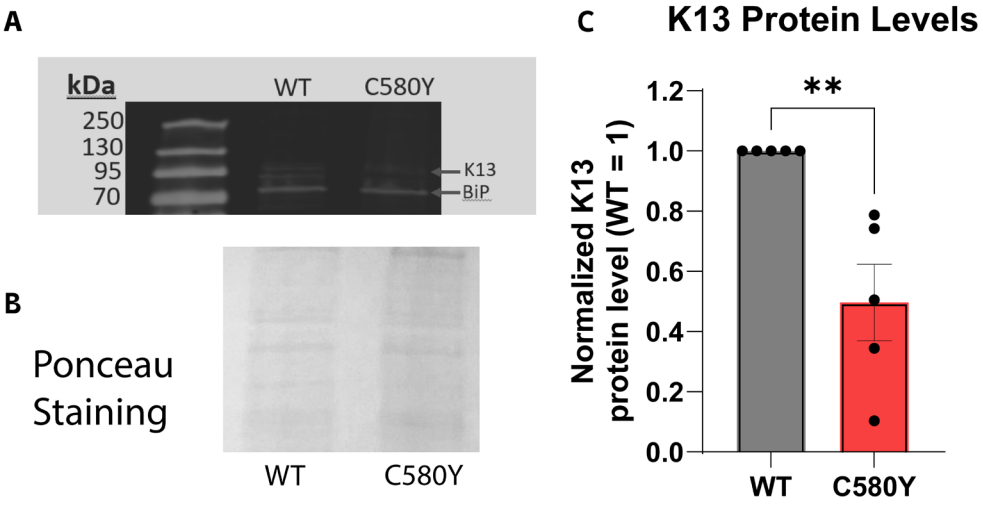

Figure 3.3 K13 protein levels are reduced in NF54 C580Y parasites. Western blot analysis of K13 protein levels in NF54 wild-type (WT) and C580Y mutant parasites. (A) Representative Western blot showing K13 (~85 kDa) and BiP (~70 kDa) as a loading/parasite marker. (B) Corresponding Ponceau S staining of the same membrane, used for total protein normalization (TPN). (C) Quantification of K13 band intensity normalized to total lane protein (Ponceau S) and reported as relative to the wild-type level (set as 1.0). The bar represent mean ± SEM from $n = 5$ independent biological replicates; points represent individual experiments. (**) $p < 0.004$ calculated using an unpaired two-tailed t-test on TPN-normalized K13 levels.

PRC1584 Disrupts Hemoglobin Uptake and Catabolism

K13 localizes at the cytostomal collar that mediates host-cytosol uptake and while C580Y parasites retain K13 at this site, the K13 protein abundance and the overall endocytic flux of hemoglobin can be reduced[13, 24, 25]. In addition, experimental mislocalization/depletion of K13 disrupts uptake and arrests development, highlighting the collar's functional role[13]. PRC1584 exhibited C580Y-specific collateral sensitivity, thus, we hypothesize that this endocytic reduction makes hemoglobin uptake and metabolism more susceptible to inhibition by PRC1584.

To quantify the effect of PRC1584 on hemoglobin digestion, we performed a hemoglobin fractionation assay that separates intact hemoglobin, free heme, and crystalline hemozoin[26, 27]. Synchronized late ring/early trophozoite parasites were exposed to either 5 μM of PRC1584 or 1 μM of chloroquine (CQ) for 5 h before fractionation. Because free heme and hemozoin are two forms of the same hemoglobin-derived heme (free heme is soluble and toxic; hemozoin is the crystalline, sequestered form), we defined 'total heme' as equal to free heme + hemozoin. We computed the within-sample free heme:hemozoin ratio (free heme ÷ hemozoin) and expressed treatment effects as $\text{ratio}_{\text{treated}} \div \text{ratio}_{\text{DMSO}}$ (reported as '× the DMSO level'). PRC1584 reduced the free:hemozoin ratio to 0.18× DMSO **(**95% CI 0.06–0.52; one-sample test on log-folds vs 1; Holm–Šídák–corrected p = 0.021), whereas CQ was 2.7× DMSO **(**95% CI 0.30–24**;** p = 0.358). We also reported the Foldbudget, defined as the fold-change in total heme (free heme + hemozoin) relative to DMSO; it indicates whether the overall heme content increased, decreased, or remained the same compared to the control. PRC1584 yielded a FoldBudget <1 (total heme decreased), whereas the CQ FoldBudget was ~1 (no net change) over the 5 h drug pulse (Figure 3.4).

Together, these data indicate that PRC1584 impairs hemoglobin uptake/vesicular delivery upstream of hemozoin formation, whereas CQ acts at hemozoin crystal formation. Although hemoglobin digestion in early rings is slow, digestion occurs in the parasite's acidic digestive vesicles; within a 5-h pulse, PRC1584 reduced both free heme and hemozoin, consistent with an upstream block in hemoglobin uptake or vesicle formation, where hemoglobin is degraded and heme is crystallized into hemozoin[10, 28]. By contrast, CQ, whose readout depends on ongoing heme release, did not show a detectable rise in free-heme under the same early-ring conditions, consistent with slow hemoglobin digestion at this stage and the assay's detection limit over a 5-h pulse (small effects may fall below the observable range).

By reducing the hemoglobin flux from the host RBC cytosol through the cytostomal collar into endocytic vesicles and onward, PRC1584 phenocopies the metabolic defects reported for K13-deficient parasites[13]. This biochemical disruption aligns with PfK13-C580Y collateral sensitivity and with the ultrastructural evidence of cytostome disruption presented below, providing a mechanistic link between cytostome integrity, endocytic flux, and the heme detoxification landscape observed here.

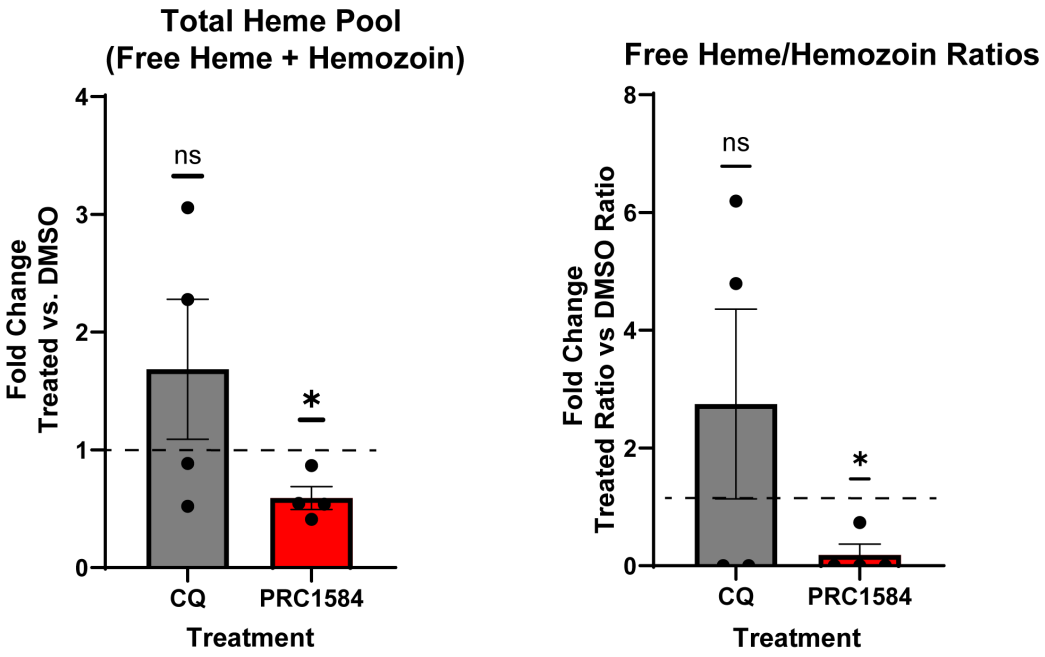

Figure 3.4 PRC1584 reduces the total heme pool without increasing the free-heme:hemozoin ratio. Synchronized late ring/early trophozoite–stage parasites were treated for 5 h with PRC1584 (5 µM), chloroquine (1 µM), or DMSO. Total heme pool (Free heme + Hemozoin) and the free heme:hemozoin ratio were quantified by fractionation and normalized to the matched DMSO control from each experiment (DMSO = 1). The free heme:hemozoin ratios were calculated as (Free heme ÷ Hemozoin)$_{treated}$ ÷ (Free heme ÷ Hemozoin)$_{DMSO}$, yielding a fold change relative to DMSO. Points represent individual biological replicates (n = 4); bars show mean ± SEM. Fold changes were analyzed on the $\log_{10}$ scale using two-tailed one-sample t-tests versus 0, with Holm–Šídák correction for multiple comparisons; results are plotted on the linear (fold-change) scale.

PRC1584 Disrupts Cytostome Formation, Digestive Vesicle Formation, and Hemozoin Crystallization.

To directly quantify the impact of PRC1584 on parasite endocytosis and hemoglobin digestion, we systematically scored digestive vesicles and hemozoin crystals from transmission electron micrographs (TEM) of synchronized late ring/early trophozoites exposed to 5 µM PRC1584 or DMSO as control for 5h. We selected this stage, duration, and concentration to (i) match the peak PRC1584 activity window from our stage-specificity assay and (ii) remain directly comparable to our fractionation assays, enabling cross-modal interpretations of uptake and DV phenotypes. In the DMSO-treated controls, parasites typically contained one to three

distinct cytostome-derived digestive vesicles within the cytoplasm (Figure 3.5B), consistent with active hemoglobin uptake. Correspondingly, well-defined cytostome structures could be visualized at the parasite periphery, with characteristic invaginations of the plasma and parasitophorous vacuolar membrane that give rise to endocytic vesicles (Figure 3.5A). In contrast, PRC1584-treated parasites frequently lacked cytostomes altogether, and those that remained appeared malformed or incomplete, with irregular membrane curvature and aborted vesicle formation (Figure 3.5A). When digestive vesicles were present, they appeared fewer in number and smaller in size compared to controls. Quantitative analysis confirmed a significant reduction in the mean number of vesicles per parasite in PRC1584-treated samples (Figure 3.6A) (Control: 1.48 ± 0.13, n = 112; PRC1584: 0.575 ± 0.776, n = 120; Welch's *t*-test, $p = 0.0001$; Mann–Whitney, $p = 0.0001$.). A similar pattern was observed when assessing hemozoin biocrystallization. In controls, parasites displayed readily identifiable hemozoin crystals within digestive vesicles (Figure 3.6A), consistent with robust hemoglobin digestion. These crystals varied in size but were consistently present. By contrast, PRC1584-treated parasites contained markedly fewer crystals, with many digestive vesicles appearing empty or containing only faint electron-dense material. Some parasites displayed malformed DVs in which the expected crystalline structures were entirely absent. Quantification revealed a sharp reduction in the mean number of hemozoin crystals per parasite under PRC1584 treatment (Figure 3.6A) (Control: 1.2 ± 0.221, n = 112; PRC1584: 0.101 ± 0.048, n = 120; Welch's *t*-test, $p = 0.0001$; Mann–Whitney, $p = 0.001$).

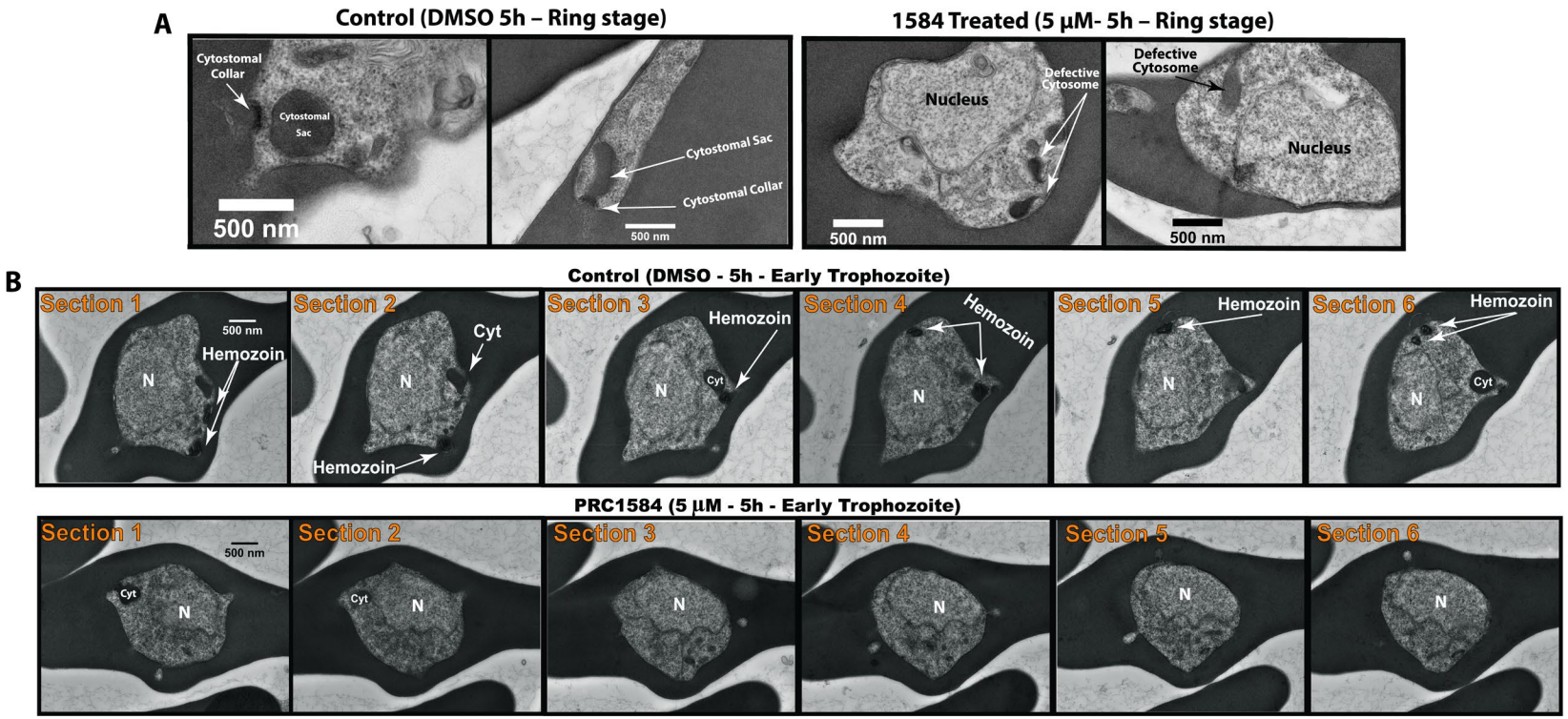

Figure 3.5. PRC1584 disrupts cytostomal endocytosis at ring stage and prevents vesicle and hemozoin formation in early trophozoites.
(A) Transmission EM of ring-stage parasites treated with DMSO (left) or PRC1584 (right). DMSO controls show intact cytostomes with a defined cytostomal collar. PRC1584-treated rings exhibit malformed cytostomes with little to no associated endocytic vesicles, consistent with impaired hemoglobin uptake. (B) Serial cross sections of early trophozoites treated with DMSO as control and PRC1584. Controls display clear endocytic digestive vesicles containing characteristic hemozoin crystals. PRC1584-treated trophozoites lack endocytic vesicles across consecutive sections and do not exhibit hemozoin crystals, indicating disrupted hemoglobin metabolism. All images are shown at matched magnification; scale bars, 500 nm.

To capture the presence/absence aspect of the phenotype, we also calculated the proportion of parasites completely lacking vesicles or crystals. Only a minority of control parasites were vesicle-negative (28%), whereas 54% of PRC1584-treated parasites contained no digestive vesicles at all (Figure 3.6B). This difference was statistically significant (Fisher's exact test, $p = 0.0001$). A similar trend was observed for hemozoin crystals: only 65% of control parasites lacked crystals, compared to 95% of PRC1584-treated parasites (Fisher's exact test, $p = 0.0001$) (Figure 3.6B).

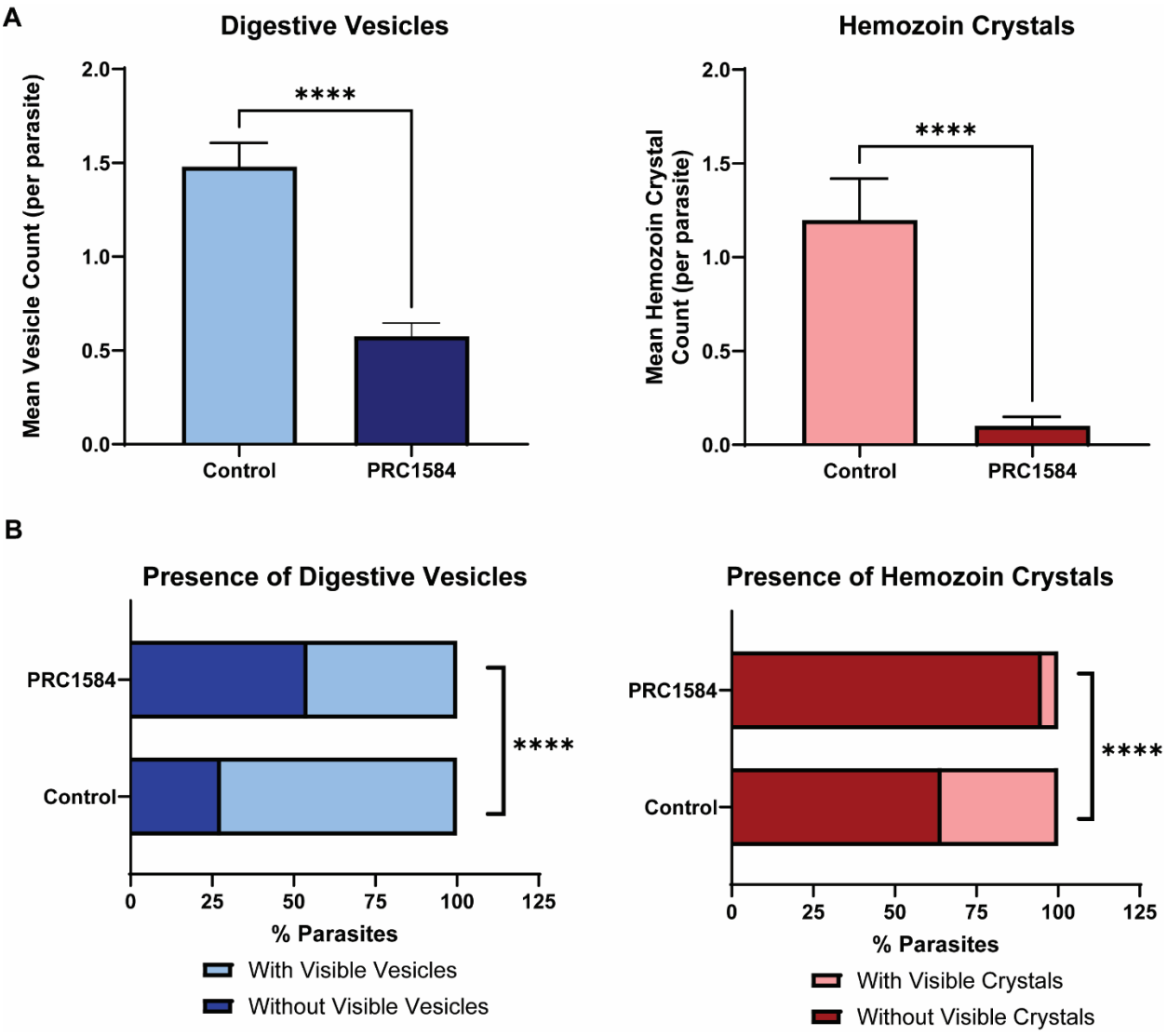

Figure 3.6 PRC1584 reduces the number of digestive vesicles and displays a marked reduction in hemozoin crystal formation.

(A) Quantification of cytostome vesicles and hemozoin crystals from transmission electron micrographs of DMSO-treated control parasites and PRC1584-treated parasites. PRC1584 treatment resulted in a significant reduction in vesicle counts compared to controls (Welch's t-test, $p = 0.0001$), with results consistent using a nonparametric Mann–Whitney test ($p = 0.0001$). ($n = 112$ Control, $n = 120$ PRC1584). Bars indicate mean ± SEM. Hemozoin crystal counts were significantly lower in PRC1584-treated parasites relative to controls (Welch's t-test, $p = 0.0001$; Mann–Whitney, $p = 0.0001$). (B) Percentage of parasites lacking vesicles or parasites lacking hemozoin crystals. Bars show the proportion of parasites that contain visible vesicles parasites or hemozoin crystals. PRC1584 significantly increased the fraction of parasites without vesicles (Fisher's exact test, $p = 0.0001$) as well as significantly increased the fraction of parasites without crystals (Fisher's exact test, $p = 0.0001$).

Vesicle quantification supports a model in which PRC1584 disrupts hemoglobin uptake and catabolism, ultimately impairing hemozoin biocrystallization. This interpretation is reinforced by the biochemical fractionation assays described above, which showed decreased accumulation of both heme and hemozoin in PRC1584-treated samples. Together, these data indicate that this compound class perturbs hemoglobin uptake and metabolism as a key component or consequence of its mechanism of action.

Elucidating PRC1584's Molecular Target(s): A Chemoproteomics Approach

While EM and fractionation assays suggest the cytostome and hemoglobin metabolism as part of the MOA, these phenotypes do not specify the molecular target(s) of PRC1584. Since the observed phenotypes link PRC1584's effect to hemoglobin uptake and early vesicle formation, we focused on a chemoproteomic approach to identify potential molecular targets for further target selection and validation. This work laid the groundwork for ongoing chemoproteomics studies.

Probe Design and Functional Validation

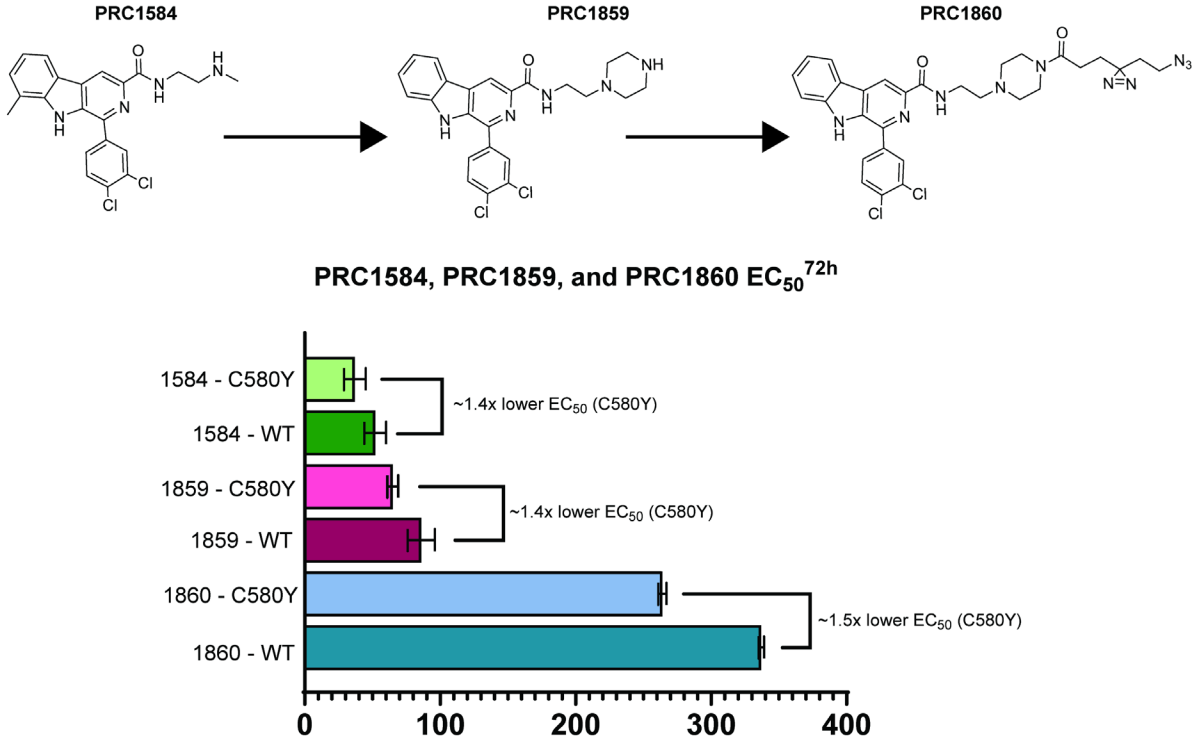

Figure 3.7. PRC1860 synthesis and 72 h EC_{50} values. Bars show mean EC_{50} ± SEM across biological replicates. Differences in the EC_{50} values (NF54-WT vs NF54-K13-C580Y) were tested by extra-sum-of-squares F-test from a global 4-parameter logistic fit (Top/Bottom/Hill shared; logIC50 separate): **** P<0.0001 for all compounds. Bracket labels indicate fold change (K13-C580Y/K13-WT).

We used a stepwise probe design to minimize artifactual readouts. First, we synthesized PRC1859, a minimally perturbed linker-only intermediate that installs the attachment scaffold at the chosen position on the β-carboline core but omits the photo/click functionality. PRC1859 serves three purposes: (i) it tests site tolerance, verifying that modification at this position preserves on-pathway pharmacology (≤ 2–4× EC_{50} shift, parent-like morphology); (ii) it isolates linker effects from photochemistry and copper-click chemistry, ensuring that any loss of activity is not due to the appended tether itself; and (iii) it provides a clean competition control matched in core structure and permeability to the probe. Only after PRC1859 satisfied these checks, the qualified diazirine-azide (QDA) probe was synthetized (PRC1860), enabling UV-triggered

capture and CuAAC click reaction for protein enrichment while retaining the validated activity profile.

Continuous exposure to all three compounds yielded dose-dependent growth inhibition, with 72 h EC_{50} values for NF54 WT and C580Y shown in Figure 3.7. As reported before in chapter 2, The parent β-carboline, PRC1584, showed collateral sensitivity in NF54 K13-C580Y versus NF54 WT with EC_{50}WT = 52 ± 8 nM and EC_{50}C580Y = 37 ± 8 nM, (C580Y/WT = 0.71×; ~1.41-fold lower). A global 4-parameter logistic fit with Top/Bottom/Hill shared across genotypes indicated the EC_{50} values were statistically different (extra-sum-of-squares F-test, $p < 0.0001$). The intermediate scaffold PRC1859 retained this pattern with intermediate potency: EC_{50}WT = 83 ± 10 nM, EC_{50}C580Y = 61 ± 4 nM (C580Y/WT = 0.73×; ~1.37-fold lower and the EC_{50} values were statistically different by extra-sum-of-squares F-test ($p < 0.0001$). PRC1859 was modestly less potent than PRC1584 (1.6-fold and 1.65-fold higher EC_{50} in WT and K13-C580Y, respectively) but maintained the same genotype selectivity, with lower EC_{50}s in K13-C580Y than WT. The analog PRC1860 containing the diazirine–azide modification likewise preserved both overall potency and genotype selectivity: EC_{50}WT = 376 ± 2 nM, EC_{50}C580Y = 258 ± 3 nM (C580Y/WT = 0.69×; ~1.45-fold lower; EC_{50} values were statistically different by sum-of-squares F-test ($p < 0.0001$). Relative to PRC1584, PRC1860 was substantially less potent, with EC_{50} values increased by 7.23-fold in WT and 6.97-fold in K13-C580Y parasites (approximately sevenfold in both lines). Despite this decrease in potency, PRC1860 preserved the PRC1584 selectivity pattern, with lower EC_{50} values in K13-C580Y than in WT, which we considered an acceptable trade-off for a functional photoaffinity probe. Together, these data show that while the addition of the diazirine–azide handle reduces potency, it does not alter the

key biological signature of greater potency in K13-C580Y mutant line supporting that the PRC1860 probe retains a similar mode of action.

PRC1860 Morphological Phenotyping

Having established that PRC1859 and PRC1860 preserve collateral drug sensitivity, with consistently lower EC_{50} values in NF54-K13-C580Y than NF54-WT, we next assessed whether the morphologic consequence of PRC1584 exposure is likewise retained after QDA tagging. We hypothesized that probe analogs would also phenocopy PRC1584-induced dormancy-like phenotype described in chapter 2; any divergent phenotype would suggest off-target effects. To test this, we collected samples from both NF54-C580Y and NF54-WT cultures that were treated with PRC1584 (1 µM), PRC1859 (1 µM), and 1860 (5 µM). Giemsa-stained smears were prepared from samples collected at 0, 24, 48, and 72 h during continuous drug exposure to assess hallmark features of drug-induced quiescence: small pyknotic parasites with condensed nuclei and reduced cytoplasm relative to DMSO controls.

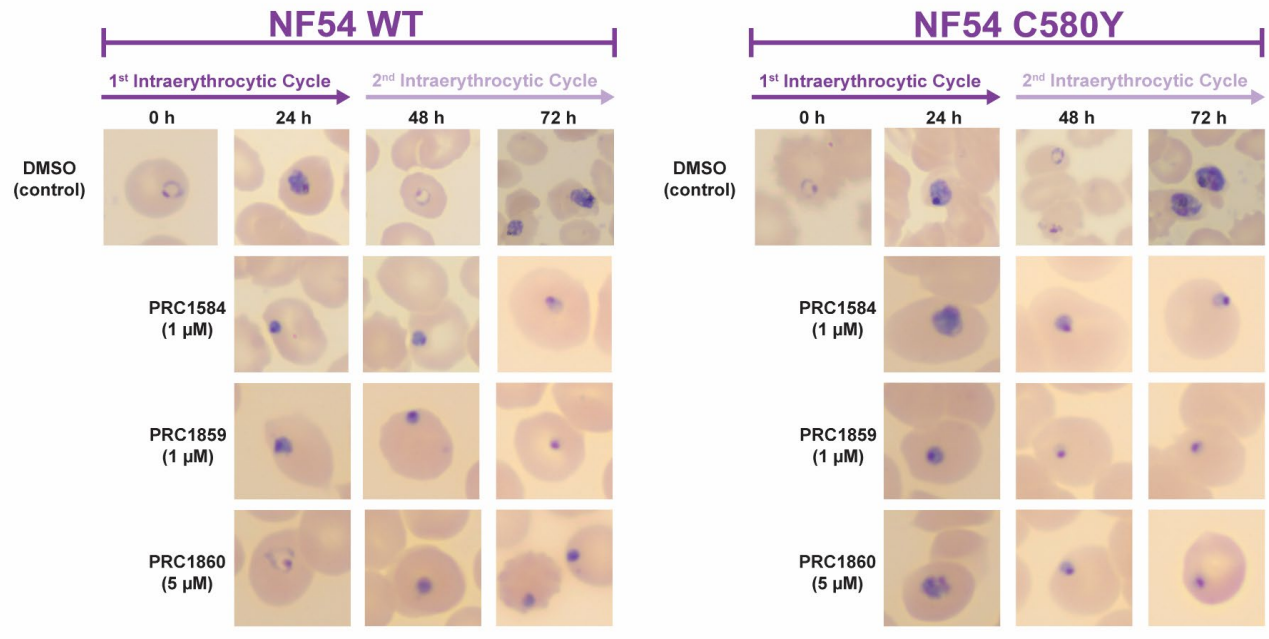

Figure 3.8 PRC1860 retains PRC1584-like Morphological Dormancy Phenotype. Representative Giemsa smears collected at 24-h intervals during 72-h exposure show PRC1584-like dormancy (pyknotic/quiescent forms) for PRC1859 and PRC1860, while DMSO controls progress normally.

Across the 72-h continuous exposure window**,** Giemsa-stained smears obtained from treated cultures showed that the intermediate scaffold (PRC1859) and the QDA-tagged photoaffinity analog (PRC1860) recapitulated PRC1584-like morphologies consistent with drug-induced dormancy-like morphological phenotype. Treated cultures displayed an enrichment of pyknotic/quiescent forms, condensed nuclei with reduced cytoplasm, whereas DMSO controls progressed normally through ring→ trophozoite → schizont stages (Figure 3.8). The qualitative phenotype tracked the potency ranking (PRC1584 > PRC1859 > PRC1860) and was more apparent in K13-C580Y mutant than NF54 WT strain at matched concentrations, mirroring their lower EC_{50} values. The sustained PRC1584-like morphology across days indicates on-target behavior for both analogs and makes it unlikely that QDA tagging introduced an off-target cytological artifact. On this basis, PRC1860 is considered a suitable chemoproteomics probe for downstream photoaffinity labeling and protein target capture.

Photoaffinity Labeling Optimization by Western Blot

To validate that the QDA-tagged probe is able to capture target(s) under *in vivo* (live parasites), we established a labeling workflow (Figure 3.9). Cultures enriched with late ring/early trophozoite stages were treated with PRC1860 or DMSO, followed by UV *in vivo* crosslinking to the potential protein targets. Parasites were then freed from the host erythrocyte by saponin treatment and lysed by snap-freeze/shear in NP-40 buffer with to release the protein content.

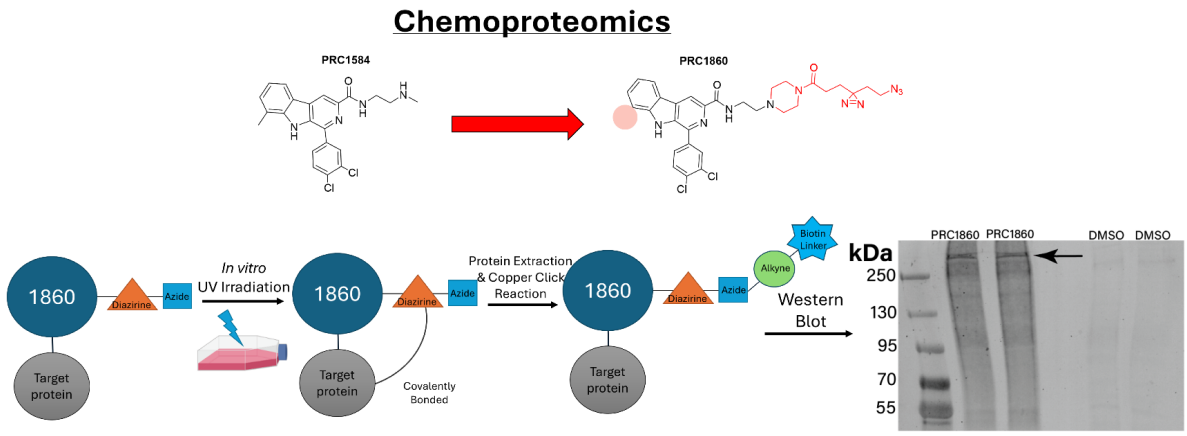

Figure 3.9 PRC1860 design, workflow, and results obtained by western blot. Initial blot detection of PRC1860 labeling in whole cell parasites. Streptavidin–LI-COR reveals probe-labeled bands in PRC1860-treated samples, with no detectable bands in DMSO controls.

Protein lysates were subjected to copper-catalyzed azide–alkyne cycloaddition (CuAAC) using azide-PEG3-biotin and a pre-mixed catalyst system added in a fixed order (biotin azide → TCEP → TBTA → $CuSO_4$). Reaction mixtures were incubated for 1 h at room temperature. To establish workable CuAAC conditions, we varied a small set of reaction parameters (protein load, detergent strength, and blocking reagent) and monitored labeling qualitatively by Western blot. Under selected conditions, PRC1860-treated samples displayed clear, probe-dependent labeling, whereas DMSO controls showed no detectable signal. Increasing protein load produced proportionally stronger bands and using a slightly higher non-ionic detergent concentration improved signal clarity, consistent with better solubilization rather than nonspecific background.

These observations confirm that PRC1860–protein adducts can be captured by CuAAC and visualized by Western blot in whole-parasite lysates. Although we did not perform a full quantitative optimization series, the qualitative improvements in signal intensity and low

background in DMSO controls provided a robust set of conditions for downstream probe development and future mass spectrometry–based target identification workflows.

Discussion

Summary of findings.

Across short-pulse and continuous exposures, PRC1584 produced a coherent mechanistic signature: (i) collateral sensitivity in NF54 K13-C580Y versus NF54 WT as evidenced by lower EC_{50} values in PfK13-C580Y mutant parasites across both 8 h and 72 h dose-dependent growth inhibition assays (Figure 3.2), (ii) no increase in free-heme:hemozoin ratio despite a reduction in total heme (Figure 3.4), and (iii) ultrastructural and cytological defects consistent with failure of cytostomal endocytosis and hemoglobin metabolism, including fewer digestive vesicles and loss of hemozoin crystals (Figures 3.5–3.6). TEM and fractionation assay sample sizes are modest, so results should be considered alongside effect sizes and consistency among methods. Together, these data favor a model in which PRC1584 impairs hemoglobin uptake and digestive vesicle formation, starving the parasite of protein precursors rather than provoking a heme-burst toxicity. In addition, the PRC1584-derivative probe (PRC1860) developed for future chemoproteomic analysis conserved PRC1584's biological fingerprint by inducing the dormant-like phenotype when added in ring stage. The intermediate analog PRC1859 maintained genotype selectivity with modest potency loss. The diazirine–azide probe PRC1860 also retained rank-order potency in PfK13-C580Y when compared to the WT strain (Figure 3.7) and a probe-specific labeling pattern was observed by western blot (Figure 3.9). However, it is important to mention that photoaffinity techniques tend to favor proteins that are plentiful, easily accessible, and located near membranes, whereas copper-click chemistry results may vary depending on the presence of

matrix chelators and the type of detergent used. Thus, results must be validated through orthogonal approaches including competition with its precursor, active and inactive analogs.

Proposed Mechanism of action of PRC1584.

Based on the results described above, we propose that PRC1584 acts potentially by affecting the cytostome formation that ultimately prevents the formation of the DV in the malaria parasite. In this model, drug engagement reduces the flux of host hemoglobin by limiting the formation of digestive vesicles, thereby diminishing hemozoin formation by lowering the total heme pool available for crystallization without increasing the free-heme:hemozoin ratio as supported by the observation of empty digestive vesicles by electron microscopy. This substrate deprivation for protein synthesis may cause the quiescent/pyknotic forms observed when parasites in ring stage are exposed to PRC1584 or its analogs. The collateral sensitivity observed in the PfK13-C580Y mutant further supports this hypothesis as PfK13 localizes to the cytostomal collar and supports endocytic uptake[17, 21]. Moreover, PfK13-C580Y mutant parasites exhibited reduced K13 protein levels (Figure 3.3) as described before[23] which has been linked to a reduced formation of digestive vesicles[28]. Therefore, PRC1584 further perturbs this already strained pathway, producing greater apparent potency in the PfK13-C580Y mutant when compared to K13-WT parasites.

It should be noted that PRC1584 exhibits a distinct mode of action compared to DHA. Although the potency of PRC1584 increases during the late ring and early trophozoite stages—coinciding with maximum hemoglobin uptake—and it shares a similar morphological phenotype as outlined in Chapter 2, its mechanism remains differentiated. This distinction will matter when comparing recrudescence and partner-drug hypotheses in Chapter 4.

Alternative hypotheses of PRC1584 mode of action.

Three alternatives hypothesis deserve consideration. First, PRC1584 might primarily affect vesicle release rather than cytostome formation *per se*; the EM evidence shows malformed collars and paucity of vesicles but cannot by itself differentiate entry versus delivery of vesicles. Second, decreased pigment could, in principle, reflect altered pH/protease activity in the digestive vesicles rather than reduced cargo. The free-heme:hemozoin ratio argues against catastrophic disruption of heme detoxification but does not exclude more modest alterations in hemoglobin uptake, vesicle formation, or trafficking dynamics. Third, our probe might be interacting with more than one protein, not due to unspecific interactions, but because the real target sits in a tiny cluster of proteins that work shoulder-to-shoulder at the cytostome (the collar/tether/fusion machinery). When we expose the diazirine to UV, it makes an ultra-short-lived 'sticky' species that reaches only a few atoms' distance. Meaning, if the probe is bound to one protein, the UV step can weld it either to that protein or to an immediate neighbor that's touching it. In other words, a single true binding event can leave covalent footprints on several members of the same physical complex. That's why we may see multiple labeled bands even if there is only one pharmacologic target.

Conclusions

PRC1584 drives a convergent phenotype: malformed cytostomes, reduced digestive vesicle formation, and absent pigment that is consistent with inhibition of the hemoglobin-uptake pathway rather than direct disruption of heme detoxification, which is further supported by the collateral drug sensitivity and reduced K13 protein levels observed in the PfK13-C580Y mutant.

A stepwise probe strategy development produced a diazirine–azide probe (PRC1860) that retain the parent's biological fingerprint while enabling specific labeling for future chemoproteomic mapping. While future work is guaranteed to identify PRC1584 molecular target(s), the integrated data justify a target-neighborhood model centered on cytostome formation and vesicle formation.

Methods

Chemicals. Dihydroartemisinin and chloroquine were obtained from Sigma-Aldrich (St. Louis, MO). PRC1584 was synthesized and purified, as previously described[22, 29]. All compounds were reconstituted at 10 mM in DMSO, except for chloroquine which was reconstituted in water.

***Plasmodium falciparum* Cultures.** The *P. falciparum* strain NF54 (MRA-1000) were obtained from MR4 (ATCC, Manassas, VA; BEI Resources, NIAID, NIH). The *P. falciparum* NF54-PfK13-C580Y strain were kindly supplied by David Fidock[21]. All *P. falciparum* strains were maintained in O^+ positive human erythrocytes (Grifols, Memphis, TN, USA) at 5% hematocrit in RPMI 1640 media (Thermo Fisher Scientific, Waltham, MA) containing 2 g/L glucose, 5.94 g/L HEPES, 2.3 g/L sodium bicarbonate, 5 g/L Albumax I, and 50 mg/L hypoxanthine. All reagents were obtained from Sigma-Aldrich (St. Louis, MO). Media was supplemented with 20 mg/L of gentamicin (Thermo Fisher Scientific, Waltham, MA). Parasite cultures were maintained at 37°C under reduced oxygen conditions (5% CO_2, 5% O_2, and 90% N_2) with shaking. Highly synchronous ring stage cultures (>98%) were obtained through two consecutive 5% sorbitol treatments (Sigma-Aldrich, St. Louis, MO) performed 6 h apart.

***P. falciparum* Growth Inhibition Assay.** Dose-dependent growth inhibition with the reported compounds were evaluated using a 10-point dilution series and the *in vitro* SYBR Green I assay as a readout. Synchronous ring-stage parasites (1% starting parasitemia, 1% hematocrit) were cultured in 96-well half-area dark plates and continuously exposed to each compound for 72 hours at 37 °C under reduced oxygen conditions (5% CO_2, 5% O_2, and 90% N_2). After 72 hours of incubation, parasite growth was assessed by the SYBR Green I assay as previously described[30]. SYBR Green I was excited at 485 nm, and its emission was measured at 535 nm using a Cytation5 plate reader. Parasite growth was normalized to untreated control parasites and calculated as a percentage. Background was determined using uninfected red blood cells (RBCs).

Dose-dependent assays were performed in at least two biological replicates and two technical replicates. Reported values represent the mean of biological replicates with standard error of the mean (SEM). Initial concentrations were optimized after compound screening to ensure the EC_{50} fell within the tested range. DMSO concentrations were maintained ≤0.02% in all assays. Data were fitted using a four-parameter logistic dose-response curve, and half-maximal effective concentration (EC_{50}) values were calculated using GraphPad Prism (GraphPad Software, Inc.). Assays comparing EC_{50} values across different parasite lines were performed concurrently. 8-hour washout assays were performed as described above with modifications. Parasites of the *P. falciparum* NF54 WT and C580Y strains were synchronized in the ring stage 48 h prior to the assay by two rounds of 5% sorbitol treatment (Sigma-Aldrich, St. Louis, MO) with a 6 h interval between treatments. After parasites completed one lifecycle and reinvaded RBCs, an additional sorbitol treatment was performed on the day of the assay to obtain highly synchronous early rings. Synchronized infected RBCs were plated in 96-well plates and sequentially exposed to compounds for 8-hours. After incubation, compounds were removed by

three rounds of washing with pre-warmed RPMI to avoid growth delays, and infected RBCs were transferred to a new plate. Plates were incubated under standard culture conditions, and parasite growth was assessed 72 h after the start of the assay using the SYBR Green I assay as described above. A 72-hour continuous exposure dose-response curve was included in parallel as control. Dose-response data were fitted using a four-parameter logistic dose-response curve and EC_{50} values were calculated using GraphPad Prism (GraphPad Software, Inc.). Assays were performed in at least two independent biological replicates, each with two to four technical replicates.

Parasite extraction from red blood cells. Samples for western blots and fractionation assays were prepared by growing synchronized ring-stage *P. falciparum* NF54 WT and NF54 C580Y to 15-20% parasitemia at 5% hematocrit (late ring/early trophozoite stages). Then, the parasites were incubated for 5 hours with either 5 μM PRC1584, 1 μM CQ, or an equal amount of DMSO for fractionation assays. For WBs, parasites were not treated with any conditions. After incubation, cultures were spun down, and the remaining supernatant was aspirated off. Then, cultures were treated with 0.1% saponin in 1X Phosphate buffered saline (PBS) to lyse RBCs. Samples were then again spun down, creating a pellet of parasites. These parasite lysate pellets were then washed three times with 1X PBS to remove remaining red blood cell debris and stored at −80 °C until ready for use.

Western Blotting and PfK13 Protein Level Quantification. Equal amounts of NF54 WT or NF54 C580Y parasite pellet, prepared as above, were loaded onto Mini-PROTEAN® TGX™ Precast Protein Gels (Bio-Rad Laboratories, Hercules, CA, USA). A total of 10 μl of Protein

Plus Kaleidoscope Ladder (Thermo Scientific) were run alongside samples as the molecular weight standard. Proteins were then separated in 1× TGS buffer (Thermo Scientific) for 25 minutes at 180 V. Bands were transferred onto a nitrocellulose membrane using iBlot®-2 Transfer System (Thermo Fisher Scientific, Waltham, MA, USA). Total protein was visualized on the membrane by Ponceau-S to ensure equal sample loads[31]. Pictures were transformed into 8-bit ImageJ[32], and the total protein stain density was quantified by measuring the densitometry of all the bands per lane. The membrane was destained in distilled water and blocked in LI-COR Intercept Blocking Buffer (Thermo Scientific Chemicals). We used a monoclonal K13 antibody (E9 clone; kindly provided by David Fidock) at a dilution of 1:1000 in Intercept Blocking Buffer rocking overnight at 4°C. The membrane was rinsed in PBST, incubated in 1:20,000 dilution of IRDye 800CW or IRDye 680RD secondary antibody (LI-COR Biotech) in Intercept Blocking Buffer for 1 hour at room temperature and rinsed in PBST. Membranes were imaged using the Odyssey Clx LI-COR infrared imaging system (LI-COR Biotech). Images were processed and analyzed using ImageStudio (LI-COR Biosciences) and transformed into 8-bit pictures, and the adjusted band density was calculated in ImageJ by dividing the K13 band density by the total protein stain density.

Isolation of Hemoglobin, Free Heme, and Hemozoin Fractions. The quantification of hemoglobin, heme, and hemozoin was done using a modified method developed by Combrinck et al.[26] but was later adjusted by Birrell et al[27]. For a high throughput workflow, we used the adjusted method for this experiment. Following the preparation of the samples, the parasite pellet was resuspended in 50 µL of Milli-Q water and sonicated for 5 minutes. Post-sonication, 50 µL of 0.2 M HEPES was added to the resuspended sample, and the mixture was then centrifuged at

4000 rpm for 20 minutes. The resulting supernatant was carefully transferred to a new tube, and 50 µL of 4% SDS was added. This mixture was incubated at 95 °C for 5 minutes. Following heating, 50 µL of 0.3 M NaCl and 50 µL of 25% pyridine in 0.2 M HEPES were added. The entire mixture was vortexed and transferred to a 96-well UV-Vis imaging plate. This sample constituted the hemoglobin fraction. Simultaneously, the pellet from the prior step underwent further treatment. To the pellet, 50 µL of Milli-Q water and 50 µL of 4% SDS were added, and the sample was resuspended via sonication for 5 minutes. The sample was then incubated at 95 °C for 5 minutes to solubilize the free heme. After the heating step, 50 µL of 0.2 M HEPES, 0.3 M NaCl, and 25% pyridine were added to the resuspended pellet. The mixture was then centrifuged at 4000 rpm for 20 minutes. The resulting supernatant was transferred to a separate well in the 96-well UV-Vis imaging plate, designating this sample as the free heme fraction. The remaining pellet underwent further treatment. To the vial, 100 µL of Milli-Q water and 100 µL of 0.3 M NaOH were added and sonicated for 15 minutes. Finally, 100 µL of 0.2 M HEPES, 0.3 M HCl, and 25% pyridine in HEPES was incorporated into the solution. The resulting mixture was transferred to the 96-well plate. This sample contained the hemozoin fraction.

Absorbance Measurement and Statistical Analysis Free heme and hemozoin were quantified using the UV–Vis absorbance method described by Combrinck et al[26]. After processing, each sample was read at 405 nm on a UV–Vis spectrophotometer, and the raw absorbance values were exported into Excel and organized by biological replicate, technical replicate, and treatment condition. Technical replicates from the same biological replicate were averaged to give one value per BioRep × Condition × Fraction (Free heme or Hemozoin). To correct for day-to-day

variation, all measurements were normalized to the paired DMSO control from the same biological replicate. Two metrics were calculated:

- FoldRatio = (Free heme ÷ hemozoin) $_{\text{treated}}$ ÷ (Free heme ÷ hemozoin) $_{\text{DMSO}}$
- FoldBudget = (Free heme + hemozoin) $_{\text{treated}}$ ÷ (Free heme + Hemozoin) $_{\text{DMSO}}$

Because these fold changes are multiplicative, statistical testing was performed on the $\log_{10}$-transformed values. Log_{10}(FoldRatio) and $\log_{10}$(FoldBudget) were compared to zero using two-tailed one-sample t-tests. When multiple treatments were evaluated within the same experiment (e.g., PRC1584 and CQ), a Holm–Šídák correction was applied to control for multiple comparisons. Nonparametric Wilcoxon signed-rank tests were also run as a robustness check. For visualization, results are plotted on a linear axis as fold change relative to DMSO (mean ± SEM), while all hypothesis testing is performed on the $\log_{10}$-transformed values. Data processing was carried out in Excel and statistical testing and graphing in GraphPad Prism.

Electron Microscopy. Samples were prepared by growing up synchronized ring-stage parasites *P. falciparum* NF54 WT and NF54 C580Y to 20-30% parasitemia (late ring/early trophozoite) at 5% hematocrit. On the day of treatment, parasites were resynchronized, washed twice with RPMI, and culture was then split in half. One sample was treated with 5 μM of PRC1584 and the other received DMSO equivalent and was incubated for 5 hours before splitting samples in half again. Newly aliquot samples were washed with 100 nM Cacodylate buffer and then pelleted gently (~20 μl of sample). Cells were then fixed with 2% paraformaldehyde, 2.5% glutaraldehyde, in a 100 mM Cacodylate solution for 2 hours at room temperature. After incubations, samples were spun down, supernatant was removed, and cells were washed in sodium cacodylate buffer for morphological analyses at the ultrastructural level, infected RBCs

were fixed in 2% paraformaldehyde/2.5% glutaraldehyde (Ted Pella Inc., Redding, CA) in 100 mM cacodylate buffer, pH 7.2 for 2 h at room temperature. Samples were washed in cacodylate buffer and postfixed in 1% osmium tetroxide (Ted Pella Inc.)/ 1.5% potassium ferricyanide (Sigma, St. Louis, MO) for 1 hr. Samples were then rinsed extensively in dH_20 prior to en bloc staining with 1% aqueous uranyl acetate (Ted Pella Inc.) for 1 hr. Following several rinses in dH20, samples were dehydrated in a graded series of ethanol and embedded in Eponate 12 resin (Ted Pella Inc.). Ultrathin sections of 95 nm were cut with a Leica Ultracut UCT ultramicrotome (Leica Microsystems Inc., Bannockburn, IL), stained with uranyl acetate and lead citrate, and viewed on a JEOL 1200 EX transmission electron microscope (JEOL USA Inc., Peabody, MA) equipped with an AMT 8 megapixel digital camera and AMT Image Capture Engine V602 software (Advanced Microscopy Techniques, Woburn, MA).

Morphological Phenotyping. Giemsa phenotyping was performed in parallel with 72-h EC_{50} assays. Thin smears were prepared at 0, 24, 48, and 72 h during continuous exposure, methanol-fixed, and stained with 10% Giemsa. Slides were examined at 1000× oil immersion and scored qualitatively for pyknotic/quiescent morphology (nuclear condensation, reduced cytoplasmic volume/intensity) relative to DMSO controls.

***In vivo* photo-crosslinking, CuAAC click reaction, and immunodetection.** Parasites were enriched for late rings/early trophozoites, treated with PRC1860 (or DMSO), followed by UV activation performed at 365 nm for 15 min in a clear plate (pre-warmed lamp; energy recorded; 50 µL per sample). Following *in vivo* crosslinking, infected erythrocyte cultures were harvested, and parasites were released from host cells by selective permeabilization with saponin. Cell

pellets were resuspended in ice-cold 0.01% (w/v) saponin in PBS supplemented with a 1× EDTA-free protease inhibitor cocktail and incubated at 37 °C for 5 min with gentle mixing, followed by 5 min on ice. Parasites were collected by centrifugation (e.g., 2,500–3,000 × g, 5 min, 4 °C), the supernatant containing lysed host material was discarded, and the pellets were washed 2–3 times with ice-cold PBS containing protease inhibitors to remove residual hemoglobin and saponin. At this point, parasite pellets could be either processed immediately or flash-frozen and stored at −80 °C. For detergent lysis, parasite pellets were resuspended in NP-40 lysis buffer (PBS or Tris-based buffer containing 1% NP-40 and 1× protease inhibitor cocktail) at a volume sufficient to fully disperse the pellet and incubated on ice for ~10 min. Lysates were then subjected to three snap freeze–thaw cycles (liquid nitrogen → 37 °C water bath) to enhance disruption, followed by mechanical shearing through a 29-gauge insulin syringe (5–10 passes). Insoluble material was removed by centrifugation at 10,000 × g for 10 min at 4 °C, and the clarified supernatant (NP-40–soluble parasite lysate) was collected for downstream CuAAC labeling and Western blot analysis. CuAAC used azide-PEG3-biotin with TCEP (fresh, 50 mM), TBTA (1.6 mM in 80% tert-butanol/20% DMSO), and $CuSO_4$ (50 mM), combined in the order biotin azide → TCEP → TBTA → $CuSO_4$; reactions proceeded 1 h at RT with agitation. Total protein was normalized by BCA (duplicates; 200 µL WR/well; 30 min at 37 °C) prior to SDS-PAGE and LI-COR streptavidin detection. DMSO served as a control.

Acknowledgements

I thank David A. Fidock for generously providing the anti-K13 (E9) monoclonal antibody, and Wandy Beatty for expert transmission electron microscopy imaging and guidance that made the

ultrastructural analyses possible. I’m grateful to Dr. Maria B. Cassera for mentorship and to members of the Cassera Lab for thoughtful discussions and help with assays and figure review.

References

(1) Organization, W. H. *World malaria report 2024: addressing inequity in the global malaria response.* ; 2024.
(2) Dondorp, A. M.; Nosten, F.; Yi, P.; Das, D.; Phyo, A. P.; Tarning, J.; Lwin, K. M.; Ariey, F.; Hanpithakpong, W.; Lee, S. J.; et al. Artemisinin resistance in Plasmodium falciparum malaria. *N Engl J Med* **2009**, *361* (5), 455–467. DOI: 10.1056/NEJMoa0808859 From NLM Medline.
(3) Straimer, J.; Gnädig, N. F.; Witkowski, B.; Amaratunga, C.; Duru, V.; Ramadani, A. P.; Dacheux, M.; Khim, N.; Zhang, L.; Lam, S.; et al. K13-propeller mutations confer artemisinin resistance in Plasmodium falciparum clinical isolates. *Science* **2015**, *347* (6220), 428–431. DOI: doi:10.1126/science.1260867.
(4) Burrows, J. N.; Duparc, S.; Gutteridge, W. E.; Hooft van Huijsduijnen, R.; Kaszubska, W.; Macintyre, F.; Mazzuri, S.; Möhrle, J. J.; Wells, T. N. C. New developments in anti-malarial target candidate and product profiles. *Malaria Journal* **2017**, *16* (1), 26. DOI: 10.1186/s12936-016-1675-x.
(5) Okombo, J.; Fidock, D. A. Towards next-generation treatment options to combat Plasmodium falciparum malaria. *Nature Reviews Microbiology* **2025**, *23* (3), 178–191. DOI: 10.1038/s41579-024-01099-x.
(6) Witkowski, B.; Amaratunga, C.; Khim, N.; Sreng, S.; Chim, P.; Kim, S.; Lim, P.; Mao, S.; Sopha, C.; Sam, B.; et al. Novel phenotypic assays for the detection of artemisinin-resistant Plasmodium falciparum malaria in Cambodia: in-vitro and ex-vivo drug-response studies. *Lancet Infect Dis* **2013**, *13* (12), 1043–1049. DOI: 10.1016/S1473-3099(13)70252-4 From NLM Medline.
(7) Abu Bakar, N.; Klonis, N.; Hanssen, E.; Chan, C.; Tilley, L. Digestive-vacuole genesis and endocytic processes in the early intraerythrocytic stages of Plasmodium falciparum. *J Cell Sci* **2010**, *123* (Pt 3), 441–450. DOI: 10.1242/jcs.061499 From NLM Medline.
(8) Spielmann, T.; Gras, S.; Sabitzki, R.; Meissner, M. Endocytosis in Plasmodium and Toxoplasma Parasites. *Trends Parasitol* **2020**, *36* (6), 520–532. DOI: 10.1016/j.pt.2020.03.010 From NLM Medline.
(9) Bakar, N. A.; Klonis, N.; Hanssen, E.; Chan, C.; Tilley, L. Digestive-vacuole genesis and endocytic processes in the early intraerythrocytic stages of Plasmodium falciparum. *Journal of Cell Science* **2010**, *123* (3), 441–450. DOI: 10.1242/jcs.061499 (accessed 9/9/2025).
(10) Milani, K. J.; Schneider, T. G.; Taraschi, T. F. Defining the morphology and mechanism of the hemoglobin transport pathway in Plasmodium falciparum-infected erythrocytes. *Eukaryot Cell* **2015**, *14* (4), 415–426. DOI: 10.1128/ec.00267-14 From NLM.
(11) Garnie, L. F.; Egan, T. J.; Wicht, K. J. Heme Detoxification in the Malaria Parasite Plasmodium falciparum: A Time-Dependent Basal-Level Analysis. *bioRxiv* **2025**. DOI: 10.1101/2025.03.06.641703 From NLM.
(12) Rosenthal, P. J.; Meshnick, S. R. Hemoglobin catabolism and iron utilization by malaria parasites. *Mol Biochem Parasitol* **1996**, *83* (2), 131–139. DOI: 10.1016/s0166-6851(96)02763-6 From NLM Medline.
(13) Tutor, M. V.; Shami, G. J.; Siddiqui, G.; Creek, D. J.; Tilley, L.; Ralph, S. A. The Plasmodium falciparum artemisinin resistance-associated protein Kelch 13 is required for formation of normal cytostomes. eLife Sciences Publications, Ltd: 2023.
(14) Ariey, F.; Witkowski, B.; Amaratunga, C.; Beghain, J.; Langlois, A. C.; Khim, N.; Kim, S.; Duru, V.; Bouchier, C.; Ma, L.; et al. A molecular marker of artemisinin-resistant Plasmodium falciparum malaria. *Nature* **2014**, *505* (7481), 50–55. DOI: 10.1038/nature12876 From NLM.

(15) Birnbaum, J.; Flemming, S.; Reichard, N.; Soares, A. B.; Mesén-Ramírez, P.; Jonscher, E.; Bergmann, B.; Spielmann, T. A genetic system to study Plasmodium falciparum protein function. *Nature Methods* **2017**, *14* (4), 450–456. DOI: 10.1038/nmeth.4223.
(16) Mbengue, A.; Bhattacharjee, S.; Pandharkar, T.; Liu, H.; Estiu, G.; Stahelin, R. V.; Rizk, S. S.; Njimoh, D. L.; Ryan, Y.; Chotivanich, K.; et al. A molecular mechanism of artemisinin resistance in Plasmodium falciparum malaria. *Nature* **2015**, *520* (7549), 683–687. DOI: 10.1038/nature14412 From NLM.
(17) Birnbaum, J.; Scharf, S.; Schmidt, S.; Jonscher, E.; Hoeijmakers, W. A. M.; Flemming, S.; Toenhake, C. G.; Schmitt, M.; Sabitzki, R.; Bergmann, B.; et al. A Kelch13-defined endocytosis pathway mediates artemisinin resistance in malaria parasites. *Science* **2020**, *367* (6473), 51–59. DOI: 10.1126/science.aax4735 From NLM Medline.
(18) Yang, T.; Yeoh, L. M.; Tutor, M. V.; Dixon, M. W.; McMillan, P. J.; Xie, S. C.; Bridgford, J. L.; Gillett, D. L.; Duffy, M. F.; Ralph, S. A.; et al. Decreased K13 Abundance Reduces Hemoglobin Catabolism and Proteotoxic Stress, Underpinning Artemisinin Resistance. *Cell Reports* **2019**, *29* (9), 2917–2928.e2915. DOI: 10.1016/j.celrep.2019.10.095 (accessed 2025/09/05).
(19) Hott, A.; Casandra, D.; Sparks, K. N.; Morton, L. C.; Castanares, G. G.; Rutter, A.; Kyle, D. E. Artemisinin-resistant Plasmodium falciparum parasites exhibit altered patterns of development in infected erythrocytes. *Antimicrob Agents Chemother* **2015**, *59* (6), 3156–3167. DOI: 10.1128/aac.00197-15 From NLM.
(20) Gupta, D. K.; Patra, A. T.; Zhu, L.; Gupta, A. P.; Bozdech, Z. DNA damage regulation and its role in drug-related phenotypes in the malaria parasites. *Sci Rep* **2016**, *6*, 23603. DOI: 10.1038/srep23603 From NLM.
(21) Gnadig, N. F.; Stokes, B. H.; Edwards, R. L.; Kalantarov, G. F.; Heimsch, K. C.; Kuderjavy, M.; Crane, A.; Lee, M. C. S.; Straimer, J.; Becker, K.; et al. Insights into the intracellular localization, protein associations and artemisinin resistance properties of Plasmodium falciparum K13. *PLoS Pathog* **2020**, *16* (4), e1008482. DOI: 10.1371/journal.ppat.1008482 From NLM Medline.
(22) Mathew, J.; Ding, S.; Kunz, K. A.; Stacy, E. E.; Butler, J. H.; Haney, R. S.; Merino, E. F.; Butschek, G. J.; Rizopoulos, Z.; Totrov, M.; et al. Malaria Box-Inspired Discovery of N-Aminoalkyl-beta-carboline-3-carboxamides, a Novel Orally Active Class of Antimalarials. *ACS Med Chem Lett* **2022**, *13* (3), 365–370. DOI: 10.1021/acsmedchemlett.1c00663.
(23) Behrens, H. M.; Schmidt, S.; Henshall, I. G.; López-Barona, P.; Peigney, D.; Sabitzki, R.; May, J.; Maïga-Ascofaré, O.; Spielmann, T. Impact of different mutations on Kelch13 protein levels, ART resistance, and fitness cost in Plasmodium falciparum parasites. *mBio* **2024**, *15* (6), e0198123. DOI: 10.1128/mbio.01981-23 From NLM.
(24) Schmidt, S.; Wichers-Misterek, J. S.; Behrens, H. M.; Birnbaum, J.; Henshall, I. G.; Dröge, J.; Jonscher, E.; Flemming, S.; Castro-Peña, C.; Mesén-Ramírez, P.; et al. The Kelch13 compartment contains highly divergent vesicle trafficking proteins in malaria parasites. *PLoS Pathog* **2023**, *19* (12), e1011814. DOI: 10.1371/journal.ppat.1011814 From NLM.
(25) Rahman, A.; Tamseel, S.; Dutta, S.; Khan, N.; Faaiz, M.; Rastogi, H.; Nath, J. R.; Haldar, K.; Chowdhury, P.; Ashish; et al. Artemisinin-resistant Plasmodium falciparum Kelch13 mutant proteins display reduced heme-binding affinity and decreased artemisinin activation. *Communications Biology* **2024**, *7* (1), 1499. DOI: 10.1038/s42003-024-07178-2.

(26) Combrinck, J. M.; Mabotha, T. E.; Ncokazi, K. K.; Ambele, M. A.; Taylor, D.; Smith, P. J.; Hoppe, H. C.; Egan, T. J. Insights into the role of heme in the mechanism of action of antimalarials. *ACS Chem Biol* **2013**, *8* (1), 133–137. DOI: 10.1021/cb300454t From NLM.
(27) Birrell, G. W.; Challis, M. P.; De Paoli, A.; Anderson, D.; Devine, S. M.; Heffernan, G. D.; Jacobus, D. P.; Edstein, M. D.; Siddiqui, G.; Creek, D. J. Multi-omic Characterization of the Mode of Action of a Potent New Antimalarial Compound, JPC-3210, Against Plasmodium falciparum. *Mol Cell Proteomics* **2020**, *19* (2), 308–325. DOI: 10.1074/mcp.RA119.001797 From NLM.
(28) Wiser, M. F. The Digestive Vacuole of the Malaria Parasite: A Specialized Lysosome. *Pathogens* **2024**, *13* (3). DOI: 10.3390/pathogens13030182 From NLM.
(29) Mathew, J.; Zhou, B.; Haney, R. S.; Kunz, K. A.; Do Amaral, L. S.; Roy Chowdhury, R.; Butler, J. H.; Li, H.; Chakraborty, A. J.; Tabassum, A.; et al. beta-Carboline-3-carboxamide Antimalarials: Structure-Activity Relationship, ADME-Tox Studies, and Resistance Profiling. *ACS Infect Dis* **2024**, *10* (11), 3951–3962. DOI: 10.1021/acsinfecdis.4c00653 From NLM Medline.
(30) Smilkstein, M.; Sriwilaijaroen, N.; Kelly, J. X.; Wilairat, P.; Riscoe, M. Simple and inexpensive fluorescence-based technique for high-throughput antimalarial drug screening. *Antimicrob Agents Chemother* **2004**, *48* (5), 1803–1806. DOI: 10.1128/aac.48.5.1803-1806.2004.
(31) Romero-Calvo, I.; Ocón, B.; Martínez-Moya, P.; Suárez, M. D.; Zarzuelo, A.; Martínez-Augustin, O.; de Medina, F. S. Reversible Ponceau staining as a loading control alternative to actin in Western blots. *Anal Biochem* **2010**, *401* (2), 318–320. DOI: 10.1016/j.ab.2010.02.036 From NLM.
(32) Schneider, C. A.; Rasband, W. S.; Eliceiri, K. W. NIH Image to ImageJ: 25 years of image analysis. *Nat Methods* **2012**, *9* (7), 671–675. DOI: 10.1038/nmeth.2089 From NLM.

CHAPTER 4

CONCLUSIONS AND FUTURE DIRECTIONS

From phenotype to mechanism: PRC1584 as a tool and lead for disrupting hemoglobin uptake in *Plasmodium falciparum*

Executive Summary of Dissertation

This dissertation characterized the novel β-carboline PRC1584 and converged on the cytostome-mediated endocytic pathway as a central component of its mechanism of action. By integrating stage-specific pharmacology, quantitative heme/hemozoin measurements, ultrastructural analysis of cytostomes and vesicles, K13-linked collateral sensitivity and protein levels, and photoaffinity probes derived from the parent scaffold (PRC1859/PRC1860), I developed a cytostome-focused model that explains both the phenotypic and genotypic responses to PRC1584. Chapter 2 shows that PRC1584 is active against ring stages, eliminates DHA-induced dormant rings, maintains low-nanomolar potency in field isolates, and exhibits a high barrier to resistance. Chapter 3 dissects the underlying mechanism: total heme levels decline without an increase in the free-heme:hemozoin ratio, consistent with curtailed hemoglobin uptake and metabolism rather than a heme "burst" (in contrast to chloroquine, which increases the ratio without acutely depleting the total heme pool). Electron microscopy reveals malformed cytostomes and fewer digestive vesicles, and K13-C580Y parasites display collateral sensitivity and reduced K13 protein levels, pointing toward perturbation of hemoglobin uptake, vesicle formation, or hemoglobin metabolism rather than direct inhibition of hemozoin crystallization. Finally, the PRC1860 probe

preserves the parent phenotype and supports UV-dependent labeling of candidate targets, establishing conditions for enrichment and LC–MS/MS-based target nomination.

Mechanistically, PRC1584 appears to limit heme detoxification by restricting hemoglobin flux into the digestive pathway. This mechanism (i) complements endoperoxides, (ii) rationalizes collateral sensitivity in K13-C580Y parasites, and (iii) selectively eliminates DHA-induced dormant rings, addressing a key contributor to delayed clearance and recrudescence. From a drug-discovery standpoint, heme/hemozoin measurements and vesicle metrics provide mechanism-linked pharmacodynamic readouts that can guide analog triage and schedule design (for example, DHA followed by PRC1584 during the dormancy window). The failure to select resistant mutants in vitro, together with the K13 sensitivity profile, suggests that PRC1584 acts on a complex, high-barrier target or pathway linked to hemoglobin uptake, supporting its potential use in combination regimens with a low risk of resistance emergence.

Beyond PRC1584 itself, this work establishes a set of generalizable tools and standards: short-pulse assays that resolve dynamics obscured by 72-h readouts; an integrated fractionation/UV–Vis workflow that distinguishes substrate depletion from heme accumulation; a structured EM and cytology rubric for cytostome and vesicle phenotypes; and a chemoproteomic engagement assay with stringent specificity controls (UV-dependence and optimized CuAAC conditions). Together, these methods provide a reproducible framework for evaluating modulators of hemoglobin uptake and metabolism and for comparing analogs on the basis of mechanism rather than potency alone. In summary, by following an initially intriguing phenotype through multiple experimental lenses, this dissertation identifies a critical aspect of parasite endocytic physiology and lays the groundwork for future studies in target identification, probe refinement, and rational combination therapy design.

Defining PRC1584's biological profile, stage specificity, and time–kill/recovery behavior

In Chapter 2, I demonstrated that PRC1584 has strong activity at low nanomolar concentrations against asexual blood stages, showing peak effectiveness during the late ring and early trophozoite stages (see Fig. 2.3). Continuous 72-h drug exposure produced the classic sigmoidal dose–response curves across different *P. falciparum* lines (Fig. 2.4, S2.3, S2.4, S2.5, S2.6). Briefly, stage-specific pulses induced development arrest, subsequently leading to a quiescent or pyknotic morphological state. This phenotype by PRC1584 shares similarities with DHA but is distinguished by recovery kinetics (see Fig. 2.4, S2.4). Short-pulse washout assays (8 h during the late ring and early trophozoite stages, Figure S2.4), revealed that long incubations such as 72 h can mask sharp early-stage potency: after matched short exposures and drug removal, DHA controls recrudesced by day 3–5 (WT) and day 1–4 (K13-C580Y), whereas PRC1584-treated cultures showed delayed or no recrudescence out to day 17–30 in both lines (Fig. 2.6, S2.7). Thus, these results address killing based on recovery rather than steady-state potency as detailed in the next section.

Consistent with this, DHA-induced dormant rings showed minimal recrudescence by day 14 when subsequently exposed to PRC1584, indicating sustained suppression of parasite recovery under the assay conditions (Fig. 2.6, 2.7). Taken together, these data identify late rings and early trophozoites as the principal window of vulnerability for PRC1584, rather than a generalized late-stage cytotoxic effect.

PRC1584 eliminates ring stages and DHA-induced dormant forms.

PRC1584 is active against ring stages, with short, stage-resolved pulses showing maximal effect during the late ring–to–early trophozoite transition, which anchors the staging logic used throughout this work. In the same experimental framework, Chapter 2 shows that a

brief DHA pulse drives a subset of rings into a quiescent state, yet these DHA-induced dormant rings are eliminated when PRC1584 is applied in the post-DHA window, reducing survival and delaying or abolishing recrudescence relative to DHA-only controls. A plausible explanation supported by the broader dataset is that dormant rings, despite reduced metabolic activity, continue to utilize cytostome-mediated hemoglobin uptake at minimal levels to sustain heme and amino acid supply. By limiting this upstream process during the ring and early trophozoite stages, when hemoglobin uptake ramps up, PRC1584 disrupts the program that sustains dormancy, even under post-DHA conditions. Functionally, this positions PRC1584 as an orthogonal antimalarial agent for DHA-tolerant rings, and it motivates the development of schedule-based combination therapies in which a artemisinin derivative rapidly debulks parasites and PRC1584 follows within the dormancy window to prevent rebound from the dormant parasites.

PRC1584 potency is retained across different genetic backgrounds including field isolates. Beyond NF54-derived lines, Chapter 2 described results showing robust *ex vivo* activity against 31 Tororo (Uganda) field isolates, yielding a mean EC_{50} of 70 nM (range 26–177 nM). Although responses varied by ~7-fold, as expected for polyclonal clinical samples, all values remained in the low-nanomolar range, aligning with laboratory potencies (Fig. 2.2, Table S2.1). For context in the same assay set, DHA averaged 1.8 nM (0.5–4.4 nM) and chloroquine 17.2 nM (6.9–27 nM). These data argue that PRC1584's potent activity extends to circulating parasites, supporting translational relevance.

PRC1584 is refractory to *in vitro* resistance selection.

Multiple selection approaches failed to select for PRC1584 resistant parasites. In single-step selections in the drug sensitive 3D7 strain using 5× EC_{50} values for 14 days on a 10^9-parasite inoculum or 100 nM for 14 days on 10^7 parasites, all cultures were cleared within the first four days and no recrudescence was observed during 60 days of post-pressure monitoring, yielding a minimum inoculum of resistance (MIR) > 10^9 infected RBCs (Fig. S2.1, S2.2). In addition, a separate attempt under constant drug pressure selection for 60 days in the Dd2-B2 strain using 3× EC_{90} values, cultures similarly cleared by day 4 with no regrowth over 60 days, whereas the control compound DSM265 (5× EC_{50} run in parallel) produced recrudescence in 68/96 wells (log10 = MIR 5.45), confirming assay PRC1584's high barrier to resistance selection. Finally, in a pulsed-exposure regimen (6 h at 8× 72 h EC_{50}, repeated over four cycles) applied to both highly synchronous rings and asynchronous cultures, parasites re-emerged between pulses, but all cultures extinguished after the fourth cycle, preventing further assessment of shifted potency (Fig. S2.1B). Across these protocols—single-step, constant pressure, and repeated pulses—no resistant parasites were recovered, indicating a high barrier to resistance for PRC1584 under the tested conditions. Taken together, these experiments indicate that, under the conditions tested, recovery of PRC1584-resistant parasites was not achieved, consistent with a high experimental barrier to resistance. The basis for this barrier remains unresolved; possibilities include engagement of a target with low mutational tolerance and/or dependence on multiple components of the endocytic/hemoglobin-uptake pathway, but these alternatives require direct testing. From a development standpoint, the absence of readily selected resistance supports pursuing combination regimens and schedule-based designs, while further resistance-risk assessment should continue.

Hemoglobin uptake and metabolism.

In the late ring and early trophozoite stages, PRC1584 reduces hemoglobin ingestion, yielding a reduction of the total heme pool with a secondary decline in hemozoin formation without an increase in free heme (Fig. 3.4). This was quantified by the fractionation/spectroscopic assays: a short exposure to PRC1584 resulted in a decrease of the total heme levels while chloroquine remained essentially unchanged, arguing against inhibiting hemozoin formation (Fig. 3.4). Ultrastructure and cytology align with this biochemical signature showing defective cytostomes, fewer digestive vesicles, and reduced hemozoin crystals (Figs. 3.5, 3.6), further supporting our hypothesis that PRC1584 affects hemoglobin uptake. Mechanistically, the phenotype is associated with K13 protein levels: western blot analysis demonstrated that the PfK13-C580Y variant exhibits reduced K13 protein levels compared to the NF54 wild type (Fig. 3.3). This reduction weakens cytostomal uptake and may account for the increased sensitivity of PfK13-C580Y mutant parasites to PRC1584 observed in both 8-hour and 72-hour assays. Essentially, tracking the heme/hemozoin levels provides a mechanistic approach to help select the best analogues and improve timing strategies. In future work, the same stage-matched short-pulse design used for the fractionation assays could be coupled to established cargo–reporter pulse–chase methods, in which parasites are briefly exposed to fluorescent hemoglobin or 10-kDa dextran, washed, and then chased to quantify cytostomal uptake under PRC1584 versus DMSO treatment.

Proposed MOA-comparability Workflow for Future Analogs

Beyond its therapeutic potential, PRC1584 functions as a chemical probe that reproducibly depresses hemoglobin ingestion at the cytostome during the late ring to early trophozoite

transition. This consistent “ingestion-down” signature provides a practical way to assess if new analogs share the same primary mechanism.

To determine whether new analogs share PRC1584’s hemoglobin ingestion-centered mechanism, a staged, mechanism-anchored workflow is proposed. First, determine if new analogs show their greatest effect in late rings/early trophozoites. Second, assess ultrastructure for cytostome defects with accompanying diminished hemozoin in early trophozoites. In the same window, run the fractionation/spectroscopy, PRC1584 reduces the total heme pool with a secondary decline in hemozoin, distinguishing upstream ingestion blockade from heme crystallization (e.g., chloroquine-like patterns). Third, use genetic sensitivity as an orthogonal check: maintenance of PfK13-C580Y collateral drug sensitivity (greater susceptibility in PfK13-C580Y mutant parasites than NF54 WT under short-pulse and continuous exposure) supports a shared mechanism at the cytostome/uptake axis. Finally, connect chemistry to biology via chemoproteomic competition: the photoreactive probe PRC1860 preserves the parent phenotype and yields specific protein labeling; dose-dependent reduction of this signal by an unlabeled analog indicates a shared binder neighborhood and on-pathway behavior. When all of these stage-matched assessments—pharmacology, ultrastructure, heme/hemozoin levels, genetics, and competition-labeling data—align, an analog can be classified as “PRC1584-like” regarding its mechanism of action. If there are differences in these areas, it suggests a different or combined mechanism and informs further profiling approaches.

Conversely, variants that show differences solely in potency would require additional profiling to identify any possible pathway deviations or the coexistence of mixed mechanisms. In practice, this methodology could guide structure–activity optimization to generate compounds that

preserve their efficacy and consistently support the intended hemoglobin uptake-based mechanism of action.

Development of chemoproteomic tools that preserve on-pathway performance

In Chapter 3, I advanced two chemical biology tools derived from PRC1584: an intermediate scaffold (PRC1859) and a full photoaffinity probe bearing a diazirine–azide handle (PRC1860). Both analogs preserved parent-like potency and reproduced the PRC1584 phenotype under 72-h exposure while maintaining PfK13-C580Y collateral sensitivity, arguing that the photoreactive tag and linker do not force an off-target effect (Figs. 3.7). Under the final CuAAC conditions selected from preliminary tests (varying protein load, detergent, reaction time, and blocking reagent; data not shown), PRC1860-treated samples displayed clear, probe-dependent labeling with minimal background, while DMSO controls showed no detectable signal (Fig. 3.9).This establishes a robust platform suitable for future proteome-wide mapping applications using new optimized chemoprobes. While I did not perform proteomics analysis for target candidate identification, the lack of labeled proteins in the DMSO control and the preservation of phenotype collectively de-risk the chemoproteomic strategy.

An integrated working model

Across chapters, a consistent picture emerges: PRC1584 disrupts cytostome function—either formation of the collar or formation of the hemoglobin-loaded vesicles. When uptake is curtailed, total heme falls and hemozoin follows. Mechanistically, PRC1584 acts upstream of the digestive or food vacuole, whereas chloroquine works within the DV on heme crystallization—i.e., chloroquine is downstream of PRC1584's primary effect. In PfK13-C580Y mutants with

already inefficient collars, PRC1584 pushes ingestion below a viability threshold at lower drug concentrations, yielding collateral sensitivity. PRC1584 also remains lethal in cultures with DHA-induced dormant rings; whether this reflects residual dependence on endomembrane trafficking/vesicle homeostasis or an alternative survival program (e.g., autophagy or stored-nutrient use) is unresolved. Functionally, the result is the same: restricting hemoglobin uptake and vesicle formation deprives susceptible and dormant populations of the source of amino acids.

Limitations and Future Directions

First, most biochemical and imaging readouts are time-window snapshots; finer kinetic resolution of hemoglobin uptake would strengthen causality. Second, cytostomal defects could, in principle, be a downstream stress response; time-resolved PRC1860 photo-labeling—UV 'stamping' at 1–15 minutes post-dose with parallel parent compound competition—will test for early, specific target engagement before morphological change. Third, most experiments used NF54-WT and NF54-K13 C580Y. Within the genotypes tested, collateral sensitivity was specific to the PfK13-C580Y mutation as it was not observed in K13-R539T and the Pfcoronin-R100K-E107V mutants. To define allele specificity and genetic modifiers, follow-up work should expand to additional K13 alleles (e.g., R561H, Y493H, M476I) and to non-K13 backgrounds linked to reduced artemisinin response, including reported chromosome-10 contributors (e.g., kelch10 variants/segmental copy-number changes) as well as UBP1, MDR2, ARPS10, and other endocytosis/trafficking factors. A stratified clinical-isolate panel across these genotypes will clarify whether the C580Y-linked collateral sensitivity generalizes or remains mutation-restricted. Finally, to independently validate the fraction assay results, assessing live parasites under real-time uptake assays using fluorescent larkers, and including additional controls (lower

temperature, ATP depletion and inhibitors with unrelated mechanism of action) as well as pH-sensitive dextran to assess changes in the pH of the digestive vesicles which is necessary to activate the proteases for hemoglobin digestion.

Therapeutic implications

A druggable choke point upstream of the digestive vacuole.

By reducing hemoglobin ingestion at the cytostome, PRC1584 reduces the flux of heme into the DV. This mechanism is upstream to quinoline-like inhibitors that block heme detoxification inside the DV and to endoperoxides that require free heme to generate radicals. Targeting ingestion provides an alternative way to control parasite metabolism by depriving the parasite of nutrients.

PRC1584 class as potential irresistible antimalarials: Rational combinations and sequence design.

PRC1584 showed activity against both proliferating ring stages and DHA-induced dormant forms and therefore, it is a potential partner for novel artemisinin-based combination (ACTs) therapies. Two potential scheduling concepts could be applied. A front-loaded “hit → starve” combination with DHA administered first to rapidly reduced parasitemia, followed by PRC1584, with the goal of steepening early clearance and stop recrudescence. Another option is a sustained “starve → sweep” approach where PRC1584 is giving first to reduce parasitemia by targeting rings stages, followed by a longer-half-life partner (e.g., lumefantrine) to kill parasites that may scape treatment by a similar mechanism to DHA-induced dormancy. Potential antagonistic

effects warrant consideration when combining a hemoglobin digestion blocker with DHA as it may limit heme availability and consequently reduce endoperoxide activation.

It would be recommended to assess novel DHA combination using a 2×2 timing matrix (PRC1584→DHA versus DHA→PRC1584) across physiologically relevant concentrations equivalent to the *in vivo* maximum and minimum concentrations detected within 24 hours of administration, evaluating endpoints including kill slope, recrudescence, and heme content. A field isolate panel categorized by K13 genotype can help identify geographic applications and the range of collateral sensitivities. Extending this framework to a panel of field isolates stratified by K13 genotype would define the breadth of collateral sensitivity and highlight geographic settings where PRC1584-based combinations may be most impactful.

Summary

PRC1584 shifts the therapeutic approach from "detoxifying heme" to "denying heme." When used in combination therapy, PRC1584 functions as a stage-targeted starvation agent, complementing rapid-acting partners and offering an alternative option in settings with K13-C580Y circulating mutants. Development should prioritize schedule-aware PK/PD to ensure exposure across the late ring and early trophozoite stage and to cover intervals when rings may enter a paused state—whether naturally or drug-provoked—with the goal of minimizing survival of these parasites. The findings presented in this work underscore the therapeutic potential of this “irresistible” β-carboline class of antimalarials that may act through a novel mechanism of action involving hemoglobin uptake and metabolization. The distinctive properties of this class provide opportunities for the advancement of innovative new combinations, including potentially future

ACTs, particularly in the setting of ART-R, by specifically targeting DHA-induced dormancy, a critical survival strategy of *P. falciparum*.